Addis Ababa University

Addis Ababa Institute of Technology

African Railway Centre of Excellence

Investigation of Fatigue Failure of Railway Axle by Finite Element Method.

A Research Submitted to the School of Graduate Studies of Addis Ababa University in Partial Fulfilment of the Requirements for the Degree of Masters of Science in Railway Engineering (Rolling stock)

Student Name: Nyimila Anosisye Mwandenuka

Registration Number: GSR/5982/12

Advisor Name: Eng.Demis Alemu (PhD)

Co-Advisor: Mr Awel mohamemdSeid

October,2021

Addis Ababa

Ethiopia

Approval

The undersigned has examined the thesis entitled "Investigation of fatigue failure mechanism of railway axle in a wheelset by Finite Element Simulation Analysis" presented by Nyimila Anosisye Mwandenuka of registration number GSR/5982/12, in partial Fulfilment of the Requirements for the Degree of Masters of Science in Railway Engineering (Rolling Stock).

Submitted by:		
Nyimila Anosisye Mwandenuka	_____	_____
Student	Signature	Date
Approved by:		
Eng.Demis Alemu (PhD)	_____	_____
Advisor	Signature	Date
Mr. Awel MohammedSeid	_____	_____
Co-Advisor	Signature	Date
Mr.Kajela Temesgen	_____	_____
Internal Examiner	Signature	Date
Kamil Dino Adem(PhD)	_____	_____
External Examiner	Signature	Date
Abrham Gebre (Associate Professor)	_____	_____
Director of ARCE	Signature	Date

Declaration

This thesis, titled "Investigation of fatigue failure mechanism of railway axle in wheelset using finite element simulation analysis," was completed as part of the requirements for the award of a Masters of Science in Railway Engineering degree (rolling stock). I swear that this thesis, with the title mentioned, is based on my idea, which is also based on the training I received while studying railway engineering (rolling stock), and is not a copy of anyone else's work. Where someone else's work has been published, his/her contribution has been acknowledged in my work through proper citation.

Student	Signature	date

Acknowledgement

First, let me take this opportunity to thank God for enabling me to be in good health as well as for enabling me to attend this course for a period of two years. Special thanks also go to the Chief Advisor Eng. Dr. Demis Alemu and the Co-Advisor Mr.Awel Mohammed for the support and advice they provided and enabled me to achieve the completion of this thesis. I would also like to thank the trainers who taught me various subjects in the railway engineering course (rolling stock) courses that have helped to expand my knowledge and skills to do the thesis. For their representation, I would like to name some of them as Dr.Celestine Nkundineza who taught a research methodology course that gave me an understanding of how to do and write a thesis. Eng. Dr. Demis Alemu who taught a Finite element methods lesson that helped me a lot on how to do analysis based on a selected topic for the thesis.

Congratulations to the railway centre of excellence under Addis Ababa University, Addis Ababa institute of technology for initiating, funding and supervising railway engineering training. I would also like to thank the director of the railway centre of excellence Dr.Abrhaham Gebre for his dedicated leadership and for being able to make me selected to join his training centre. My last thanks to my employer who is the National Institute of Transport (NIT) in Tanzania, especially the management under the head of the institution Eng. Professor Zakaria Mganilwa for giving me permission to attend training, and cover the cost of training in Ethiopia.

Abstract

Railway axle like other part of a wheelset is very important for achieving the propulsion of a rail vehicle. However, in case of safety of passengers, railway staff and Freight, care required to avoid failure of the railway axle in-service. In this thesis, the investigation of fatigue failure mechanism of the railway axle carried out using Finite Element Method (FEM). The software used is ANSYS workbench in which the analysis of the railway axle model performed in the wheelset assembly together with a track. The static structural analysis of the axle in ANSYS workbench performed by applying the axle load on the top of the axle boxes in order to investigate and analyse the axle damage, fatigue life and the maximum stress that cause the damage of the axle and factor of safety. In addition, Static structural analysis performed in ANSYS workbench for small-scale (rough and smooth) specimens to investigate and analyse the fatigue strength limit of materials used for axle manufacturing. The finding show that the maximum stress is 661.35MPa for $\emptyset\, 7mm$ rough specimen and 564.97MPa for $\emptyset\, 11.5mm$ smooth specimen. After the analysis performed in ANSYS workbench, a simulation also performed on nCode to verify fatigue life, damage and maximum stress of the axle. The results obtained from the simulations verified by comparing with the results obtained from the experiment, which are available literature review. The results obtained according to the axle weight of 25tons, 30tons and 35tons in terms of stresses are 86.66MPa, 103.98MPa and 121.3MPa respectively in ANSYS workbench. The maximum fatigue stress obtained due to nCode simulation is 170.6MPa.Recommended from international standard is 200MPa.For small scale specimens, the results agreed with the experimental results in literature review. In case of fatigue of a full axle, there is a variation between the simulation and experimental results and its standards.

Keywords: Railway axle, Fatigue damage, Fatigue life and Simulation analysis.

Table of Contents

List of Figures

List of Tables

Acronyms and Abbreviations

List of Appendices

Chapter 1. Introduction

1.1 Background

In view of the various factors, it is important that the axle design of the railway car take into account the long-term use of the intended function. The goals of the design and manufacture of railway axle are to ensure that they can operate without damage for at least 30 years. The issue has prompted a number of experts to conduct research into the causes of railway axle failure if in use before reaching the expected time. The goal is to improve or eliminate the problem that causes axle failure when in use so that it does not continue to cause harm to consumers[1].

The design of the railway axle should take into account how it can withstand the force of fatigue when in use. Various methods are used to detect the presence of causes of axle failure. Non-destructive testing (NDT) is used to detect the presence of small cracks and to ensure that they do not grow before reaching another axle inspection cycle through NDT. In 1996 to 2003, five axles failed in the UK. Four of those five broke into two pieces and caused serious damage. It is reported that although the occurrence of axle fractures when in use is not very common but the effects are intermittent when they occur. In this regard, care is still required to ensure that no railway axle can fail before the next inspection period[2].

There are many disadvantages due to the axle to withstand the force of fatigue. In Europe, following a report released by the European Railway Agency (ERA) for the period 2007 to 2012 more than 400 accidents of railway vehicle were due to damage of railway axle. Experimental results show that although the design of the railway axle as well as its manufacture based on the resistance of the fatigue load, but still cracks occur due to repeated load. Moreover, the tests performed to detect cracks using NDT equipment are not sufficient to enable the investigator to detect the problem early before it causes harm [3]

The complication of loading conditions of the axle, to withstand the vertical force, braking force and the reaction force of the wheel, but also it requires enduring the impacting loads of line and the pulling force and reaction force of driving device, and so on. Its design and manufacture have focused on the durability of the material to withstand the fatigue load so that it can last a long time. One reason is that many failures are due to long-term use and that the growth of cracks is due to the weakness of the materials[4]. Therefore, for improving the reliability and safety of the axle during service, it is extremely significant to research and assess

the failure mechanism of the railway axle. In this thesis, the investigation of fatigue failure carried out by using finite FEM. Fatigue failure analysis; include full-scale specimen and small-scale specimens. For small-scale specimens the tension analysis carried out on rough and smooth specimens in ANSYS Workbench.

1.2 Problem Statement

Many researchers have researched the cause of railway axle failure when in use due to fatigue load. They have found that although the design of the railway axle adheres to the fatigue limit, reports still indicate some of the train accidents caused by the failure of the railway axle. As reported by Hutar et al[3] quoting the ERA in their study, nearly 400 cases of train accidents during the period 2007 to 2012 in the European Union. Those accidents occurred due to failure of the railway axle [3]. In the period from 1996 to 2003; there have been five mid-length axle faults on vehicles operating in the UK, in which four axles were completely broken into two pieces [2]. Failure of railway axle cause a derailment of the railway vehicles. The derailment of railway vehicle has several impacts to human life and environment such as;

Death and injury to passengers and the general public, Possible environmental damage - chemical spillages, flammable or explosive cargoes, Destruction of public property and consequent financial losses, Disruption of rail (and possibly) road traffic, Loss of public and commercial confidence in the transport system.

The existing research investigate the failure of railway axle in different ways. Some of them investigated the physical broken axle to find out what caused the axle to fracture. Other research[5], [6] based on fatigue test of a small specimen because full-scale test of real axle is very expensive.

1.3 Research Questions

i. Why railway axle fails while in service operation?
ii. What are the main mechanisms of axle failure?
iii. What to do in order to omit and control those mechanisms of axle failure?
iv. Which methods to implement to investigate fracture of axle?

1.4 Objective

The main objective of this research was to investigate the fatigue failure of railway axle. The analysis of railway axle model performed in ANSYS workbench software linked with nCode

to analyse maximum permissible stress, axle damage, factor of safety and the fatigue life of the axle.

1.4.1 Specific Objectives

i. To create railway axle model using CAD software for FEM analysis in ANSYS workbench and in nCode software.
ii. To analyse maximum fatigue failure using analytical method
iii. To analyse maximum permissible stresses, axle damage, factor of safety and fatigue life of the railway axle in ANSYS workbench and nCode simulation.

1.5 Significance of the Study

The investigation of axle failure mechanism aims to improve safety in railway transportation sector. It is known that the failure of railway axle like other part of a wheelset, cause a train derailment. The derailment of the train has several disadvantages such as lose of human life, loss of properties and destruction of railway infrastructure etc. Understanding the proper causes of the axle failure is important because it is suggesting the proper design of the axle to avoid failure and to suggest the proper methods of investigating the crack propagation on the railway axle to prevent failure while it is in-service.

1.6 Scope and limitation of axle fatigue failure investigation

The investigation of railway axle failure focused on finding the fatigue failure mechanism that lead the axle failure in service. Static structural investigation performed in ANSYS workbench software, then linked to nCode software to verify fatigue failure so that the measure taken to prevent the failure of railway axle in service. This is achieved by improving the design, manufacturing process, good surface finishing and painting and reducing fatigue loading. It has been found that before axle collapse, there are cracks that occur due to certain causes. These cracks as time increases, they grow and eventually cause the axle to break completely. That is why it is important to monitor the axles while in service to observe the crack formation before the axle failure.

The limitations of this investigation based on experimental test. In this analysis both small-scale specimens and full test piece performed by using software only. Experiment test did not performed in this investigation.

Chapter 2. Literature Review

The review of this literature comes from many different sources. Many researches done regarding to investigate what are causes of railway axle failure. Although scientists and engineers have conducted in-depth research on the fatigue, failure mechanism of axles, and infinite life design and periodic non-destructive testing used to ensure their service reliability, but still there are some accidents reported. For example on their research[4],report indicate that in 2004, the train derailment accident occurred in Italy, which was caused by axle fracture. In 2008, a high-speed train in Germany overturned due to hollow axle failure despite being traveling at a slow speed while crossing the Rhine Bridge in Cologne. The axle broke when it was used for a short period of time, which is estimated to be 3.09 million kilometres, which means 109 loading cycles withstood. Quoting from the Railway Safety Performance Report of the ERA in 2011, the number of broken axles in the European Union between 2006 and 2009 was 329 in total.

Rail axes are the heaviest parts of railroad cars, which have the highest concentration of stress. In addition to bending, common problems, the axles can be stressed at the same time. Those are the driving mechanisms and disc brake valves. In this way, the axles perform the same as shafts it works. It has been shown in the literature that the complex and easy conditions of stress, overcrowding, poor handling and exploitation, material-related faults and poor mechanical properties are the most common causes of failure - breakdown of the rail shaft. In their study they found that, axle breakage occurred under exploitation conditions at the source of the stress concentration in the cross section located at the axle section between the roller bear and the rail wheel [7].

The authors Zhu et al[4] of the study on "Analysis of the mechanism of failure on the shaft wheel of a power engine rail" indicate that, the state of the loading of the axis is very complicated. It not only withstands vertical force, braking force and wheel impact force, but also withstand impact loads, pull force, and impact force of the steering device, and so on. Rail axes designed for unlimited life depending on the fatigue limit of the material. While many cases of their failure are caused by defects that were caused during service and the extension of important dimensions as a source of cracks[4] .

In the study of rail shafts and axle fractures toward the fatigue failure in-service condition and the accumulation of fatigue damage. The study of adverse with un-expectable conditions as well as adverse conditions of exploitation and maintenance of railway infrastructure makes it

possible to break the shaft with real axles. Examining traction shafts, axle breakage, and breakdown processes, the study comes with the in use conditions and the outcomes presented through the service stress spectrum. In addition to railway axle condition in service, their results also included unknown conditions natural environment shaft vibrations and the sliding wheels caused by stick–slip processes movement processes during full train or stop motion. Figure *2.2* up to Figure 2.4 show axle fracture as referred to position as in Figure 2.1[8].

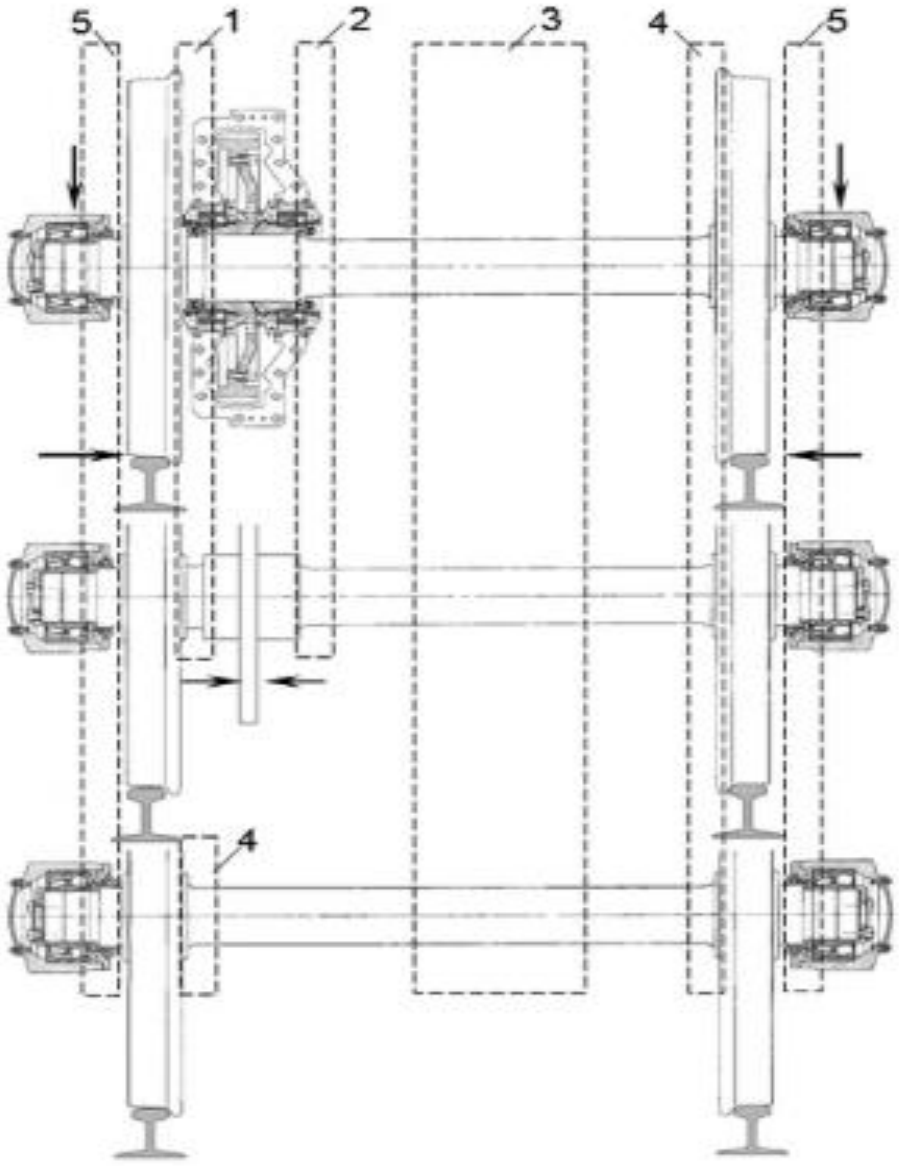

Figure 2.1: Distribution of fracture places in the railway traction shafts and axles

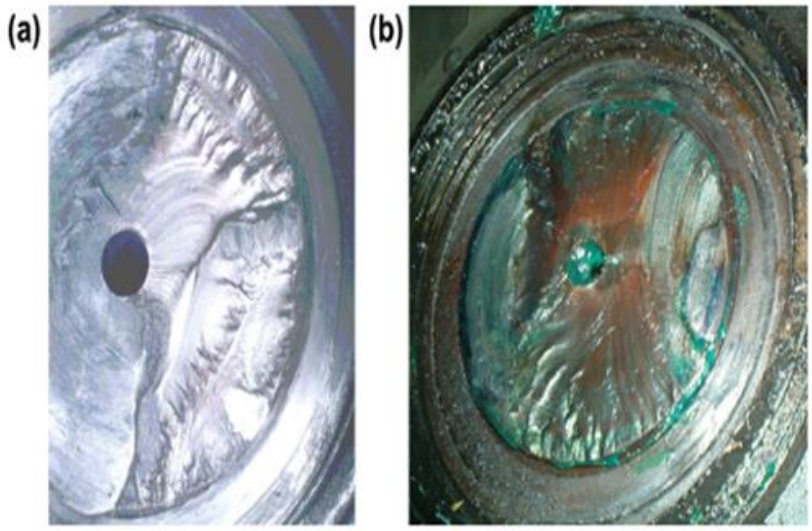

Figure 2.2: Typical fractures of traction shafts–axles

Figure 2.3: Fracture of the traction shaft in section 3 (Fig.2.1)

Figure 2.4: Fractures of traction shafts–axles in section 2 (Fig. 2.1).

Ognjanovic et al [8] on their study concluded that, the structural parameters of the rail shafts make the occurrence of shaft failure impossible in normal service conditions. They identified two causes of rail shafts and axle breakage. The first was the natural vibrations of the rail and wheels caused by the stick–slip process in wheel/rail contacts. The second was bearing and breaking of the shaft - breaking the axle and bearings. The result of their work was a statistical analysis obtained due to service and condition that provided through the spectrum of service stress, which represents the traction shaft, together with the railway axle condition as well as the fatigue life. Tolerance of broken gravity devices was tested. Using experimental results obtained from the sample (available), the distribution tolerance region obtained by data change and presentation, by bending back and by back torsion. Next, they used FE analysis to identify

the concentration of stress at a complex assembly with the complex effects of the attached components like gears and wheels. Examples of reliability calculations include the effect of axle during operations (the scope working stress) and the accumulation of fatigue damage. The effects of material damage on the surface layer were included in the analysis[8].

Ognjanovic et al[8] suggest possible barriers against breakage of shafts (axles). The formation of cracks prevented by strengthening the surface layer. With surface hardening (turning off), the resistance to crack activation increases. The best solution is permanent control of natural vibrations and online monitoring of fertility. Similarly, online crack activation monitoring on shafts and rails can be a very acceptable solution.

Executive and R. The court examined five axles, which failed in service and failure results, and comments on the causes of failure. Most were due to the slow growth of fatigue cracks on the axles. It was found that electrical drills, rust and corrosion stress are a source of fatigue One study based on the accident at Rickerscote, Stafford, occurred on March 8, 1996[7]. Unfortunately, the derailed wagons blocked the adjacent line and run into by a travelling post office train going in the opposite direction. One person has been killed and there were 10 injuries. The fractured axle shown in Figure 2.5(a). The axle manufactured in 1970 and satisfied the specifications in place at that time. Since its last ultrasonic test, the axle had only travelled 110 000 km. The accident had destroyed any information on crack initiation, but examination of the axle did reveal a small amount of corrosion, mostly only about 0.03mm deep, with one corrosion pit 0.05mm deep. Based on their observations, one found that, it is possible that damage due to fatigue occurred in a rusty hole near the center of the axis where the paint had come. The rust hole added stress inside the axis to initiate fatigue of the cracks. The crack grew and eventually broke into two pieces. The axle break in the salt truck occurred on January 29, 1998 in Shields Junction, Scotland. The fracture was exactly in the middle of the axle section. Figure 2.5(b) shows that crack activation occurred in two or more locations, with two major fatigue cracks growing on similar planes until a rupture occurred. The exact points of initiation destroyed in the accident. Complete ductile fracture occurred when only about 15 per cent of the cross- sectional area of the axle was not broken, as shown Figure 2.5(c).

(a) Railway axle broken into two pieces from the freight wagon

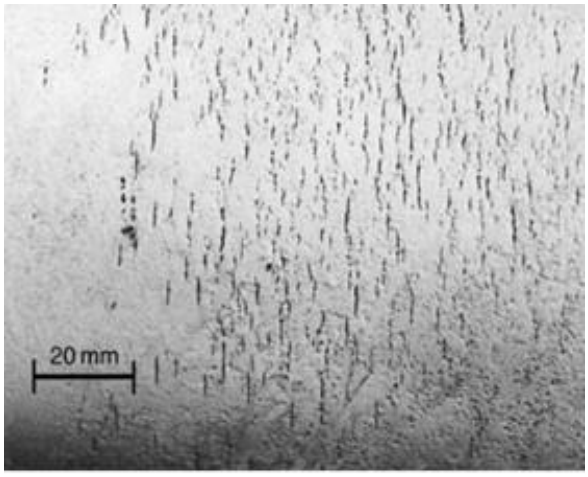

(b) Crack surface of fractured freight wagon axle

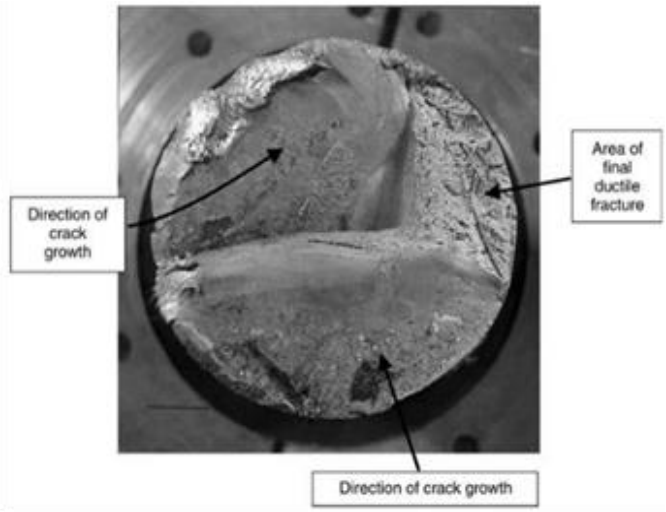

(c)The surface of broken railway axle involved in the accident

Figure 2.5: Indicate appearances and the features of the broken axles: (a) Railway axle broken into two pieces from the freight wagon, (b) Crack surface of fractured freight wagon axle, (c) The surface of broken railway axle involved in the accident[7].

In Figure 2.5(c). As illustrated in Figure 2.5(b), the axle had many surface cracks, which the magnetic particle inspection method emphasized. The axle was sectioned, and the deepest non-fractured crack found was 12mm deep into the axle's body.

According to the research, the damaged bitumen coating on the axle allowed salt solution to come into touch with the axle, and become stuck around the surface. Stress corrosion fatigue cracking was caused by high mechanical fatigue stresses in the center region of the axle, along with the highly corrosive liquid on the axle surface, as evidenced by the repeated cracking in

Figure 2.5(b). Fracture of an axle and derailment occurred near Bennerley Junction, Nottingham, on 21 June 2002. Several of the two-axle coal-carrying wagons were derailed and damaged the track, but there were no injuries. The broken shaft was tapered with a minimum diameter at mid-span of 171mm wherever the fracture occurred. The diameter of the axle adjacent to the wheels was 189mm. The damage area shown in Figure 2.4 regarding 120mm of the broken surface across the axle was coated with fine, parallel lines (beach marks), indicating that cracking occurred throughout an amount of slow cleft growth. The ultimate 50mm across the fracture face shows that ductile failure occurred once about twenty-five per cent of the cross-sectional space of the axle remained unbroken, as referred on Figure 2.6 by the bottom area of the fractured surface. Then, the shaft finally bent and bust into 2 pieces. The corners of the fracture face were broken throughout the derailment; this destroyed the purpose of initiation of the fatigue crack. The ductile final fracture as indicated in Figure 2.5, by the rough surface end and therefore the absence of any sides on the fracture surface[2].

Assessment of the potential for fatigue in high-speed rail bundles due to foreign material damage (FOD) conducted by Wu et al[9]. To identify the defect, 50 rail axles made of intermediate steel alloy steel (MSAS) and hard replacement of low carbon steel (HCS) were carefully detected with 46 alloy axle defects and 50 alloy steel defects carbon was discovered, subjugated. In their discovery Wu et al[9], axle surface defects included scratches and impact defects. The examination included wear and tear problems and minor cracks. For MSAS axles, scratches and impact defects were at 710-1191mm from the axial end away from the gearbox, and most of the 46 defects are between 830 and 1050 mm. According to Wu et al[9], two experimental techniques were carried out: one was typical of monotonic tension.

These devices were created and fabricated using experimental materials obtained from MAS Chinese axles in compliance with EN13104. Since FOD is performed on a regular basis at the axle body, the tendency to fatigue and fatigue of the outer surface of the axle was generally very important, according to the analysis.

Thus, models of traditionally designed bars used for uniaxial real estate in Figure 2.7(b) and models of glass clocks used for fatigue and high frequency rotations were prepared from the region of interest in Figure 2.7(a). MTS-810 servo measuring equipment adopted to detect properties of monotonic tension. As clearly shown in Figure 2.7(b), the 0.2% the reduction strength of 0.2% of Rp0.2, the final strength of the Rm force and the breakdown length of the calculated lengths as MP1 591, 726 MPa and 18.8%, will be under control. The second set of

characteristics was the Fracture mechanics parameters, which employed the stress intensity factor range (ΔK) and its threshold (ΔKth) of a long fatigue crack to assess crack initiation, growth, and residual life owing to FOD of high-speed railway axles.

For greater fitting accuracy, four types of stress ratios were used, i.e., R=−1, 0, 0.1, and 0.5, were used for better fitting accuracy. The ΔKth -decreasing approach of fatigue crack growth studies employing the Amsler-HFP 5000 testing machine with a frequency of 120–150 Hz[9] was used to calculate Kth. The title of the study is "Probabilistic fatigue assessment for railway axles and derivation of a simple damage calculation format." Berretta S, Regazzi D [10], describe a process for determining the danger of a railway axle failing due to fatigue under service loading for a simple fatigue assessment that complies with recent structural requirements. Their goal was to find a safety factor for damage calculations that would allow designers to use a simple semi-probabilistic method to building axles with a desired level of fatigue resistance.

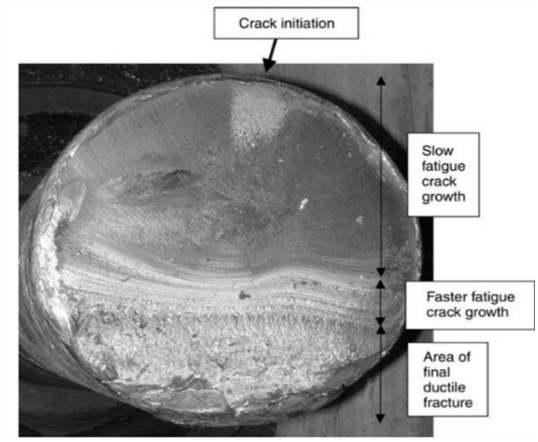

Figure 2.6: Fatigue surface of axle Brocken in the accident [2]

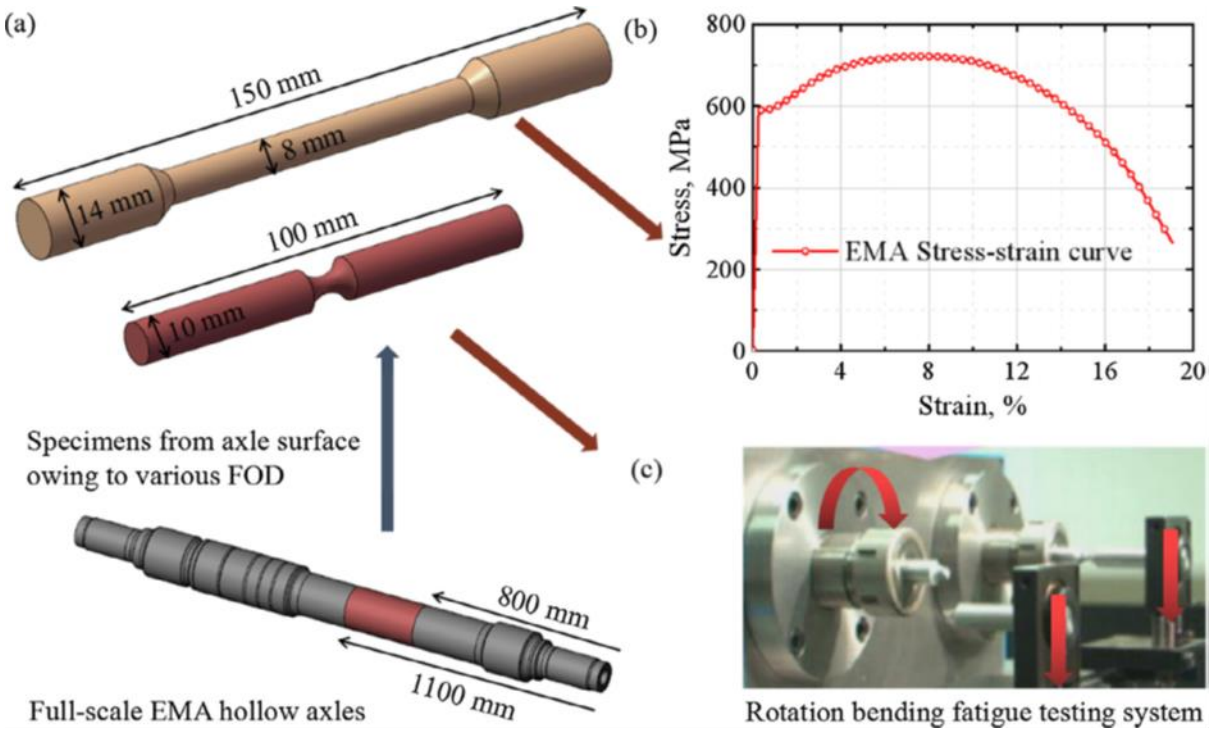

Figure 2.7: Specimen preparations taken from the outer surface of full-scale hollow axles that have been exposed to a variety of external damage causes:(a) Specimens from axle surface owing to various FOD,(b) Stress/strain graph of specimens,(c) Rotating bending testing system[9].

The design curve, which corresponds to the characteristic curve divided by an acceptable safety factor, is used to make the assessment (both for constant and variable amplitude loading)(γ_{Mf}) reported in Table 2.1. Considering that a railway axle is a safety critical component, according to EUROCODE 3 the safety factor should be in the range 1.15–1.35.

Table 2.1: Recommended values for partial safety factor γ_{Mf} [10]

Assessment Method	Consequences of failure	
	Moderate consequences	Severe consequences
Damage tolerance	1.00	1.15
Safe life	1.15	1.35

In their finding Berretta S, Regazzi D [10], the probabilistic fatigue assessment they consider an axle with a local fatigue strength described by a Gaussian distribution with parameters ($\mu_{\log S_D}$,$\sigma_{\log S_D}$) that subjected to a constant stress S_L for an infinite number of cycles *(or $n > N_D$)* as shown in Figure 2.8. The failure probability simply calculated as:

$$P_f = \phi(-\beta) \qquad 2.1$$

Where;

$$\beta = \frac{\mu_{\log S_D} - \log S_L}{\sigma \log S_D} \qquad 2.2$$

Using the ideas of stress spectrum and damage, a probabilistic assessment of fatigue under varying amplitude may be made. To begin, the S–N diagram must be expressed as follows

$$N = \frac{C}{S^k} \qquad 2.3$$

Where $C = N_D . S_D^k$ It is easy to recognize that, because of the variability of fatigue life, C is a random variable (Figure 2.8) which belongs to a lognormal distribution with parameters:

$$\mu \log C = \log\left(N_D . S_D^k\right) \text{ and } \sigma \log C = \sigma \log N \qquad 2.4$$

Where σlogN is the dispersion of fatigue lives that could be estimated with an appropriate interpolation of fatigue data[10] The damage of a stress spectrum divided into l classes

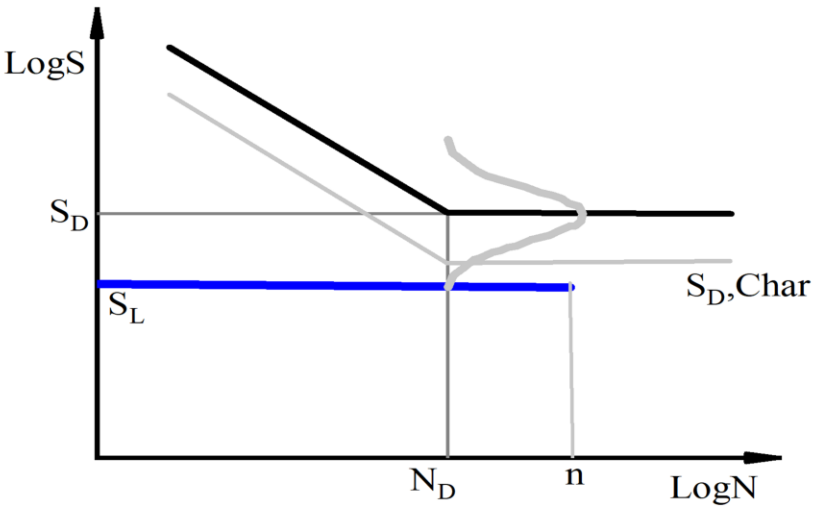

Figure 2.8: Scheme for a simple probabilistic fatigue assessment under a constant amplitude stress S_L[10]

expressed as:

$$D = \frac{1}{C} \sum_{i=1}^{l} n_i . S_i^k \qquad 2.5$$

(1) that can be rewritten as:

$$\text{Log D} = -\text{logC} + \log\left(\sum_{i=1}^{l} n_i . S_i^k\right) \qquad 2.6$$

(2) This equation shows that $log\ D$ is a Gaussian random variable with the same scatter as the fatigue life ($\sigma logD = \sigma logN$. the calculation of the failure probability simply done as:

$$P_f = \text{prob}[D > D_{crit} = \phi(-\beta) \qquad 2.7$$

With;

$$\beta = \frac{D_{crit} - \mu\text{logD}}{\sigma \log D} = \frac{D_{crit} - \mu\text{logD}}{\sigma \log N} \qquad 2.8$$

There have been tests conducted by EURAXLES and they have been able to detect high-level fatigue, which has led to the approval of the required maximum level of fatigue. Due to this challenge, it has been difficult to achieve accurate S-N curved drawing. The graph that expected to draw S-N so that it is adaptable in comparison with a small amount of data as Figure 2.9(a) shows the data. At the same time it is known that the roughness of the surface and the volume of its area have led to a decrease in fatigue strength in the area, as well as changes in the slope of the S-N curve including changes in knee position [10,11].

Furthermore, the researchers was able to discover the S-N axle diagram based on their research and other earlier studies, and its whole slope has been lowered. These were created using an S-N diagram and the data received, as well as those saved for axle fatigue. The essential data is divided into three portions, with $\text{UTS} = 700$ [MPa], being the most important.

(i) The ND knee position has been identified as one of the smallest specimens (ii) the slope k has found out from the S–N diagram of full-scale axles that estimated using ML method diagram of small-scale specs at $N = 10^4$ cycles; (iii) a log- normal is a consideration for fatigue limit distribution and fatigue strength.

The estimated S–N diagram parameters for EA4T are listed in Table *2.2*. The fatigue limit calculated here is remarkably similar to the value obtained in [11], which used full-scale data and assumed a Gaussian distribution for fatigue strength. Figure 2.9 (b) shows a potential S–N

diagram for A4T, along with the full-scale test data available. The S–N diagram, as expected, is slightly conservative in terms of data points.

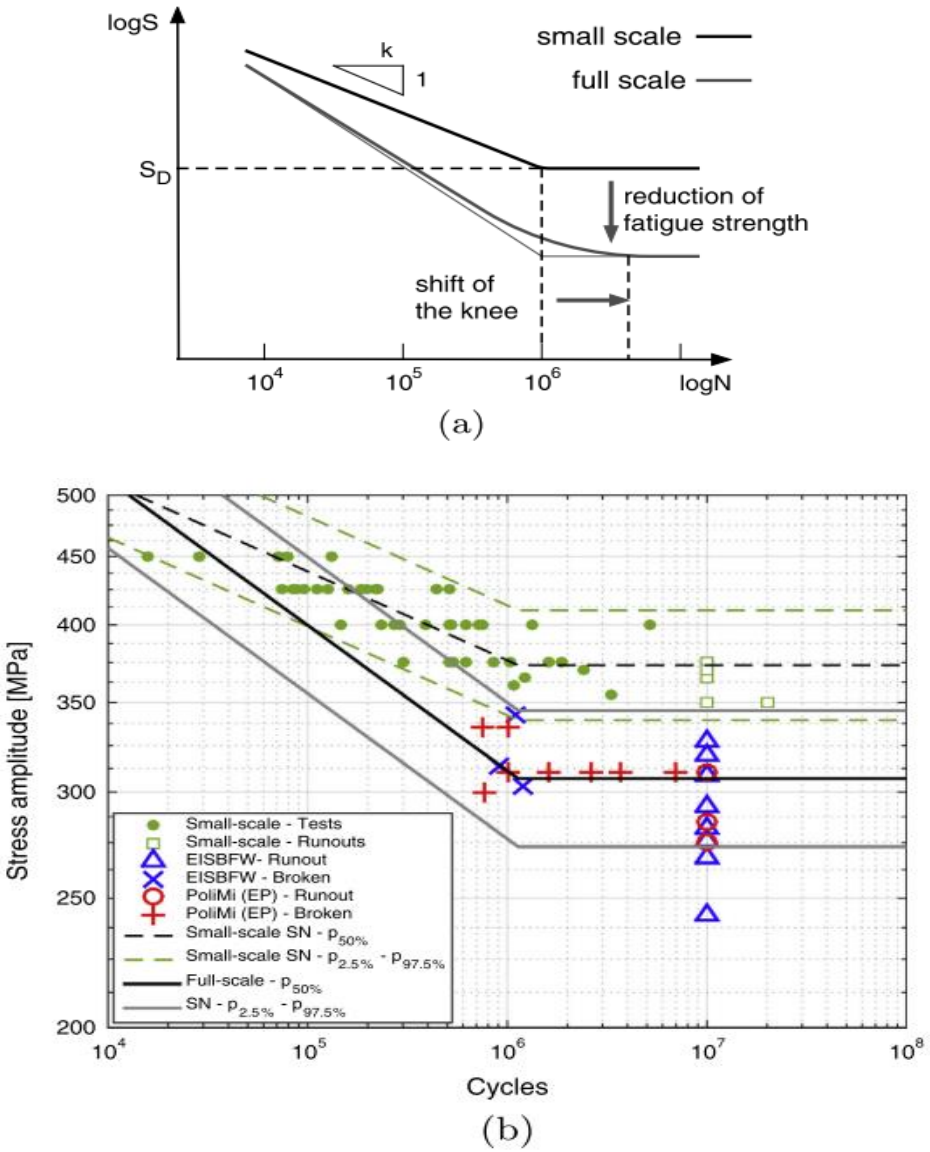

Figure 2.9: EA4T prospective S–N 1diagram: (a) Schijve's schematic (derived from [12]); (b) full-scale comparison with available data 10 and 11]

Table 2.2: Parameters for the estimated S–N diagram for EA4T[10]

N_D $[cycles]$	S_D $[MPa]$	k	$\sigma log\ S$
$1.2\ .10^6$	307.3	9.2	0.026

Table 2.3 lists the parameters of the EA1N S–N diagram. Figure 2.10, shows the resulting prospective S–N diagram for A1N, which matches the full-scale test data for A1N. The fatigue threshold of small-scale specimens is nearly identical to the fatigue threshold of full-scale axles, and the small-scale specimens' slope is nearly identical to the slope of full-scale axles.

Table 2.3: Parameters for the estimated S–N diagram for EA1N.

$N_D\ [cycles]$	$S_D\ [MPa]$	k	$\sigma log\ S$
$2.2\ .10^6$	252.3.3	18.8	0.059

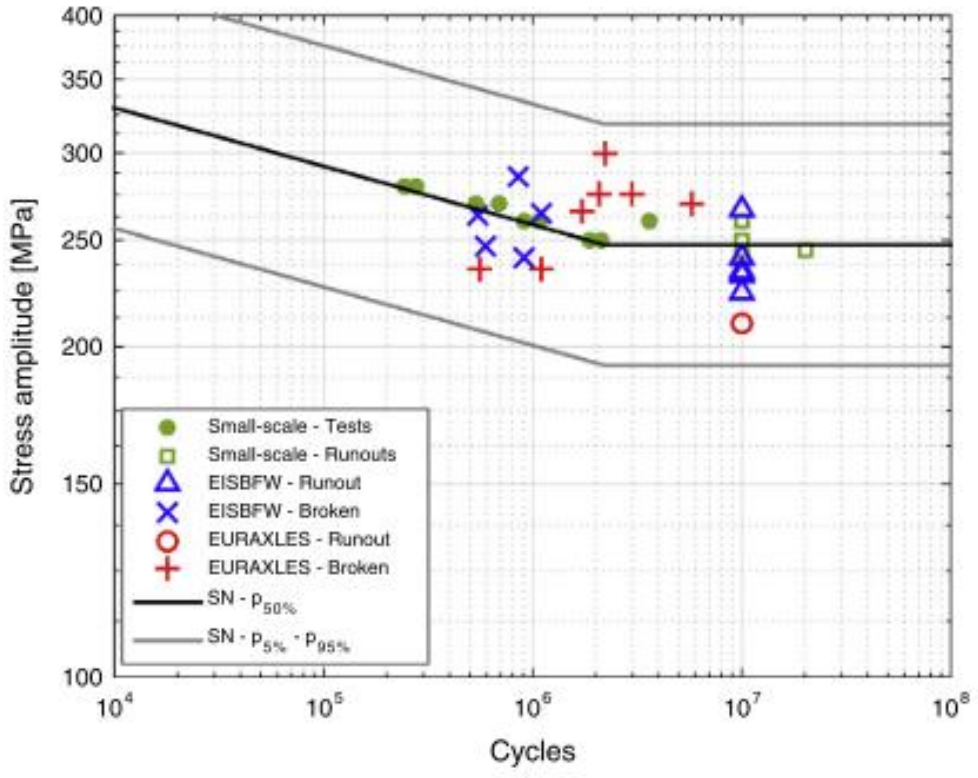

Figure 2.10:Reference S–N diagram for full-scale axles (in terms of local stress) made of EA1N[10]

The researchers discovered that surface flaw is the most common cause of axle failure in their study on the Analysis of Transverse Cracks Forming in a Railway Axle. The reason of a surface flaw on the wheel seat of a certain type of dynamic axle was systematically investigated in that research. The macroscopic chemical component of the inspection axle was determined using a spectrometer during the test. Energy disperse spectroscopy and X-ray photoelectron spectroscopy analyses were used to determine the chemical composition surrounding the crack.

Optical microscope was used to examine the fracture microstructure, while scanning electron microscope and confocal laser scanning microscope were used to characterize the crack microscopic characteristics. The problem is a transverse crack that runs circumferentially along the wheel seat, according to the report. It was established that the presence of stress concentration, which the wheel and axle interference fit caused, resulted in wear abrasion and fretting fatigue-initiated fatigue cracks because of surface pressure. Fretting fatigue damage to railway axles frequently occurs along the contact edge inside the wheel seat, where the tension is concentrated. Surface abrasion, peeling material, and plastic deformation are some of the most common types of damage[12].

Experimental Procedure of the research[12] conducted according to the requirements of China's railway standard TB/T1027.

- The chemical composition of the investigated axle was tested using spectrometer.
- Surface magnetic particle inspection and macroscopic observation conducted on the axle with cracks.
- Optical microscope (OM), scanning electron microscope (SEM) and confocal laser scanning microscope (CLSM) observed the surface morphology and vertical metallographic near the cracks on the wheel seat.
- The fracture morphology also observed using scanning electron microscope, when the crack opened along the depth direction.

Fatigue limit experiments on micro-notched specimens led to the calculation of fatigue thresholds for small cracks of the studied steel, based on examination of scale effects in fatigue limit and the rate of crack growth for a high strength steel used for high-speed railway axles. This allows for the examination of the scale effect and the fatigue resistance of full-scale axles when it comes to threshold stress for short cracks caused by small non-metallic impurities. The goal of the paper[5] was to better understand property of fatigue full-scale components by investigating scale fatigue effects limit and crack propagation rate of a high-strength steel serving for Axles of high-speed railways. The exercise started examination of the scale effect' between small specimen fatigue limits and full-scale fatigue limits. A group of fatigue limiting threshold was conducted on micro-notched specimens subjected to rotating bending fatigue for this purpose. The findings led to the formation of link between defect size and fatigue limit under rotating bending, known as the "Kitagawa diagram," for the steel in question. After that, the study looked into the growth rate of short cracks under rotating bending. The outcome of the experimental results were then utilized to create an EPFM crack growth model, which

included a "mechanical threshold" the applied stress determined factor of safety. This model was compared to data on fracture propagation from a "full-scale" axle during fatigue testing of a new test rig. The fatigue tests on railway axles. A minimum of 15 smooth sarface test specimen having a 10 mm diameter (RfL). And an equal number of notch pieces with 0.1mm depth, an opening angle of 30°, and a radius of r=0,04 mm at notched root (RfE). In the course of the examination, rotating bending forces, which were performed with test pieces of 10 mm diameter. The test bars on the axle were removed as near as possible to the axle's surface body. The RfL and RfE values are estimated for 10^7 cycles for the 50 percent probability of failure, and the test results are assessed using the ISO 12107 statistical "staircase" approach. EN 14261: March 2009 specifies the maximum limit of fatigue commonly used steel grades, with a focus on measuring the notch sensitivity coefficient q, which is required to calculate the safety parameter S [6].

Table 2.4: The fatigue to be achieved in according with EN 13261 are given[6]

Steel grade	RfL [MPa]	RfE [MPa]	q [-]
EA1N	Min. 250	Min. 170	Max. 1.47
EA4T	Min. 350	Min. 215	Max. 1.63

The fatigue limits determined from knowing the value of S, the security coefficient. Knowing the fatigue limits, the maximum admissible stresses obtained. For calculating the safety parameter (S), the notch sensitivity coefficient (q) has to be determined. The notch effect q obtained using the values of RfL and RfE. RfL is a fatigue limit determined from smooth surface small test piece, and RfE is the fatigue limit determined from notched small test pieces. From evaluated fatigue limit RfL and standard deviation, a probabilistic curve of fatigue strength constructed. Figure 2.11 shows a distribution of fatigue test results of a small scale specimen as carried out by Jorge et al [13]

$$q = \frac{RfL}{RfE} \qquad 2.9$$

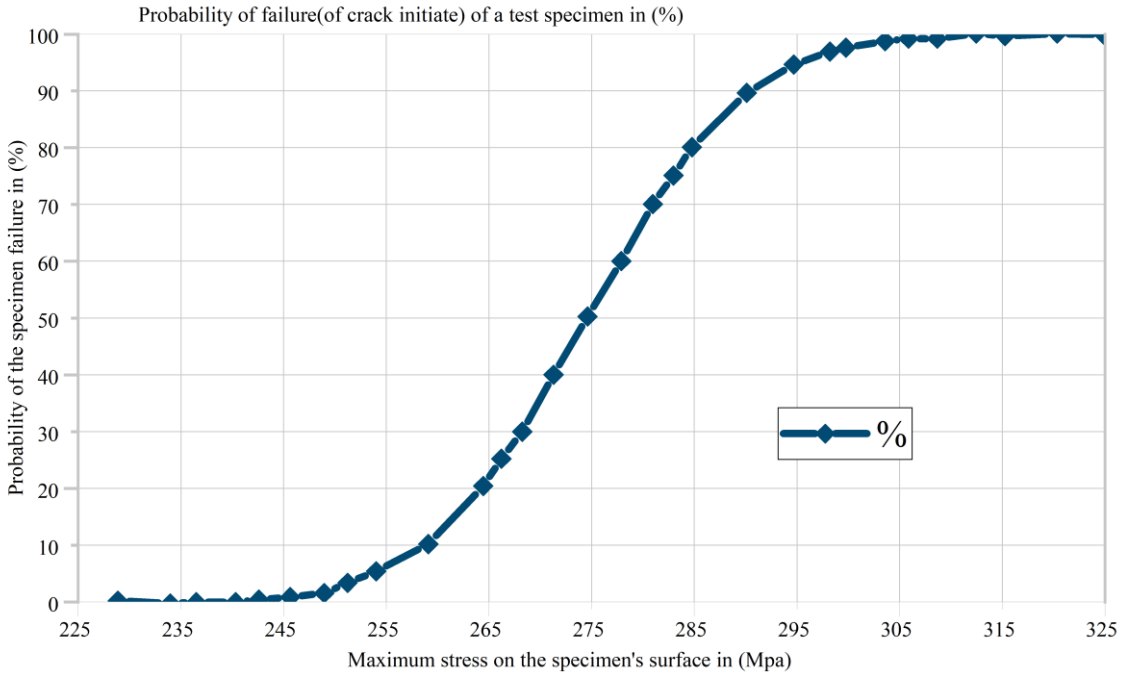

Figure 2.11: Distribution of fatigue test results of a small-scale specimen (steel grade EA1N)[13]

Table 2.5: Mechanical properties of steels for railway axles at +20°C in accordance EN 13261:2009 and DIN 10083[6].

Steel grade	Re [MPa]	Rm [MPa]	A5 [%]	Z [%]	KUlongit. [J]	KUtransv. [J]
EA1N	Min. 320	550 – 650	min.22	Not defined	Min.30	Min.20
EA4T	Min. 420	650 - 800	min.18	Not defined	Min.40	Min.25
34CrNiMo6 (DIN10083)	Min. 600	800 - 950	min.13	Min.55	Min.45	-

Where:

Re = yield strength

Rm = ultimate strength

A = Elongation

KUlongit = impact test, longitudinal test piece

KUtransv = impact test, transversal test piece

According to their conclusions [6], the values estimated and a vast number of fatigue tests were used to verify the axles' fatigue qualities. Because it is necessary for ensuring the In-service of railway axle safety. Unfortunately, a full-scale test of a genuine axle is an extremely costly test, and there are always a tiny amount of uncertainty in the results. Some issues were caused because there is a proper clarification missing in the expectations and definitions supplied in railway axle standards, in addition to minor discrepancies across testing facilities. The fatigue investigation allows for the assessment and determining model parameters. Designer acquires knowledge regarding material fatigue qualities and full-scale axle properties from investigated results.

2.1 Factors Affecting Railway Axle Structural Durability

The critical areas, which affected more by fatigue in rail- way axles, are at the press-fits (example seat for bearing, wheel seat, and seat for driving gears, the brake disc seat, the bearing seat, or labyrinth seal seat) and the radii of the axle. Among the factors for consideration the level of structural durability are stresses, which are the consequences of external loads, and the fatigue strength, which determined by material properties, design, manufacturing technology and environ- mental factors. From literature the experimental measurement show that the fatigue stresses vary with time. This variation is a result of varying force levels when the wheelset is rolling during service. The stress cycle created due to wheel and axle rotations is a function of the in-service conditions such as driving along straight track, driving round a curve or when crossing points, and has an amplitude-modulated characteristic Grubisic et al[14]. In the findings Grubisic et al[14], the fatigue strength of axles S_e depends on properties of the material, local stress conditions at individual axle areas and on the manufacturing technology.

According to Grubisic,V; Fischer,B if the value of S_e is related to the ultimate material strength R_m for axles with a diameter of about 200mm and stress concentration at fillet radii $K_t \leq 1.5$, approximately. Then the expression $Se \approx (0.21 – 0.25)R_m$ used for the axle's free surface and $Se \approx (0.12–0.16)R_m$ for press-fits, the lower values are related to the materials with higher R_m values. For example, the fatigue properties of an axle press-fit of the components at the wheel seat for different materials as presented in Figure 2.12 [14]

2.2 Axle steels that are standard

The steel grades EA1N and EA4T are the most common in European standards. EA1N is a general-purpose normalized carbon steel, while EA4T is a high-performance quenched and tempered low-alloyed steel. The fatigue characteristics of these steel grades are used as a

reference in axle design requirements. In terms of material fatigue characteristics, European standards mandate that all manufacturers check material performance so that one have properly dimensioned axles. Because of this forecast the behaviour of the axle under in-service stresses, it is important to estimate the fatigue limits to evaluate both the material and the product. A full-scale specimen of Cervello, S [11],was studied as part of the Euraxles project, which was a European Research initiative. Cervello, S. compiled a summary of the key findings from the full-scale axle fatigue test campaign, which included a variety of axle configurations. Work package 3 (WP3) of the Euraxles project was responsible for the experimental activity. WP3's main goal was to develop new fatigue limits for standard steel grades while also taking into account the impact of surface conditions that are not typical of newly machined axles, such as surface corrosion that can occur during service or surface blasting as a technique to increase paint adhesion. Axle locations tested included free body transitions or groves, and wheel seats, where relative micro slippage occur at high bending rates, resulting in the so-called fretting fatigue phenomenon.

Another component of their research [11], was the stress concentration impact that occurs during transitions where the body exhaustion limit is determined. Throughout each test, those parameters tested with strain gauges, and the results were used in the Euraxle project to verify their assumptions using a FE model.

Table 2.6: Design limits for EA1N and EA4T steels according European Standards[11]

	EA1N	EA4T
F1 – fatigue strength axle body (MPa)	200	240
F4 – fatigue strength press-fits (MPa)	120(solid axle)	132 (hollow axles)
Safety factor	1.2	1.33

An increase in groove depth or a decrease in groove radius in press-fitted railway axles can induce fretting wear and strain. On a heat-treated axle on its faces, an evaluation of fretting fatigue behavior was performed. The wheel seat and wheel hub bore were cleaned first, then lubricant was applied to reduce surface friction and prevent scratching throughout the process, according to EN 13260. At the contact region's center, FEM calculated a pressure of roughly 100Mpa. Inspection Magnetic particle of more than 600 axles after 300,000 kilometers revealed fretting fatigue cracks. Long and shallow with a fracture of diameter up to 0.5mm were discovered throughout the circumference of the wheel seat. The cracks in the place began

2-5mm from the press-edges. Fit's Stress relief grooves, including groove radius and depth, should led to increase fatigue-fretting resistance, as stated about improvement in fatigue fretting resistance[15]. Bayractar,F; Guclu,M[16] explains the conditions makes fracture and the life of the axle up to fracture. Materials of machine elements are important for the life of the component considering the working conditions. According to Bayractar,F; Guclu,M; the ultimate axle materials strength, should be more than 650Mpa.Also they stated that when radius increases, ultimate axle materials strength decreases. The effective stress calculated as $\sigma_{ef} = 315\text{Mpa}$ for a full load. Table 2.7 show the infinite life for the values less than 50% reliability.

Table 2.7: The life valued corresponding to σ_{ef} = 315 Mpa Damage[16]

Damage probability [%]	Reliability [%]	Life [Load cycles]
10	90	2.6×10^6
50	50	Infinity
90	10	Infinity

The test results shown in Figure 2.12 indicate that only a relatively small improvement of the fatigue strength achieved through utilization of a higher strength material in the press-fit assuming a similar diameter relationship. A greater improvement of the axle fatigue resistance, manufactured from high-strength materials, found by increasing the diameter ratio d_s/d_g as indicated in Figure 2.12 which area at the axle part is most critical, depending on the layout of the railway axle. Roughly for values of $ds/dg \leq 1.16$, usual press-fit conditions without surface treatment and typical stress concentration of the free axle surface $K_t \leq 1.3$, the most critical area is the press-fit, which indicated by failures in service. In addition to the choices of material and design approach, other important factors in determining the fatigue life are the manufacturing technology and sur- face treatment. Thus, to increase the fatigue strength of press-fits different coatings and a combination of press- fit and bonding are used. Other methods of surface treatment such as induction hardening and rolling used rather than choosing a high-strength material[14].

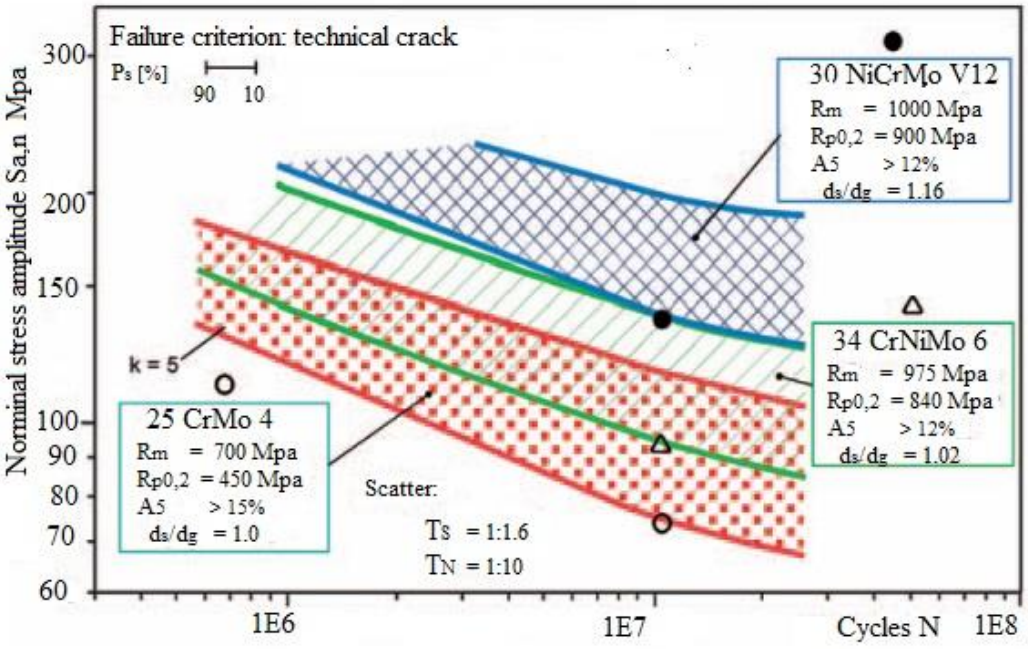

Figure 2.12: Woehler curves for wheel seat areas of different axles and materials under rotating bending, diameter of axles up to 190mm **[**13**].**

Luke et al[17], carried out the experiment and finite element modelling, adjusting fretting fatigue load settings on small-scale specimens to obtain stress-strain findings. The goal of the investigation was to forecast the beginning of cracks due to fretting fatigue conditions by using different fatigue characteristics.

2.3 Experimental procedures for testing specimens

Experiment for crack initiation under fatigue fretting loading is required because of relative changes inside the press fit of axle and wheel connections at contact zone. Testing procedures for experiment to simulate loading scenarios, cyclic axial load with a constant stress amplitude (or a maximum stress) applied to the specimen end by means of a standard testing machine (resonant testing machine).The experiment of different length of fattened pad specimens conducted by Luke et al obtained the results as follows;

1. Overall specimen length L=100mm, uniform specimen length l_s=21mm

- N=10^6 cycles at Q=1.5 kN and σ_{appl}=270-350 MPa
- N=2.10^5 cycles at Q=1.5 kN and σ_{appl} = 350 MPa
- N=10^6 to 5.10^6 cycles at Q=3 kN and σ_{appl} = 350 MPa

2. Overall specimen length $L = 142\text{mm}$, uniform specimen length $l_s = 100\text{mm}$

N=10^6 cycles at $Q = 1.5$ kN and $\sigma_{appl} = 250 - 350$ Mpa

2.4 Test due to Constant Amplitude

The test piece for fatigue were created utilizing parts from three distinct European railway axle manufacturers, all of which are Euraxles project partners. Steels EA4T and EA1N were used in the production specimens for fatigue tests. One of the instruments used to perform high-cycle fatigue under constant amplitude is the Rumul Te-stron (load regulated). This fatigue testing system allows for loading frequencies of approximately and produces fatigue test results in a short period. Using pure alternating sinusoidal loading, the loading ratio completed all fatigue tests. A fixed number of cycles was set at cycles for the runout test. The specimens were fatigue tested in stairwells according to ISO 12107[18] procedures. The S-N values was used to describe the situation in the investigation results with four parameters. The fatigue limit at the curve was determined using two different ways. To estimate fatigue endurance strength at cycles (fatigue limit) the staircase method and a maximum log-likelihood technique were utilized. The slope (k), standard deviation, and life cycles in the Wohler curve parameters were estimated using a modified maximum log-likelihood technique [18]. The results evaluation of Filippini et al[18] fatigue data under constant amplitude loading shown in Table 2.8 and Figure 2.13.

2.5 Application of S-N curve

An S-N curve, also called a Wöhler curve, with a results obtained as a number of testing fatigue at different levels of stresses. Figure 2.14 referrers the results for tested of un-notched

Table 2.8: Parameters for the SN curve and the fatigue endurance strength of EA4T and EA1N steels estimated by the ML method (small-scale specimens, constant amplitude loading)[18].

Steel grade	S_D Mpa	N_D Cycles	K	σlogs
EA4T	373.19	1133300	15.05	0.020966
EA1N	251.6	2230000	18.80	0.01588

specimens of a CrMo steel (SAE 4130). In Figure 2.14 the stress amplitude (S_a), fatigue life N is usually plotted tests $S_m = 0$, and thus the stress ratio is $R = S_{mim}/S_{max} = -1$. The variable on a logarithmic scale. In the literature, the stress amplitude is presented both on a linear scale and

on a logarithmic scale. Here, it is preferred to adopt the log scale because it frequently leads to an approximately linear relation between $\log S_a$ and logN for a substantial range of N-values. Fatigue at high amplitudes and fatigue lives up to some 10^4 cycles is called low-cycle fatigue (or high-level fatigue), see Figure 2.13.

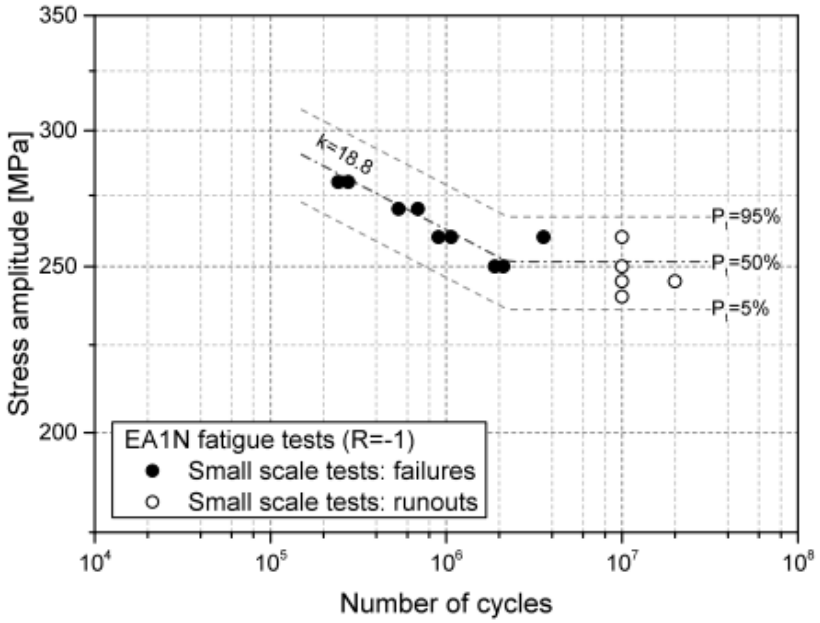

Figure 2.13: SN curve of small specimens of EA1N steel[18].

High-cycle fatigue occurs when a significant number of cycles, such as 10^5 or more (or low-level fatigue). A fixed number of cycles does not accurately describe the difference between low and high-cycle fatigue. Low-cycle fatigue relate with macro-plastic deformation in every cycle, which is the most significant difference between the two states. High-cycle fatigue is more closely linked to the material's elastic behaviour on a macro scale. In actuality, high-cycle fatigue is the more common scenario, while low-cycle fatigue is linked to specific structures and load spectra.

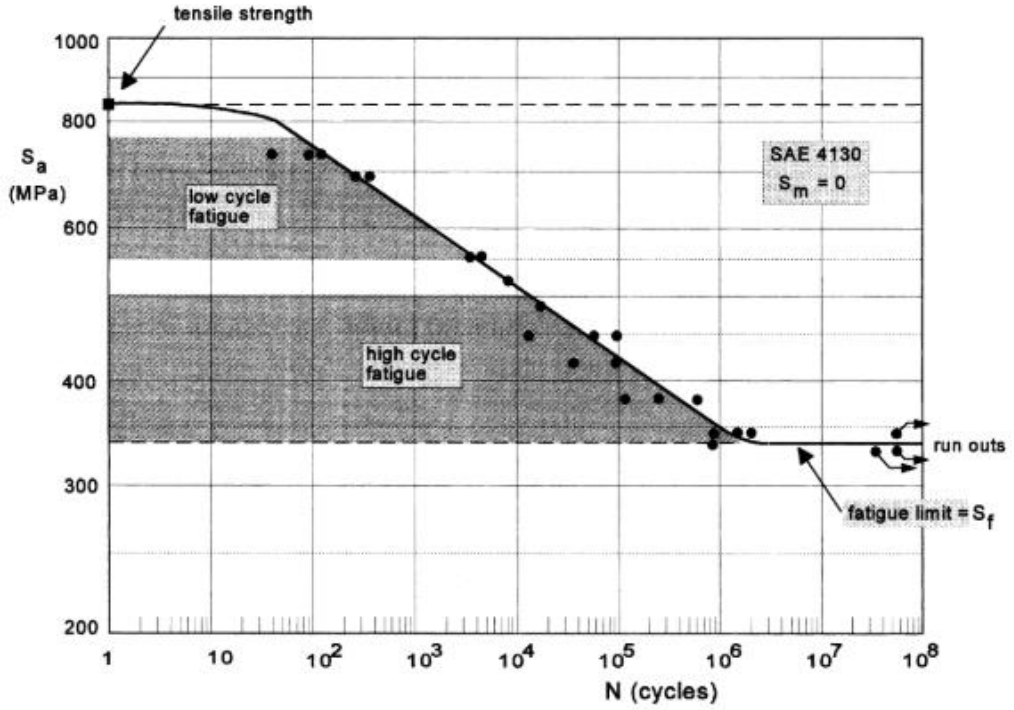

Figure 2.14: Fatigue test results of un-notched specimens of a low-alloy steel (SAE 4130)[19]

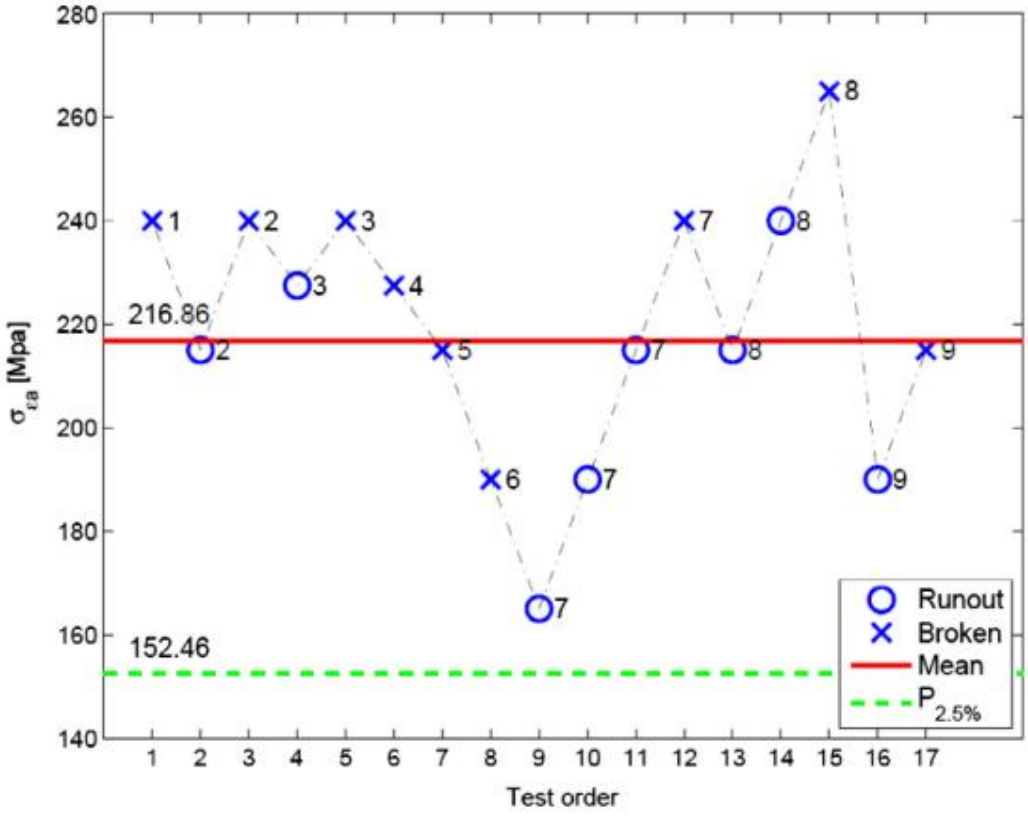

Figure 2.15: Fatigue test results of F1 A1N unpainted corroded axles, staircase sequence[11]

2.6 Description of the axle that was tested

Roughly 10 unpainted A1N axles that had been in operation for about 10 years (1 M km) on an SNCB passenger car were examined for the purpose of investigating fatigue of full-scale specimens of railway axle Cervello,S[11], Figure 2.15 shows the runout and broken axle under various pressures. Although many investigations for axle failure have been done to examine failure mechanisms, according to various literature reviews. The examination of axle fatigue failure was executed on a full-scale specimen and on more than 15 pieces of the same size for notched and smooth Small-scale specimens.

In this research, the investigation will base on finding fatigue failure due to fatigue loading in-service. For small-scale specimens the analysis carried out by varying the size of 10-notched specimens and 10 smooth specimens. In case of full axle, investigation conducted on the axle model assembled with a wheel, axle box and sliding on the top of the track.

Chapter 3. Methodology

For the purpose of determining the causes of railway axle fatigue damage, the FEM analysis simulation was performed. It was decided to employ the following methodologies for this investigation.

3.1 Data collected

The information used in this research is secondary. These secondary data were gathered through a survey of the literature. Existing published research, papers, journals, and reference books incorporated into literature review. International standards, such as the European Railway Axle Standard, were studied to obtain data for simulation analysis. That information are;

- The axle size to investigate
- The chemical make-up of the substance used in railway axles
- Mechanical properties of the materials and
- The size of a small-scale for fatigue of materials investigation are some of the important data collected for the computer simulation the railway axle fatigue damage.

Table 3.1: Types of wheelsets and the size of axle and wheel (EN 13261).

Wheelset Type	BA 004	BA 092	BA 314	BT 4
Axle load(tons)	23.5	25	25	
Wheelset weight(kg)	998	1394	1064	1244
Designed for	Heavy freight wagon	Passenger wagon	Heavy freight wagon	Passenger & freight wagon
Maximum Speed(km/h)	120	200	120	160
`Axle size(mm), weight(kg)	Ø130×191, 390	Ø120×179 374	Ø130×191 404	Ø120×170 386
Wheel size(mm), weight(kg)	Ø920 304	Ø920 304	Ø920 330	Ø1000 429
Axle material	A1NEN13262 2003	A1NEN13262 2003	A1NEN13262 2003	A1NEN13262 2003
Wheel material	ER7 EN13262	ER7 EN13262	ER7 EN13262	ER7 EN13262

These data for the analysis of railway axle failure obtained from Literature review, where the most design of rolling stock components is due to the International Standard organization (ISO)

and European Nations (EN) the components of the Wheelset it designed according to EN 23261.The wheelset consist of Railway axle, Bearing and Wheels. Axles designed according to the type of wheelset. Table 3.1 shows types of wheelset and the size of axle and wheel. The selected wheelset for the analysis of wheel axle is type BA 314 which are used for freight locomotive. The properties of the railway axle is due to JIS and European EN standards[20] as used for railway axle design and quality. The chemical composition and mechanical properties of railway axle materials are shown in Table 3.2 and Table 3.3 respectively [20].

Table 3.2: Chemical composition of railway axle material

	C	Si	Mn	P	S	Cr	Mo	Ni	V
AET4(EN)	0.22-0.29	0.15-0.4	0.5-0.8	-0.02	-0.015	0.9-1.2	0.15-0.3	-0.3	-0.002
RM	0.23	0.21	0.50	0.015	0.005	1.06	0.16	0.006	0.002

Table 3.3: Mechanical properties of railway axle materials[20]

	Yield strength (MPa)	Tensile strength (MPa)	Elongation (%)	Absorbed energy (J)
EA4T (EN)	≥420	650–800	≥24	≥30
RM	538.7	725.3	23	124

3.2 Create Wheelset, axle box and Tack 3D model

The model in this analysis created by using solid works 2019 software. Each part created in separate window and then assembled by using mate. The modelling parts included in the simulation are railway axle, wheels, and track and axle box as shown in the Appendix. The analysis of railway axle performed in the Wheelset assembly acting on the railway track. Railway axle including other parts of the wheelset assembly model for simulation analysis created by Solid works software. 3D Railway axle model and a wheelset created according to the required of EN standards dimensions. The dimensions of the railway axle displayed into 2D drawing as shown on Figure 3.1 and the wheelset assembly shown on Figure 3.2.

3.3 Import 3D model into ANSYS software

The created 3D assembly wheelset model from Solid works converted to ‘Para solid’(x*t).This file imported to ANSYS Workbench 2020 R2 software for simulation (Figure 3.3a).

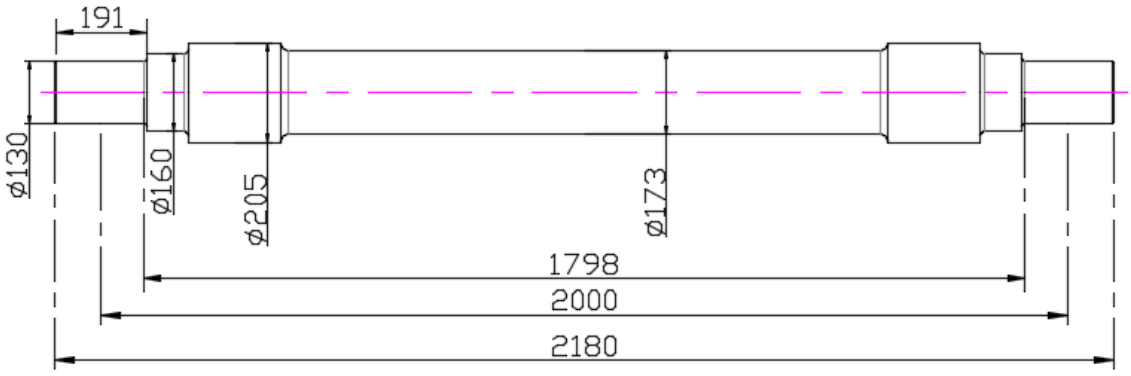

Figure 3.1**:** Axle dimensions according to EN 13261

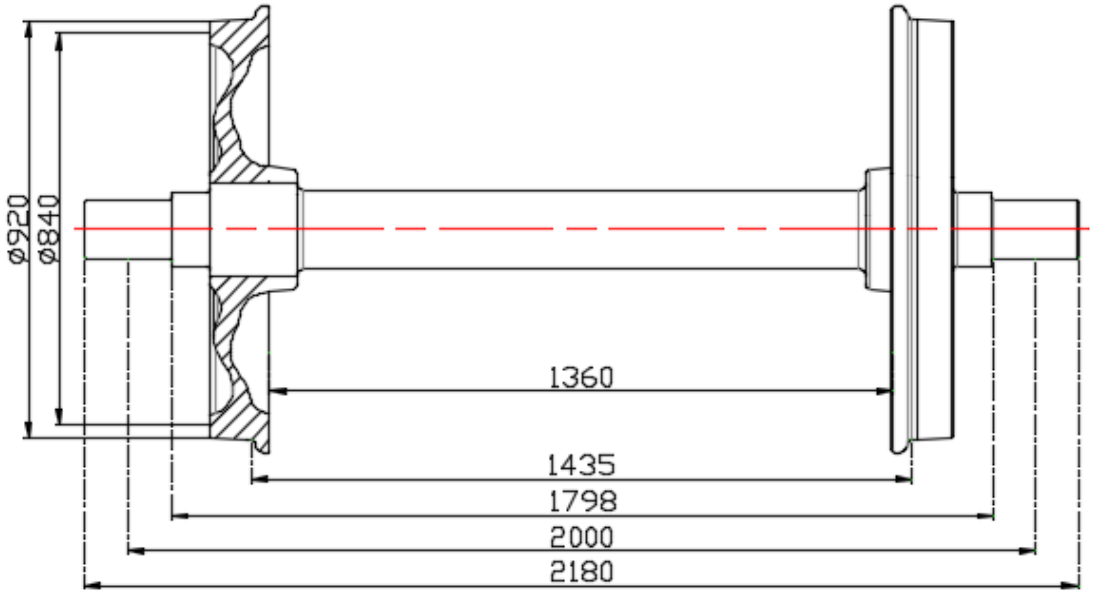

Figure 3.2: Wheelset assembly according to EN 13261

Axle's main characteristics

- The bearing size is ø130 × 191mm according to EN 13261.
- Axle weight is 404kg, the material is A1N EN 13261 2003.

Main parameters of the wheel

- High resistance to the mechanical impact of the thermos during the stopping action
- The wheel diaphragm has a low level of axial distortion.
- Residual pressure is low, and the material has good strength qualities.
- Rolling ring diameter is ø920mm and the minimum repair diameter is ø840mm.
- The material category is 13262 EN ER7 and the nominal weight is 330kg.

The mechanical characteristics of the materials for wheel are 520 MPa, 820MPa yield strength and ultimate strength respectively.

3.4 Materials assignment

Each part in the model assigned the required material properties according the data collected. This procedure performed in the content of engineering data in ANSYS workbench by assigning the mechanical characteristics of the parts. Physical properties and Mechanical characteristics of the components shown in Table 3.4.The material selected Ni-Cr-Mo steel SAE4340_350A which located under the category source of nCode-matml. This type of materials prefer to performed simulation in nCode for the purpose of fatigue analysis of the railway axle model.

Table 3.4: Physical and Mechanical properties of Assembly

Part name	Modulus of Elasticity (GPa)	Density (kg/m^3)	Yield Strength (MPa)	Ultimate Strength (MPa)	Poison's ratio(-)
Axle	210	7850	320	550-650	0.3
Wheel	210	7850	550	820	0.3
Rail	200	7850	510	943	0.3
Axle box	210	7800	320	550	0.3

3.5 Model Connections

In ANSYS Workbench 2020 R2, the connections between the wheels and axles, axle and axle box bounded (target and contact body), while the connections between wheels (target body) and tracks (contact body) is a frictional with coefficient of 0.3.as shown on Appendix B. Wheel movement only in X direction and displacement in Y direction.

3.6 Meshing of the model

The imported assembly model into ANSYS Workbench 2010 R2, meshed using fully integrated mechanical physical preference and element order quadratic with element size 20.0 mm finite elements Figure 3.3(b). The mesh and the number of elements used in the FE model have a significant effect on the results obtained and the computational time/cost. Although a fine, mesh would produce results that are more accurate but it increases the computational time/cost significantly. For this present work, a total of 360243 nodes and 200575 eight-node

quadratic elements used. It considered that a radius of the axle near the press-fit of the wheel contact region expected to experience higher stress.

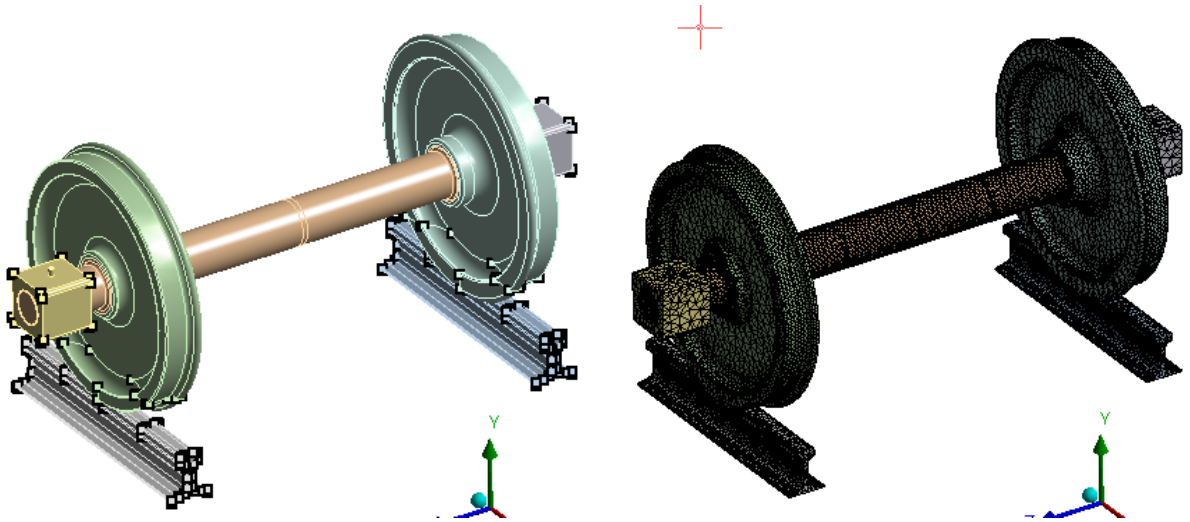

(a) (b)

Figure 3.3: (a) Imported assembled model in ANSYS (b) Assembly model mesh

3.7 Railway axle 3D model simulation

The 3D axle model was simulated using ANSYS software and subsequently in nCode software, that are linked together.

3.8 Railway axle model

The selected railway axle model for this analysis is a freight axle of the bearing size Ø130 × 191 according to EN 13261 standard. The full dimensions of the axle shown on Figure 3.1above. The analysis of the axle performed on the wheelset assembly. In this analysis, the three variations of load applied to the railway axle in the assembly model. These load values are 25tons, 30tons and 35 tons. The force (F) to be applied on the axle box calculated using mass (m) and acceleration due to gravity (g) as indicated in equation 3.1 and Table 3.5.

$$F = mg \qquad 3.1$$

Table 3.5: Axle loads

Mass(kg)	F=mg(N)	$\frac{F}{2} = \frac{mg}{2}$(N)
25000	245250	122625
30000	294300	147150
35000	343350	171675

3.9 Axle loading and boundary condition

The fixed support applied on the bottom of the two-tracks that there is no displacement of the track in any direction (i.e. X, Y, and Z).Wheels are bounded with axle, and its displacement is in Y direction only. The axle load applied in the axle box that are bounded with axle. The half load of 25tons, 30tons and 35tons applied on the top of the axle box on both side of the railway axle bearing **Error! Reference source not found.**. The maximum stress concentration on the axle radius near the wheel seat observed.

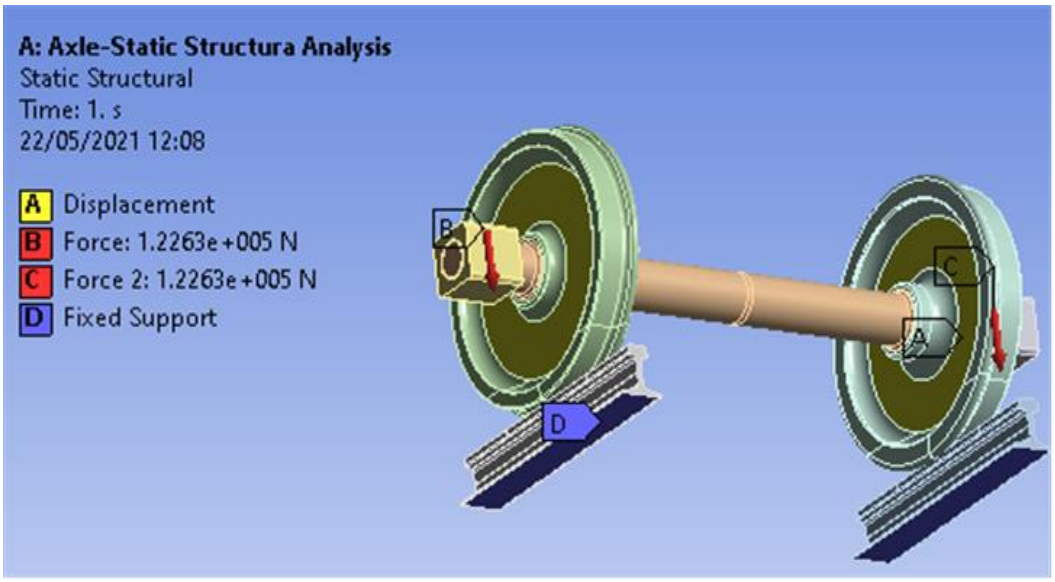

Figure 3.4: Fixed support, Displacement and applied load on the two axle boxes

3.10 Solving the model and checking convergence

The model solved and its convergence is checked. Since the model is converged, then the stress histories are calculated and then the fatigue life of axle has been determined. Then the stresses values taken from this analysis for the fatigue analysis to calculate the life and damage.

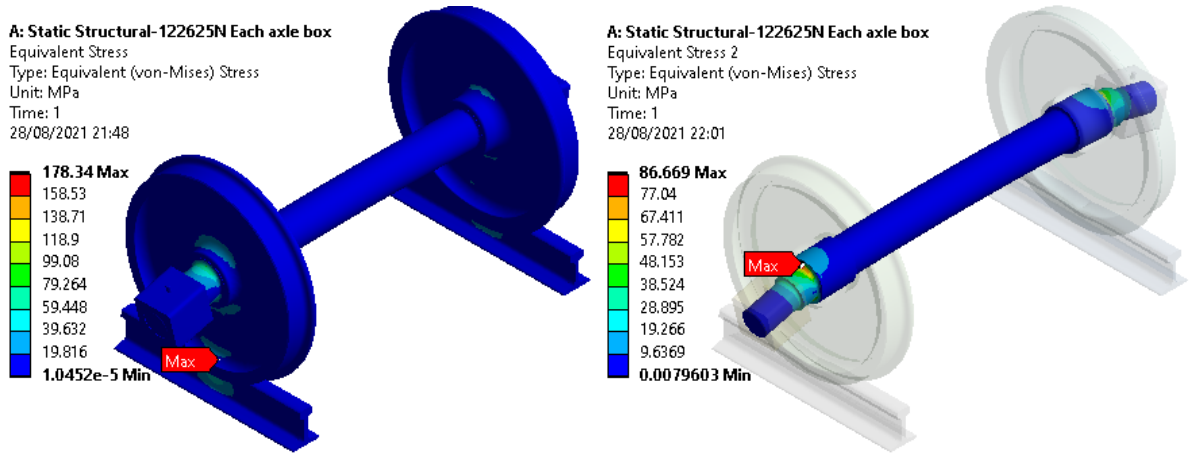

(a) (b)

Figure 3.5: Wheelset model simulation results, (a) The wheelset (b) The axle only.

Figure 3.5(a) shows the stress results of the whole mode due to the total weight of 25 tons applied on both right and left axle box. The maximum stress found is 178.34 MPa, and occur on the track. For the purpose of axle analysis, Figure 3.5(b) shows the stress results on the railway axle only. In addition, the values of maximum stress as shown on Figure 3.5(b) the maximum stress occurs at the roots outside the wheel seat. Other results for axle load of 30 tons and 35 tons shown on

Appendix E. The stresses increase due to increasing of the load.

The methods used to conduct the investigation to determine the cause of the failure of the railway axles are as shown in the flow chart on Figure 3.6. The main analysis of this investigation based on FE method using ASYS workbench. In ANSYS software, the analysis based on static structural analysis to investigate fatigue failure of railway axle mode by using fatigue tools and nCode software. The results for these simulations aimed to find out the causes of damage of the axles, maximum permissible stress for axle design and to analyse the fatigue life of the railway axle.

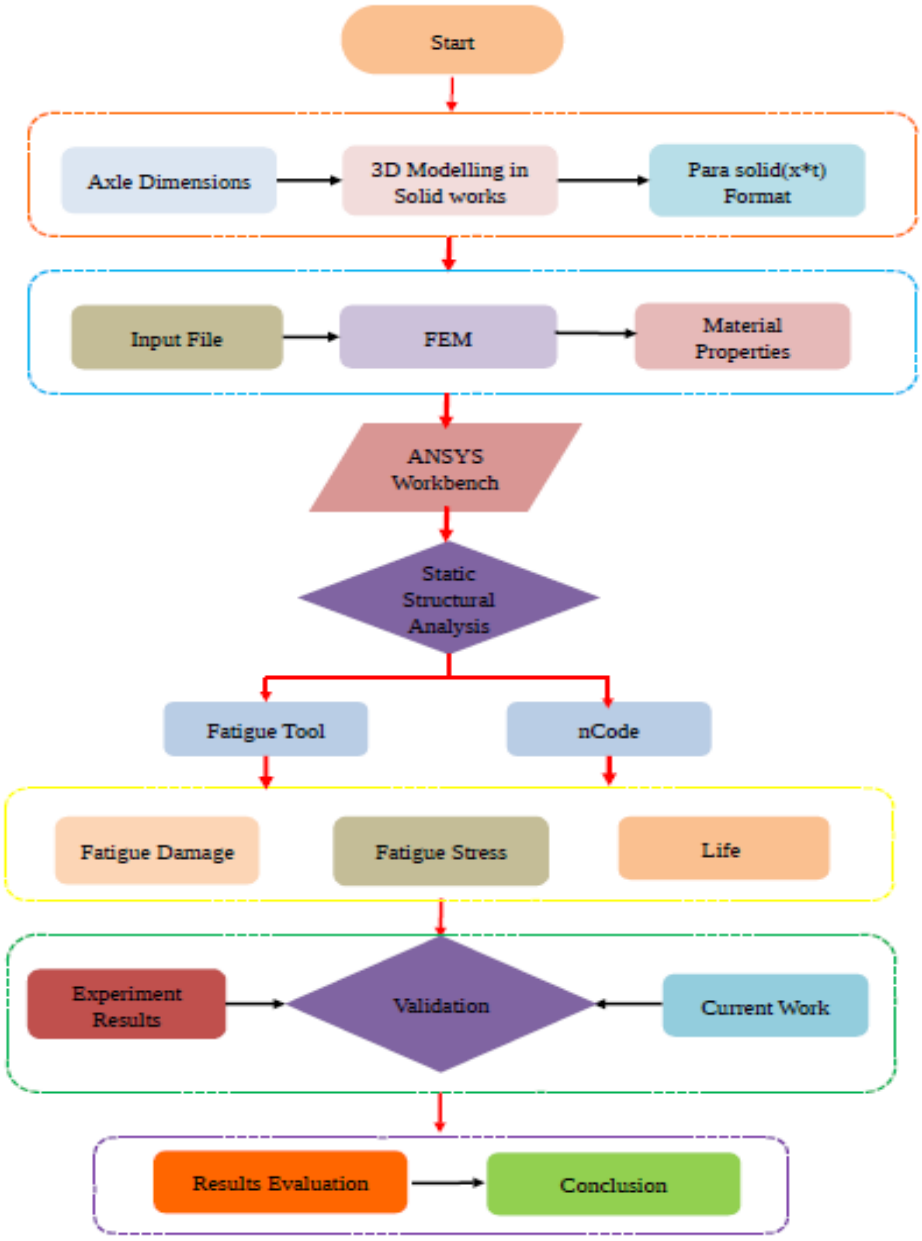

Figure 3.6: Flow chart for research methods

3.11 Fatigue test on the entire test piece

To predict Axle response to in-service stress conditions, the limits to fatigue in the axle's critical areas must be estimated. This is accomplished through the following steps:

- Estimation of limits to fatigue for the material on reduced test pieces with a diameter of 10 mm in the event that of an experiment.
- Examining the product's fatigue parameter. Tests on full-size axle test pieces whose dimensions and manufacturing technology are similar to the final product and its associated permissible fabrication flaws.

Changes in stress or strain define fatigue cycles, that can be explained as a range (Δs) or an amplitude (S_a).The average stress (S_m) has an impact on fatigue life. Several specimens are shattered under amplitude stress of constant magnitude to produce the following fatigue life curves:

- Plot the cycles it takes for a system to fail. For each specimen versus the change in stress or strain on a log-log plot.
- Using a curve fit, determine amplitude stress/strain and the life cycles until failure.
- In effect, the limit of endurance stipulates an endless existence.

3.12 Types of fatigue analysis

Fatigue analysis classified into two categories:

- Fatigue resulting from the formation of cracks and
- Crack growth-related fatigue.

The choice of the analysis type selected according to the given application as;

- When in the design phase, or for performing general fatigue analysis crack formation may be sufficient.
- For highly engineered parts or for in-service life prediction, crack growth can be selected.

3.13 Method of fatigue analysis

Fatigue crack formation analysis carried out in the following ways;

- Cracks/flaws are not explicitly considered.
- Use ANSYS to predict far-field (un-cracked body) conditions

ANSYS results fed to a fatigue analysis tool. Basic approach could be an S-N table look-up, performed by hand or via macrons, while fatigue that is more comprehensive analysed using nCode. In this analysis, nCode is used.

3.14 Complexities of Fatigue Analysis

There are many complications that required considering when performing fatigue analysis;

- Test data is typically for full reversed, uniaxial loading, but actual engineering will seek general loading conditions.

- Large scatter in fatigue test data
- Local plasticity in notch regions.

nCode has techniques that can address all of these complications.

3.15 ANSYS nCode Design life

ANSYS now offer an advantage set of fatigue analysis capability built in nCode, design life technology. nCode integrate with ANSYS workbench platform. Also, can run stand-alone using ANSYS RST, DYNAD3PLOT, ABAQUS, NASTRAN ETC.

3.16 Fatigue curves

- Stress-life curve; do not attempt at modelling plasticity and it is appropriate for high cycle fatigue.
- Strain-life curve; model material yielding and plasticity, appropriate for low cycle fatigue.

3.17 Small scale Specimen test

The small-scale Specimens analysis based on the materials used in manufacturing of the railway axles. In experimental test, Specimens taken from railway axle segments that were sliced into considerable pieces for study purposes.

3.18 Location of the test piece

The test pieces according to EN 13261[21] when taking from the largest axle section, three levels to consider are,

1. Near to the external surface for all the axles;
2. at mid-radius and in the centre of solid axles;
3. At mid-distance between external and internal surfaces, and near the internal surface of hollow axles.

The geometry of the specimens and the cut-up of a segment of axles with the positions of the specimens for experiments shown in Figure 3.7.

It is necessary to define clearly the group of the material for which the statistical distribution of fatigue properties being estimated. Specimen selection from the group taken in a random fashion. However, it is necessary to select the specimens considering the accurately to represent the group they are intended to describe. If population consists of numerous lots or materials in

batches, test specimens are drawn at random from each group in an amount proportionate to the lot or batch size. The amount of specimens taken must be equal the size of the sample (n) required. If the population has a serial nature, suppose, as an example, the properties are tied to the manufacture date, the population should be separated into time groups. Each group will be randomly sampled in numbers related to the quantities of the group.[22].

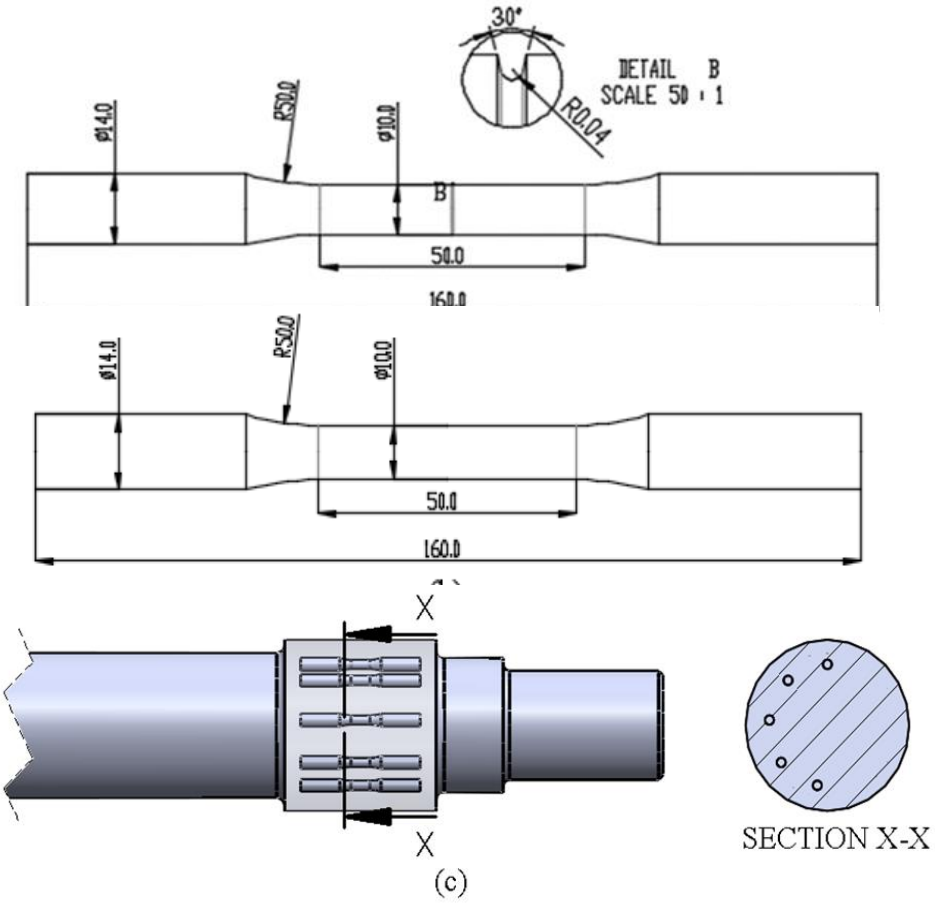

Figure 3.7: Details of fatigue test specimens (a) Rough specimen (b) Smooth specimen (c) Positions of the specimens in the railway axles segments

The materials in this analysis according to European Standards is EA1N having mechanical properties of Ultimate Strength (R_m) 550MPa and Yield Strength (R_e) 320MPa. The force applied to each specimen is due to product between the Ultimate Strength of the materials and the specimen's oginal cross section area (A_o) . The expression for calculating maximum force for testing specimen given by;

$$F_{max} = R_m \times A_o \qquad 3.2$$

In this analysis, the Variation of the diameter with respect to tensile maximum forces as in equation 3.2 applied to each specimen. Figure 3.8 (a),(b),(c) and (d) shows the mesh, constraint and loading, ultimate load, equivalent elastic strain results and equivalent stress result respectively of the specimen of 8mm diameter as an example of other specimen test.

(a) Specimen mesh

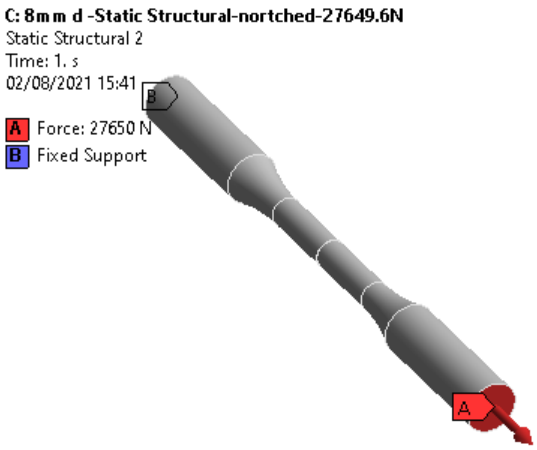

(b) Specimen constraints

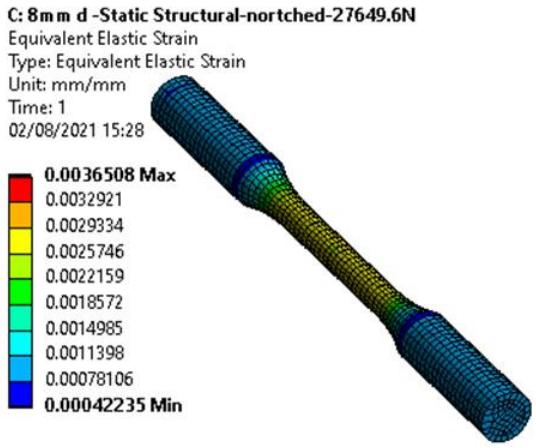

(c) Equivalent elastic strain

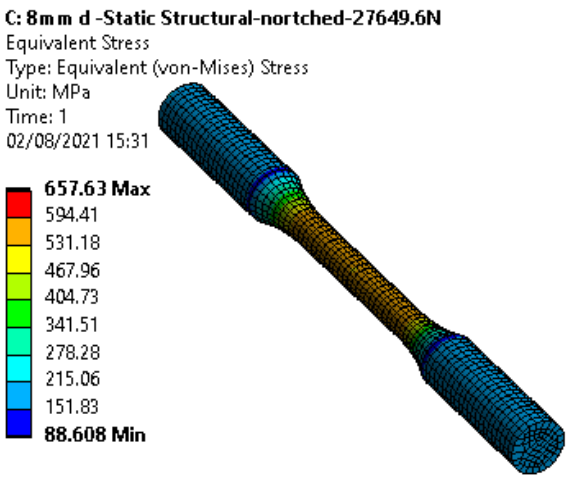

(d) Equivalent (Von-Mises) Stress

Figure 3.8: (a) Mesh (b) constraint and loading, (c) equivalent elastic strain results and (d) equivalent stress result of the specimen of 8mm diameter

The stress also calculated from equation 3.3, and the results compared with the stress obtained by ANSYS simulation analysis for rough and smooth specimens respectively.

$$\sigma_{smax} = \frac{F_{max}}{A_O} \quad 3.3$$

3.19 Fatigue analysis of specimens

The fatigue limit, fatigue curves (S-N curves), and a fatigue diagram are used to characterize the fatigue properties of materials ($K_t = 1.0$). The properties are limited to the results of constant amplitude (CA) testing on un-notched specimens. The findings of these tests are generally regarded to reflect a material's basic fatigue behavior. Fatigue qualities should be included in a material's mechanical properties, although they are frequently limited to the fatigue limit on un-notched specimens determined in rotating beam tests($S_m = 0$). When performing fatigue tests, the specimen failed due to alternating load [19]. A steady range of stress (S_r) or a consistent amplitude of stress (S_r) or a constant stress amplitude (S_a) describes the applied load on a specimen. The algebraic expression for the stress range and amplitude [23] is as follows:

The stress range is a difference between the maximum (S_{max}) stress and the minimum stress (S_{min}) in a cycle.

$$S_r = S_{max} - S_{min} \quad 3.4$$

The stress amplitude is defined as one-half of the stress range as;

$$S_a = \frac{S_r}{2} = \frac{(S_{max} - S_{min})}{2} \quad 3.5$$

Typically, in case of fatigue analysis, consider positive for tensile stress and negative for compressive stress. For fully reversed loading, S–N fatigue testing conducted using which indicates that loading is alternating about a zero mean stress.

The mean stress expressed as;

$$S_m = \frac{(S_{max} + S_{min})}{2} \quad 3.6$$

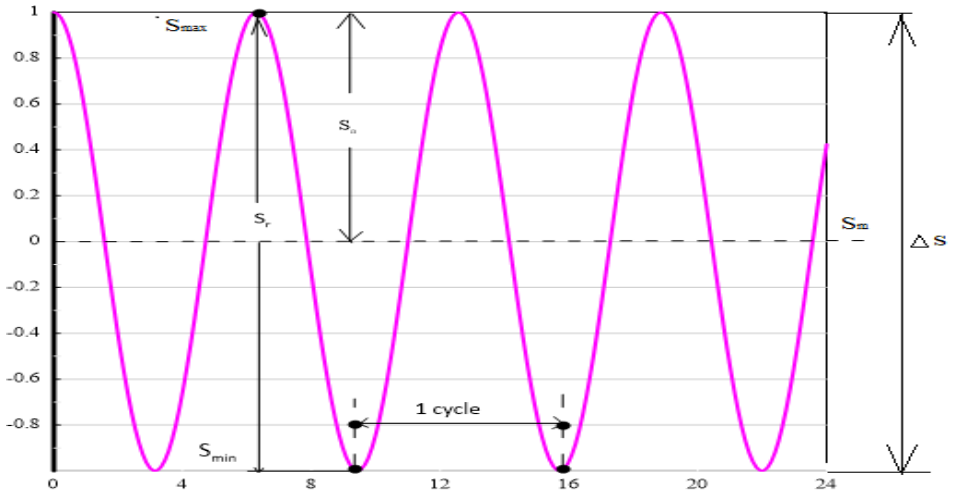

Figure 3.9: Characteristic stress levels of load cycle (reversed) [19].

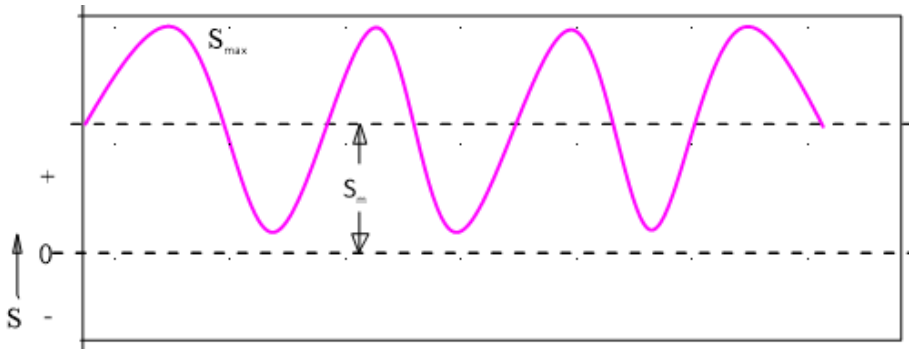

Figure 3.10: Tension-Tension with applied stress[19]

If fatigue has to be considered as part of the design analysis of a structure, it is well recognized that a stress cycle is characterized by a stress amplitude (S_a) and a mean stress (S_m), see *Figure 3.9*. Instead of S_a and S_m, a second equivalent definition is given by S_{max} and S_{min}, while a third one uses the stress range ΔS (= $2S_a$) together with the stress ratio R, defined as[19]

$$R = \frac{S_{min}}{S_{max}} \qquad 3.7$$

$$(A) = \frac{S_a}{S_m} = \frac{1-R}{1+R} \qquad 3.8$$

3.20 Stress Concentration Factor

In notch fatigue, the primary aim is to be able to anticipate fatigue behaviour of a material or parts with a stress concentration from smooth bar data. The majority of fatigue data available either is in the low cycle fatigue (LCF) regime or corresponds to fatigue lives below the endurance limit, if such a limit exists at all. The first aspect of addressing notch fatigue

resistance is to define the the notch's harshness or stress concentration. To do this, the stress concentration factor k_t employed. Here, $\boldsymbol{k_t}$ describe as the ratio of the peak stress at the root of a notch to the average stress over the net cross section[24]:

$$K_t = \frac{\text{Peak stress at notch root}}{\text{average stress over the net cross section}} \qquad 3.9$$

The stress concentration factor calculated from the results of a peak stress at notch root and average stress over the net cross section of the specimens shown on

Table 3.6.

Table 3.6: Stress concentration factor of notched specimen

Specimen diameter (mm)	Peak stress of Notched specimen (MPa)	Average stress of Smooth specimen (MPa)	K_t
7	661.35	290.92	2.273305
8	627.91	326.28	1.924451
9	675.29	356.28	1.895391
10	654.17	380.76	1.718064
11	653.43	426.93	1.530532

3.21 Fatigue notch Factor

It is clear that notches in components can lead to high cycle fatigue failures because they provide a localized area of stress concentration or stress raiser. Because of this, knowing how a notch affects FLS and being able to anticipate strength without considerable experimentation is critical. Another motivation for studying and modelling notch behaviour is that it reflects a situation in which stress gradients exist, with the highest tension at the notch root and the lowest stress below the notch.

Overall, the fatigue life and strength of a notched component are better due to tension at the notch root, as opposed to smooth bars that have the same load spread uniformly across their whole cross section. Researchers have long accepted the concept that fatigue behaviour is dependent on stress, or strains over a critical volume of material.

Since the notch is small, far-field loads or average stresses have the most impact on fatigue behaviour. The radius of the notch root also affects the fatigue limit significantly. For this reason, when tested, the nose roots will act as a smooth surface with no breaks. Increases in notched diameter have a greater impact on fatigue behaviour because the peak tension at the notched edge increases. These observations and experimental data collected and obtained for long period of time were used to generate equations for calculating the fatigue behaviour of a notched component using the fatigue behaviour of smooth bars.

The fatigue notch factor, which compares the fatigue strength of notched and un-notched bars, says that notched bars are superior (K_f)[24].

$$K_f = \frac{\text{unnotched fatigue limit stress}}{\text{notched fatigue limit stress}} \qquad 3.10$$

This equation defined, in the strictest sense, for fully reversed loading (R = -1) as well as for a specific number of cycles and a specific specimen geometry. The fatigue notch factor generally covers the range $1 < K_f < K_t$, indicating that use of K_t rather than K_f can be overly conservative to describe the notch sensitivity. An alternate quantity used to define the notch behaviour of a material is the notch sensitivity ($\boldsymbol{q}$) defined as[24].

$$q = \frac{K_f - 1}{K_t - 1} \qquad 3.11$$

Notch sensitivity for a material takes the range $0 < q < 1$. When q = 0, this represents a presence of a notch. When q = 1, this corresponds to $K_f = K_t$,notch material and notch geometry where $K_f = 1$, the case where material is insensitive to the sensitive and the behaviour governed exclusively by the local stress at root notch.

If a cycle with a stress amplitude S_a can create a micro crack in the un-notched specimen, the same cycle of the peak stress in the notched specimen (σ_{peak}) should also be capable to create micro crack at the root of the notch. If S_a in the un-notched specimen is the fatigue limit (S_{fl}) of that specimen, then S_{peak} in the notched specimen should correspond fatigue limit for notched specimen (S_{fk}). The similarity principle thus leads to[19]:Speak

$$S_{peak} = K_t S_{fk} = S_{fl} \text{ or } S_{fk} = S_{fl}/K_t \qquad 3.12$$

It implies that the fatigue limit of an un-notched specimen should be divided by K_t to obtain the fatigue limit of the notched specimen. However, it has been shown in numerous fatigue tests that the reduction factor is smaller than K_t . The reduction factor obtained by experiments is denoted by the symbol K_f. It implies that

$$S_{fk} = \frac{S_{f1}}{K_f} \qquad \text{or } K_f = \frac{S_{f1}}{S_{fk}} \tag{3.13}$$

There is a distinction between fatigue life and fatigue resistance (additionally known as limit of endurance), which is the level of stress in which failure is unlikely. The quantity of failure cycles increases when the stress reduced. Tensile strength in a static state improves with increasing fatigue strength. The two components of a fluctuating stress are the average stress (S_m) and the alternating stress S_a.

3.22 High cycle fatigue

A high amount of cycles ($N \geq 10^5$ cycles) and elastic applied stress characterize high-cycle fatigue. For most nonferrous metals, the test fatigue for high-cycle are routinely carried out for 10^7 cycles and occasionally 5×10^8 cycles nonferrous materials. High-cycle available data for fatigue are commonly displayed when plotting a stress (S_a), vs the life cycles to failure (N) according to Campbell, F [25],.The amount of cycles calculated using a logarithmic scale. The highest stress, S_{max}, lower stress, S_{min}, or the amplitude stress (S_a) are all possible values for stress. Typically, the S-N relationship is determined for a certain of the average stress, S_m value or either ratios R or A.

For ductile materials, as stated by Campbell, F [25] the test data usually fall closer to the Gerber parabolic curve; however, because of the scatter in fatigue data and the fact that notched data fall closer to the Goodman line. When it comes to real-world applications, the Goodman relationship comes in handy rather often. For more cautious Soderberg findings applied, if component design considering yield rather than ultimate strength, as is the most case. Mathematically, the three relationships expressed as:

$$\sigma_a = \sigma_e \left[1 - \left(\frac{\sigma_m}{\sigma_u}\right)^x\right] \tag{3.14}$$

For Goodman line x = 1 for the Gerber curve x = 2, and for the Soderberg curve $\sigma_u = \sigma_y$ while and σ_e is the fatigue limit for completely reversed bending.

3.23 Low cycle fatigue

Stress/strain are directly connected with cyclic loading in the elastic domain due to the elastic modulus. The responses are more complex and create a hysteresis loop when repeated loading produces plastic strains. The amplitude strain is constant throughout cycling load in the application of fatigue-control. Since plastic deformation is not completely reversible, the stress-strain response during cycling can change, largely depending on the initial condition of the metal. The metal can either undergo cyclic strain hardening, cyclic strain softening, or remain stable.

Also, the following expression for Goodman, Soderberg and Gerber used

$$\text{Goodman} \qquad \sigma_a = \sigma_e \left[1\text{-} \left(\frac{\sigma_m}{\sigma_u}\right)\right] \qquad 3.15$$

$$\text{Solderberg} \qquad \sigma_a = \sigma_e \left[1 - \left(\frac{\sigma_m}{\sigma_y}\right)\right] \qquad 3.16$$

$$\text{Gerber} \qquad \sigma_a = \sigma_e \left[1 - \left(\frac{\sigma_m}{\sigma_u}\right)^2\right] \qquad 3.17$$

From the results of the rough and smooth specimens the relative deviation (Rd) expressed as;

$$\text{Relative deviatio} \quad Rd = \left(\frac{\text{mean deviation}}{\text{mean}}\right) \times 100\% \qquad 3.18$$

$$\text{deviation} \quad d = \text{individual sample}(X) - \overline{X} \qquad 3.19$$

$$\text{Mean} \quad \overline{X} = \frac{\sum X}{n} \qquad 3.20$$

$$\text{Mean deviation Md} = \frac{\sum d}{n} \qquad 3.21$$

3.24 Probability density function

The link between observations and their probability is known as probability density. Some random variable outcomes will have a low probability density, while others will have a high probability density. A probability density function is used to determine probabilities for individual outcomes of a random variable, and a probability distribution is the overall form of the probability density (PDF). Knowing the probability density function for a sample of data can help you determine whether a given observation is likely or unlikely enough to be considered an outlier or anomaly, and whether it should be deleted. It's also useful for selecting acceptable learning methods that require specific probability distributions in the input data. The expression for calculating PDF is given as;

$$f_X(x) = \frac{P(x < X \leq x + \Delta)}{\Delta} \qquad 3.22$$

The function $f_X(x)$ gives the probability density at point$x$. It is a limit of the probability interval$(x, x + \Delta)$ divided by the length of the interval as the interval goes to zero (0)

$$P(x < X \leq x + \Delta = F_X(x + \Delta) - F_X(x) \qquad 3.23$$

So that

$$\begin{aligned} f_X(x) &= \lim_{\Delta \to 0} F_X(x + \Delta) - F_X(x) \\ &= \frac{dF_X(x)}{dx} = F'_X(x) \end{aligned} \qquad 3.24$$

If $f_X(x)$ is differentiable at x

3.25 Failure Rate

The anticipated number of occasions on which a certain item will fail during a particular period is known as the failure rate (Fr). A computed value is used to assess a product's level of reliability. Failure rate under this analysis is due to applied load to the components that generate the stresses lead to failure of materials. The expression for determining Fr is calculated as;

$$Z(t) = \lim_{\Delta \to 0} \frac{Pr(t < T \leq t + \Delta t | T > t)}{\Delta t} \qquad 3.25$$

$$\lim_{\Delta \to 0} \frac{F\big((t + \Delta t) - F(t)\big)}{\Delta t} \times \frac{1}{R(t)} = \frac{f(t)}{R(t)}$$

Since Δt is small, then the expression obtained as;

$$Pr(t < T \leq t + \Delta t | T > t \approx Z(t).\Delta t \qquad 3.26$$

3.26 Cumulative density function

A function that gives the probability that a random variable is less than or equal to the independent variable of the function.

The cumulative density function (CDF) of random variable X defined with the expression as;

$$F_X(x) = P(X \leq x) \qquad 3.27$$

For all $x \in \mathbb{R}$.The, subscript X indicate that, this is the CDF of the random variable. In addition, CDF defined for all $x \in \mathbb{R}$

Chapter 4. Results and Discussion

The analysis for investigating fatigue axle failure performed using ANSYS workbench software. The results obtained in ANSYS workbench software validated with experimental results obtained in literature review. The investigation of strength of the materials carried out by simulating small test piece and full-scale test piece. Small-scale test performed on notched and smooth specimens for the aim of estimation of fatigue limits of the materials on reduced test piece. These small- scale specimens used for determining the impact of notched materials that used to manufacture the axle in agreement with security coefficient (q) as mentioned in the design standard EN 13103[26] and EN 13104[27]. For experimental purpose, for RfL and RfE specimens, it is recommended to use more than 15 test pieces of 10mm diameter for 10^7 cycle for a non-probability of 50%. For simulation purpose the size of specimens for both RfL and RfE performed by using specimens, which is less, equal and greater than 10mm diameter, that are used in experimental investigation. These sizes of specimens are taken by varying the size from 7mm diameter to 11.5mm diameter as shown on Table 4.1and Table 4.2 respectively.

4.1 Obtained Results of small-scale specimens

Table 4.1: Results of Notched (Rough) specimens of a railway axle

Diameter d(mm)	Fmax (N)	Maximum simulated stress (σ_{smax}) MPa	Minimum simulated stress (σ_{smax}) MPa	Variation ($\sigma_{smax} - \sigma_c$) MPa
7.0	21169.2	661.35	67.84	111.35
7.5	24301.4	659.5	77.88	109.5
8.0	27649.6	627.63	88.61	107.63
8.5	31213.8	681.45	101.25	131.45
9.0	34994.0	675.29	113.52	125.29
9.5	38990.3	668.61	126.48	118.61
10.0	43202.5	654.9	140.17	122.9
10.5	47630.8	658.55	154.51	108.55
11.0	52275.0	653.43	169.57	103.43
11.5	57135.3	649.19	185.34	99.19

Table 4.2: Results of un-notched (smooth) specimens of railway axle

Diameter d(mm)	Fmax (N)	Maximum simulated stress (σ_{smax}) MPa	Minimum simulated stress (σ_{smax}) MPa	Variation ($\sigma_{smax} - \sigma_c$) MPa
7.0	21169.2	556.82	68.02	6.82
7.5	24301.4	557.01	78.09	7.01
8.0	27649.6	557.13	88.85	7.13
8.5	31213.8	557.74	101.34	7.14
9.0	34994.0	557.9	113.61	7.9
9.5	38990.3	559.64	126.59	9.64
10.0	43202.5	559.92	140.27	9.92
10.5	47630.8	562.02	154.64	12.02
11.0	52275.0	562.57	169.72	12.57
11.5	57135.3	564.97	185.5	14.97

The stress amplitude and mean stress, which are calculated from maximum and minimum stress of small-scale specimens, is shown on Table 4.3 and Table 4.4. These stress amplitude or mean stress are used to determine the life cycles of the materials.

Table 4.3: Stress amplitude calculated from data obtained in ANSYS simulation of specimens

Diameter d(mm)	Maximum simulated stress (S_{max}) MPa	Minimum simulated stress (S_{min}) MPa	S_r ($S_{max} - S_{min}$)	S_a $\left(\frac{S_r}{2}\right)$
7.0	556.82	68.02	488.8	244.4
7.5	557.01	78.09	478.92	239.46
8.0	557.13	88.85	468.28	234.14
8.5	557.74	101.34	456.4	228.2
9.0	557.9	113.61	444.29	222.145
9.5	559.64	126.59	433.05	216.525
10.0	559.92	140.27	419.65	209.825
10.5	562.02	154.64	407.38	203.69
11.0	562.57	169.72	392.85	196.425
11.5	564.97	185.5	379.47	189.735

Table 4.4: Mean stress calculated from S_{max} and S_{min}

Diameter $d(mm)$	S_{max} (Mpa)	S_{min}(MPa)	$S_m = \frac{S_{max} + S_{min}}{2}$ (MPa)
7.0	556.82	68.02	312.42
7.5	557.01	78.09	317.55
8.0	557.13	88.85	322.99
8.5	557.74	101.34	329.54
9.0	557.9	113.61	335.755
9.5	559.64	126.59	343.115
10.0	559.92	140.27	350.095
10.5	562.02	154.64	358.33
11.0	562.57	169.72	366.145
11.5	564.97	185.5	375.235

Table 4.5: Relative deviation of axle specimens

Diameter(mm)	7	8.0	9.0	9.5	10	10.5	11.0	11.5	Rd (%)
S_{max} (Rough) MPa	661.35	627.63	675.29	675.29	654.9	658.55	653.43	649.19	1.42
S_{max}(Smooth) MPa	556.82	557.13	557.9	559.64	559.92	562.02	562.57	564.97	0.36

The simulation on the full test piece was to verify the geometry of the full size of railway axle model made, to relate to the final physical product to manufacture. The maximum stress and factor of safety as found in ANSYS are shown on Table 4.6.

Table 4.6: simulation stress amplitude and safety of factor K_t.

Axle type (EA1N)	Axle load	$S_{max}(MPa)$	K_t
Non-powered axle	25tons	86.669	4.19
Non-powered axle	30tons	103.98	3.4927
Non-powered	35 tons	121.3	2.994

4.2 Fatigue stress verification Results

The maximum allowable stresses for solid axles shown in the Table 4.7. Minimal value of safety coefficient S is in accordance with standard EN 13104 equal 1.2 and for driven axle is higher because of torsion, vibrations, and dynamic forces and so on.

Table 4.7: Values of permissible stresses that can be used in strength calculations of the railway axle[6].

Axle Type	S	F1-fatigue on the free surface $F1 = 200\ MPa$	F3-fatigue in fitting part $F3 = 120\ MPa$
Non-powered (EN 13103)	1.2	166	100
Powered axle (EN 13104	1.5	133	80
Other parts in (EN 13104)	1.3	154	92

4.3 Damage verification

The damage results of the railway axle model from nCode simulation shown in

Appendix F. The damage values of the axle is due to increasing or decreasing of fatigue stresses. These stresses and damage compared with experimental results from literature review[5].

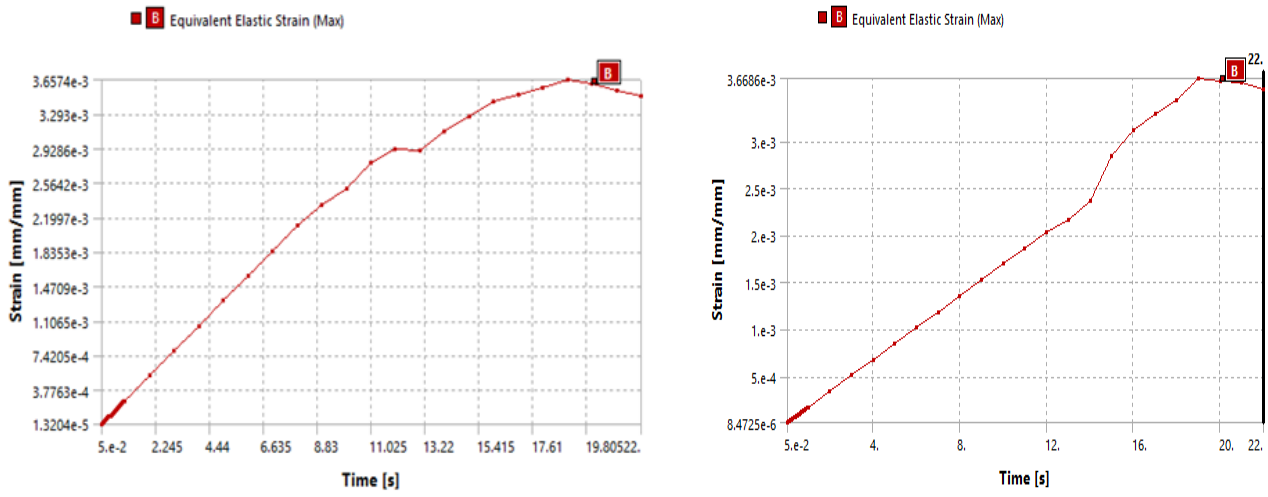

(a) (b)

Figure 4.1: Strain-Time graph notched axle specimen, (a) 8mm diameter, and (b) 10mm diameter

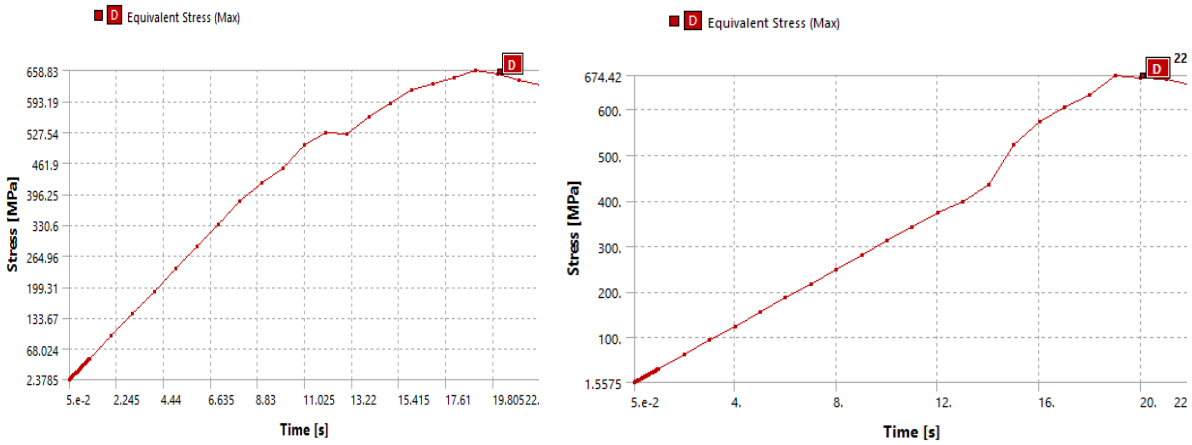

(a) **(b)**

Figure 4.2: Stress-Time graph notched axle specimen, (a) 8mm diameter, and (b) 10mm diameter

Under constant strain Figure 4.1, stress is a time-dependent decrease in stress. The material's characteristic behaviour is investigated by applying a constant amount of deformation to a specimen and measuring the load required to maintain it over time. Figure 4.2 illustrates a typical stress-time curve. At the start of the experiment, a constant rate of strain is applied to the specimen to achieve the desired elongation Figure 4.3. Once the specimen has reached the desired elongation, the strain is maintained constant for a predetermined time. The stress values are recorded at various time intervals and the results are plotted to produce a stress versus time curve.

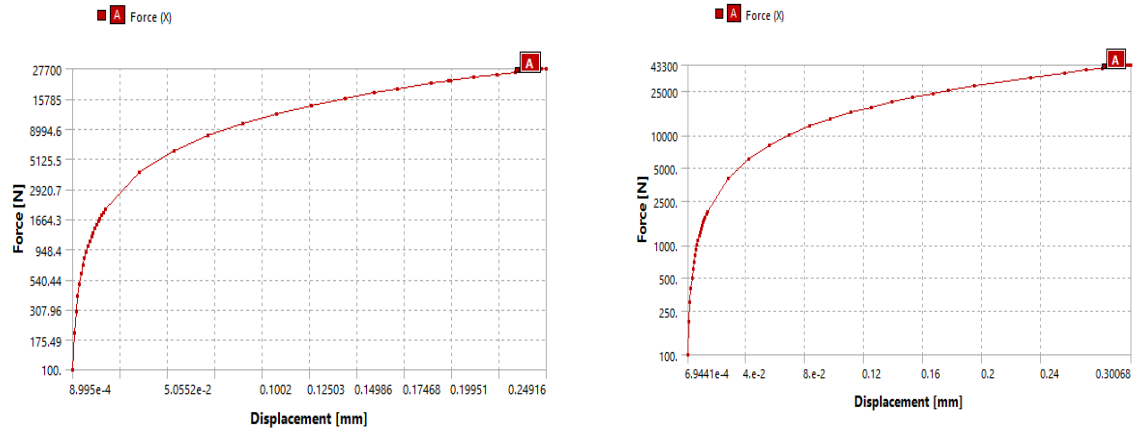

(a) (b)

Figure 4.3: Force-Displacement graph notched axle specimen, (a) 8mm diameter, and (b) 10mm diameter

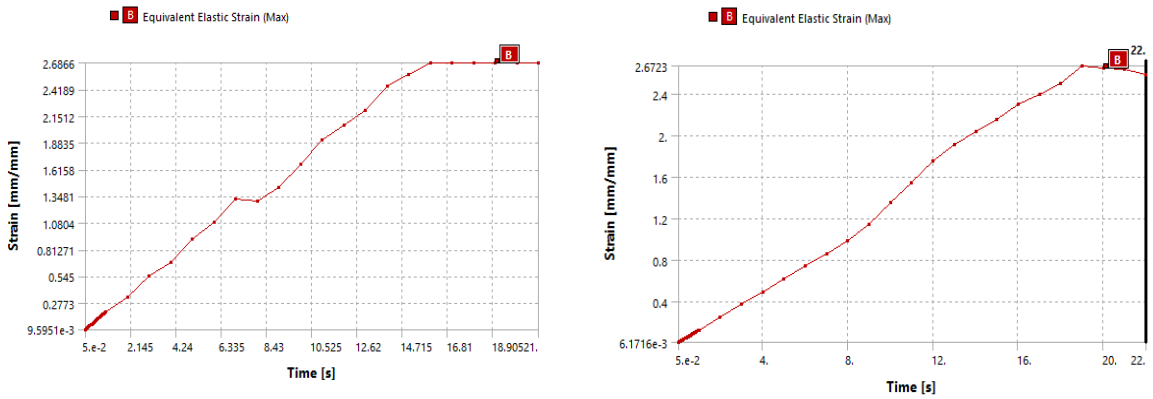

(a) **(b)**

Figure 4.4: Strain/Time graph of axle smooth specimen, (a) 8mm diameter, (b) 10mm diameter

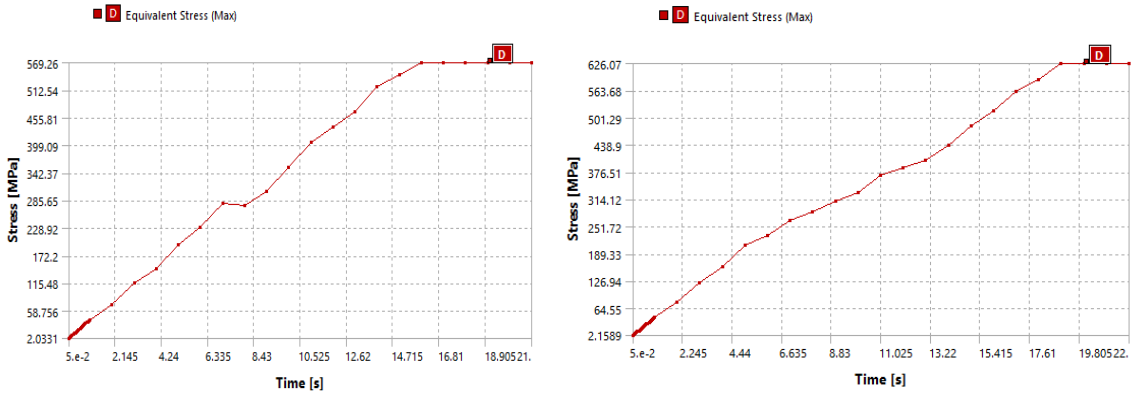

(a) **(b)**

Figure 4.5: Stress-Time graph smooth axle smooth specimens, 8mm and 10mm diameter

Tensile Stress-Strain Relationship as in Figure 4.6and Figure 4.7, this test is the most frequently used method for determining mechanical properties. Round-bars are gripped at the ends and pulled at a constant velocity (or, more precisely, at a constant strain rate) until they break. The sample is loaded and displaced and the results are plotted as stress (load/cross-sectional area) vs strain (sample elongation/original length). The elastic region is linear and reversible, as defined by Hooke's law (= E, where E is an elastic constant known as Young's modulus). The point at which linearity is violated is referred to as the elastic limit, and it is at this point that permanent deformation, or plastic strain, begins. Due to the fact that deviations frequently occur gradually, a metal's " yield strength " is defined as the stress at 0.2 percent permanent (or

plastic) strain. Continued plastic flow beyond the elastic limit results in an increase in stress, a phenomenon known as work hardening. The sample deforms uniformly during this stage, elongating and thinning while maintaining its volume, until work hardening can no longer keep up with the increasing stress caused by the sample's cross-sectional area reduction. At this point, the stress reaches its maximum value, referred to as the ultimate tensile strength and the sample begins to deform irregularly, or neck, before ductile fracture occurs. Necking can occur because of “normal” or shear localization prior to fracture.

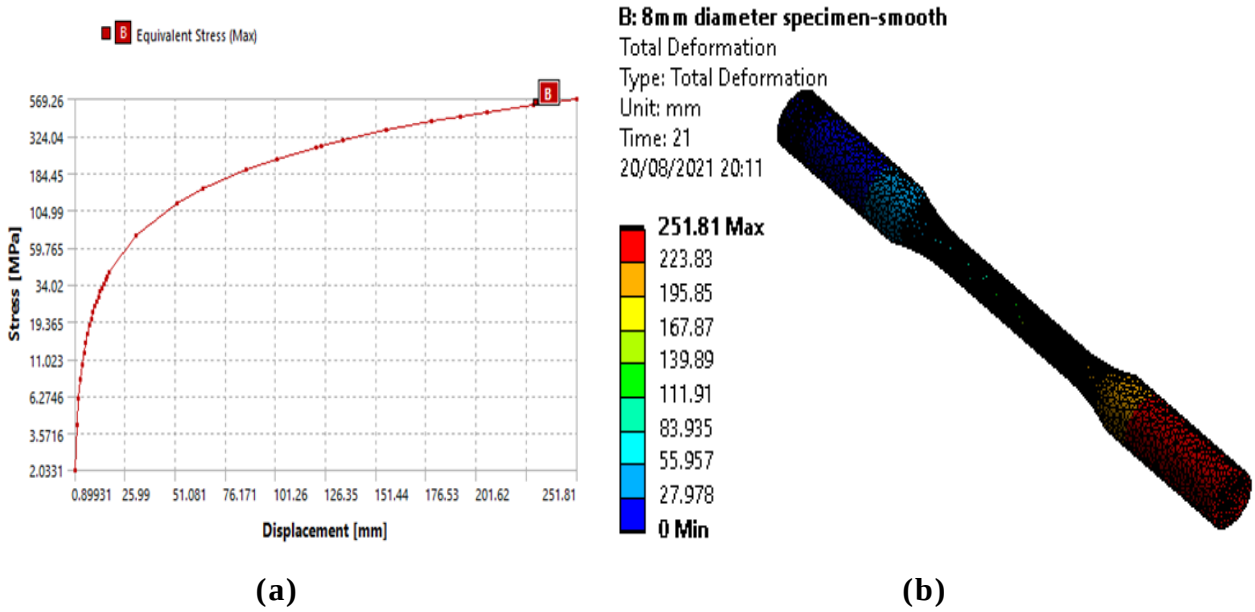

(a) **(b)**

Figure 4.6: 8mm diameter smooth specimen results, (a) Stress/displacement graph, (b) Displacement

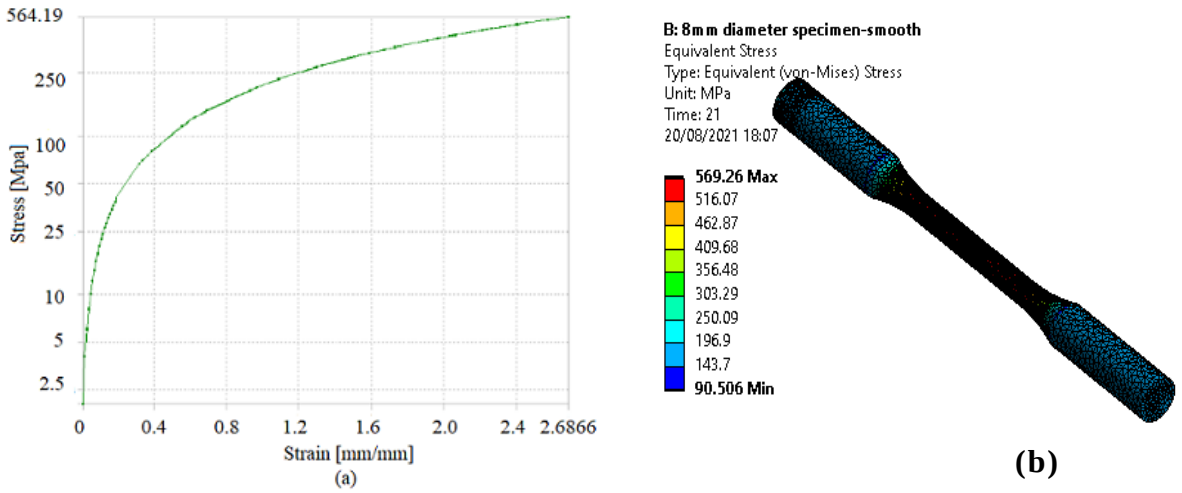

(b)

Figure 4.7: 8mm diameter smooth specimen results, (a) Stress/Strain graph (b) Stress result

4.3.1 Rough specimens

The tension simulation of the railway axle specimens carried out in ANSYS Workbench. The minimum and maximum stress of different size of the tested notched (rough) specimens indicated on Table 4.1. There is a variation between the simulated stress and calculated stress due to the maximum load (ultimate load) applied to each specimen. In addition, it observed that the value of the maximum stress of the simulation is varying. For example, the maximum stress of the specimen of diameter 7mm, 7.5mm, 8mm, 10mm and 11.5mm are 661.5MPa, 659.5MPa, 657.63MPa, 672.9MPa and 649.19MPa respectively. In case of strain or deformation, the rough specimens observed that there is a little strain and deformation before reaching the maximum stress. The simulation results of all notched and smooth specimens are indicated from Appendix H to Appendix L

4.4 Smooth specimen

For smooth specimen the same tension simulation in carried out in ANSYS workbench as simulation results of all specimens indicated from Appendix M to Appendix Q. The maximum stress observed during the simulation analysis Table 4.2 shows the small variation between tested sizes of the railway axle specimens.

The analysis of specimens in ANSYS workbench connected to nCode. After static analysis in the ANSYS Workbench, the fatigue analysis of the specimens carried out in nCode software. Due to application of maximum load or ultimate load the specimens in nCode software, it observed that the specimens fail due to static load Figure 4.8 and Figure 4.9 shows the damage failure and stress failure of the materials.

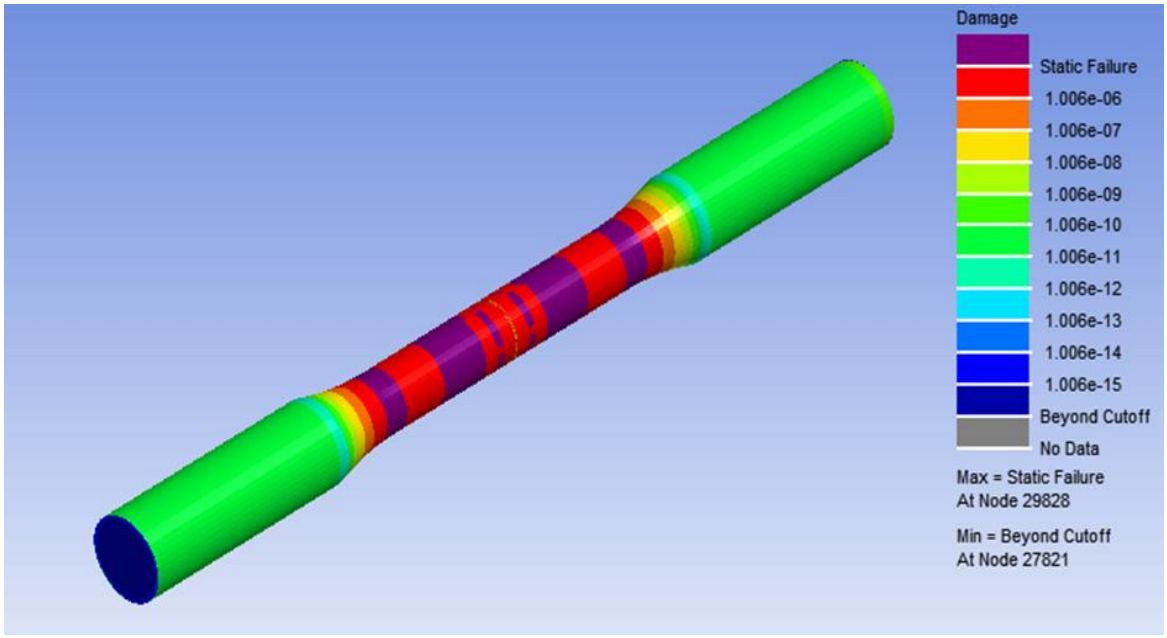

Figure 4.8: Static damage failure of a rough railway axle specimen (nCode Software)

In that case let us consider the yield load (F_e) to be applied to the specimens. The yield load as given by;

$$\mathbf{F_e = R_e \times A_o} \qquad 4.1$$

Two specimen of 10mm diameter and 8mm diameter smooth and rough tested in ANSYS Workbench by applying F_e for tension test of the railway axle specimens.

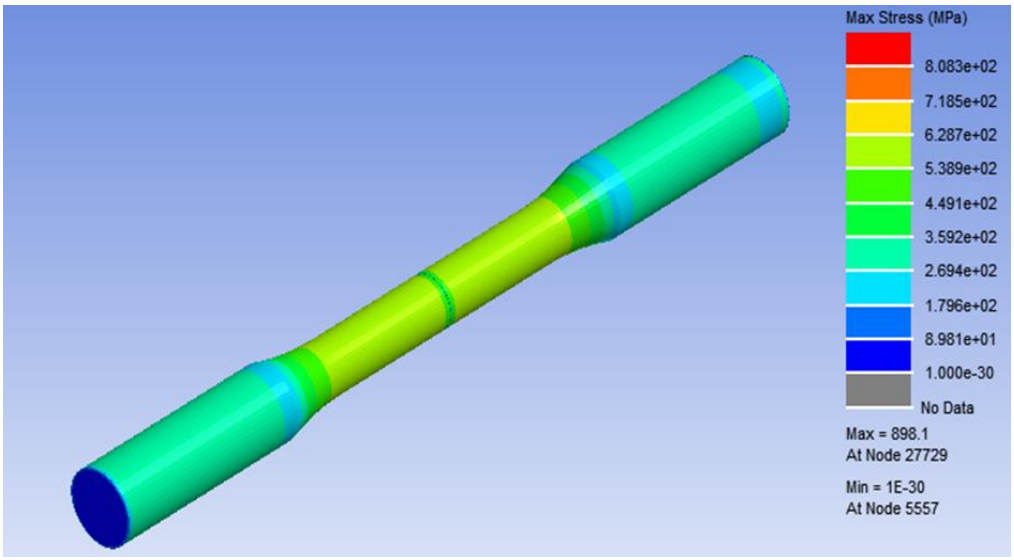

Figure 4.9: Fatigue stress of a rough railway axle specimen

In addition, in nCode software for fatigue analysis. Table 4.8 and

Table 4.9 is a result of tested rough and smooth specimens in ANSYS Workbench. Static analysis in Ansys workbench carried out by applying load F_e on a specimens and the results are show on Figure 4.10. Then the model carried in nCode simulation as Figure 4.11 and Figure 4.12 shows 8mm diameter rough specimen fatigue damage and fatigue stress results respectively due to nCode simulations.

Table 4.8: Results of rough specimens (ANSYS Workbench Simulation)

Diameter d(mm)	F_e(N)	Maximum simulated stress (σ_{smax}) MPa	Minimum simulated stress (σ_{smin}) MPa	Variation ($\sigma_{smax} - \sigma_c$) (MPa)
8.0	16087.04	382.62	51.554	62.62
10.0	25136	391.5	81.552	71.5

Table 4.9: Results of smooth specimens (ANSYS Workbench Simulation)

Diameter d(mm)	F_e(N)	Maximum simulated stress (σ_{smax}) MPa	Minimum simulated stress (σ_{smin}) MPa	Variation $\sigma_{smax} - \sigma_c$ (MPa)
8.0	16087.04	324.16	0.0017	4.16
10.0	25136	361.77	0.0026	41.77

(a) **(b)**

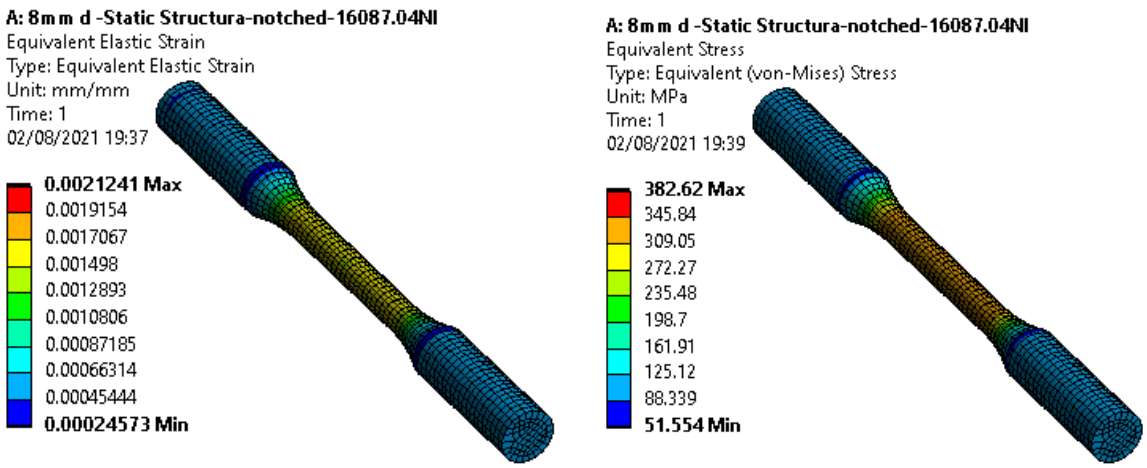

(c) **(d)**

Figure 4.10:Specimen simulation,(a) mesh,(b) Fixed support, applied load (c) Strain (d) Stress

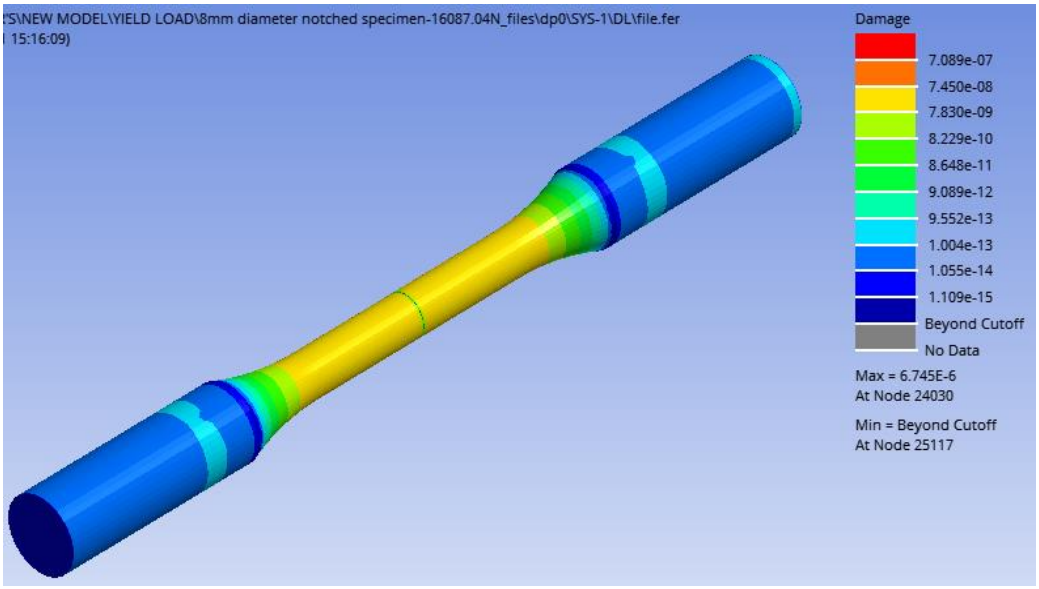

Figure 4.11: 8mm diameter fatigue damage of railway axle notched specimen materials

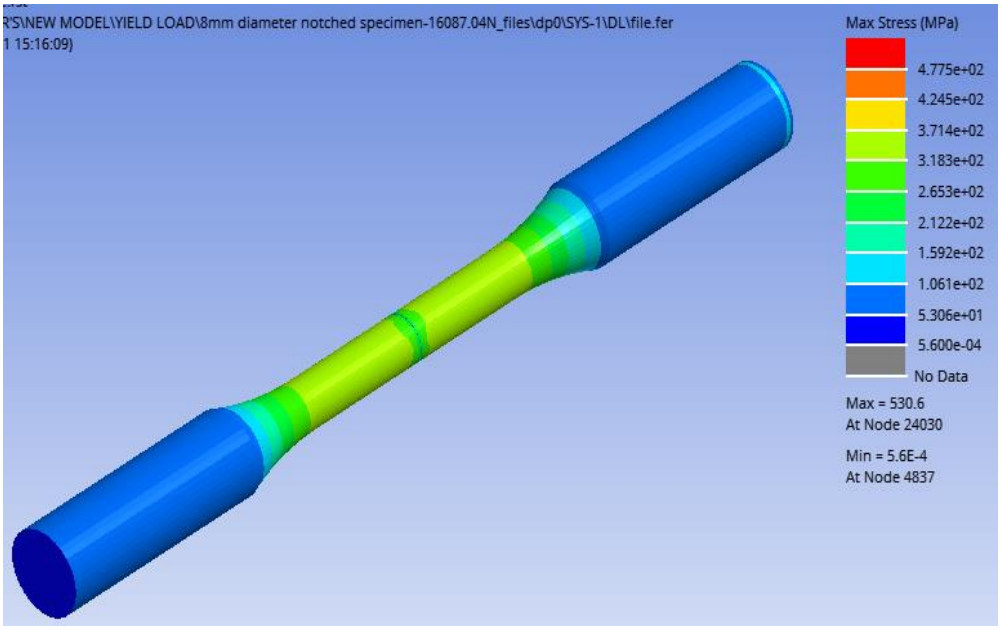

Figure 4.12: 8mm diameter fatigue stresses of railway axle notched specimen materials

The results indicate that, bellow yield point, materials is resistant to static load. Figure 4.13(a) graph shows the results of stress against life, Figure 4.13(b) is a graph showing damage against stress of the railway axle specimen of 10mm diameter in nCode simulation.

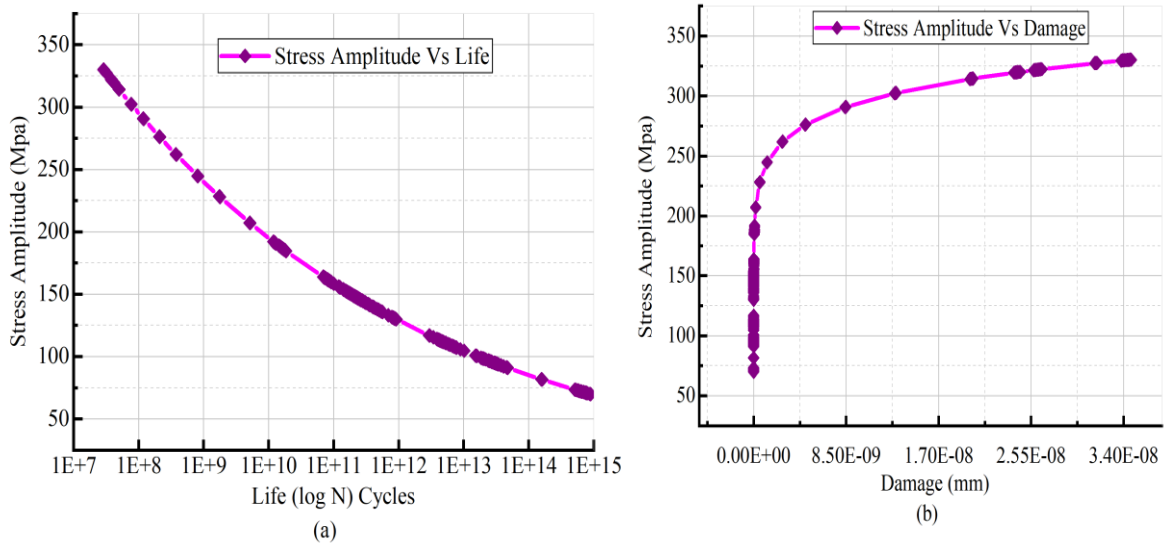

Figure 4.13: nCode simulation results graphs, (a) stress amplitude Vs life, (b) Damage Vs Stress amplitude

4.4.1 Full-scale axle mode results

Table 4.10: Axle results of the axle models

Axle load	S_{max}(MPa)	S_{min}(MPa)	life	Damage	K_f
25tons	86.669	0.00796	1e11	0.0001	4.19
30tons	103.98	0.01279	1e11	0.0001	3.4927
35 tons	121.3	0.01189	1e11	0.0001	2.994

4.5 Full Scale Fatigue Analysis

Verification of the fatigue characteristics is essential in order to have a correctly dimension of axle. To achieve proper and satisfactory performance of an axle in service these characteristics is required.

Figure 3.5 shows a full-scale model analysis performed in ANSYS workbench Table 4.10 and Error! Reference source not found. illustrate the simulation results of the railway axle model. The limits calculated on full-size test pieces to validate the features of axle fatigue are consistent with those used to derive the maximum allowed stresses in accordance with EN 13103 and EN 13104 [26], [27]. The fatigue limit values for steel grade EAIN utilized in the design process are as follows:

- $200 N/mm^2$ Outside the fitting and $120 N/mm^2$ beneath the fitting for solid axle.
- $200\ N/mm^2$ Outside the fitting, $110\ N/mm^2$ beneath the fitting, except the journal; $94\ N/mm^2$ beneath the fitting on the journal; $80\ N/mm^2$ for the surface of the bore for hollow axle.

To obtain maximum permissible stress according to EN 13103 for non-powered axle, the fatigue limits have to be divided by the security coefficient value S. Table 4.11 indicate Maximum permissible stresses for solid axles of steel grade EA1N.Figure 4.14 indicate the transition areas between journal and collar bearing surface, collar bearing surface and wheel seat.

Table 4.11: Maximum permissible stresses for solid axles of steel grade EA1N[26]

Security coefficient - a S	Zone 1-b N/mm^2	Zone 2-c N/mm^2
1,2	166	100

Key

a- minimum value

b- Zone 1: axle body, plain-bearing seats, fillets

c- Zone 2: wheel seats, brake disc seats, rolling bearing seats, collar surface Table 4.11

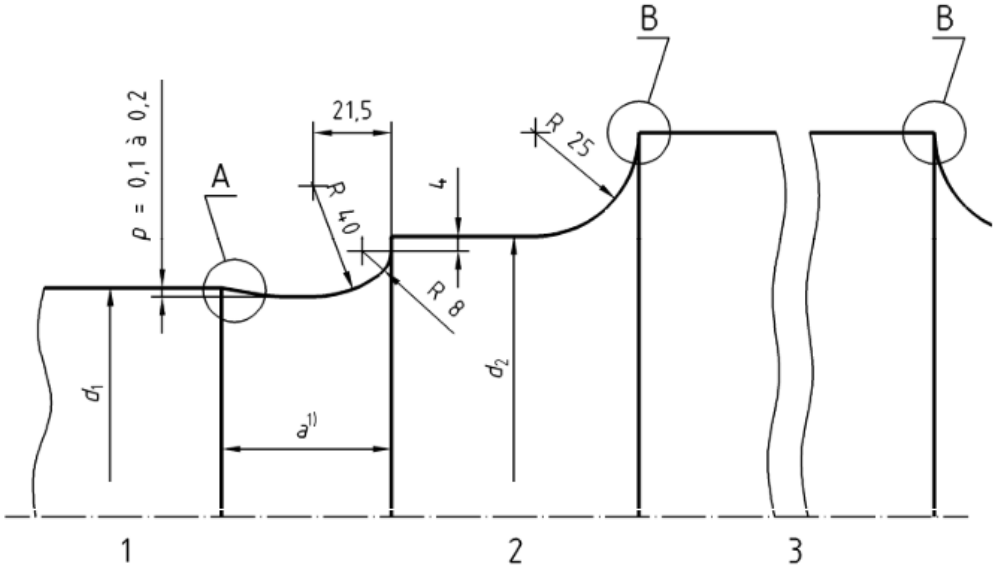

Figure 4.14: Transition areas between journal and collar bearing surface, collar bearing surface and wheel seat[26]

In Figure 4.14, 1-is a journal, 2-is a collar bearing surface and 3-is a wheel seat. In the analysis carried out in ANSYS workbench of the full axle model, by considering three types different weight. The values of this axle weight are 25tons, 30tons and 35tons for the axle load. As mentioned earlier, two cases of analysis, the first is to apply the force on both sides and the second to apply the load in the middle of the railway axle. The results obtained for axle weight of 25tons, 30tons and 35tons in terms of stresses are 86.66Mpa, 103.98 and 121.3Mpa respectively for the first case, while in the second case the results obtained are 86.49Mpa, 103.5Mpa and 120.62Mpa respectively.

After conducting an analysis on ANSYS workbench, also an analysis has been done on nCode to determine fatigue stresses, life and damage. In nCode the results obtained are as follows, stress 170.6Mpa, damage 2.253×10^{-11} and life cycles of 4.438×10^{10}. These results were compared to those acquired from experimental findings, which available in literature and standards set internationally. Although the stress obtained from simulations is less to compare with the results sought in the publications after tests and internationally set standards, materials

observed that, it is strong enough to withstand fatigue. This is because the life of the materials in case of fatigue obtained due to this maximum stress is (4.438×10^{10}), greater than 10^7 which is the recommended life cycle of the test materials to survival.

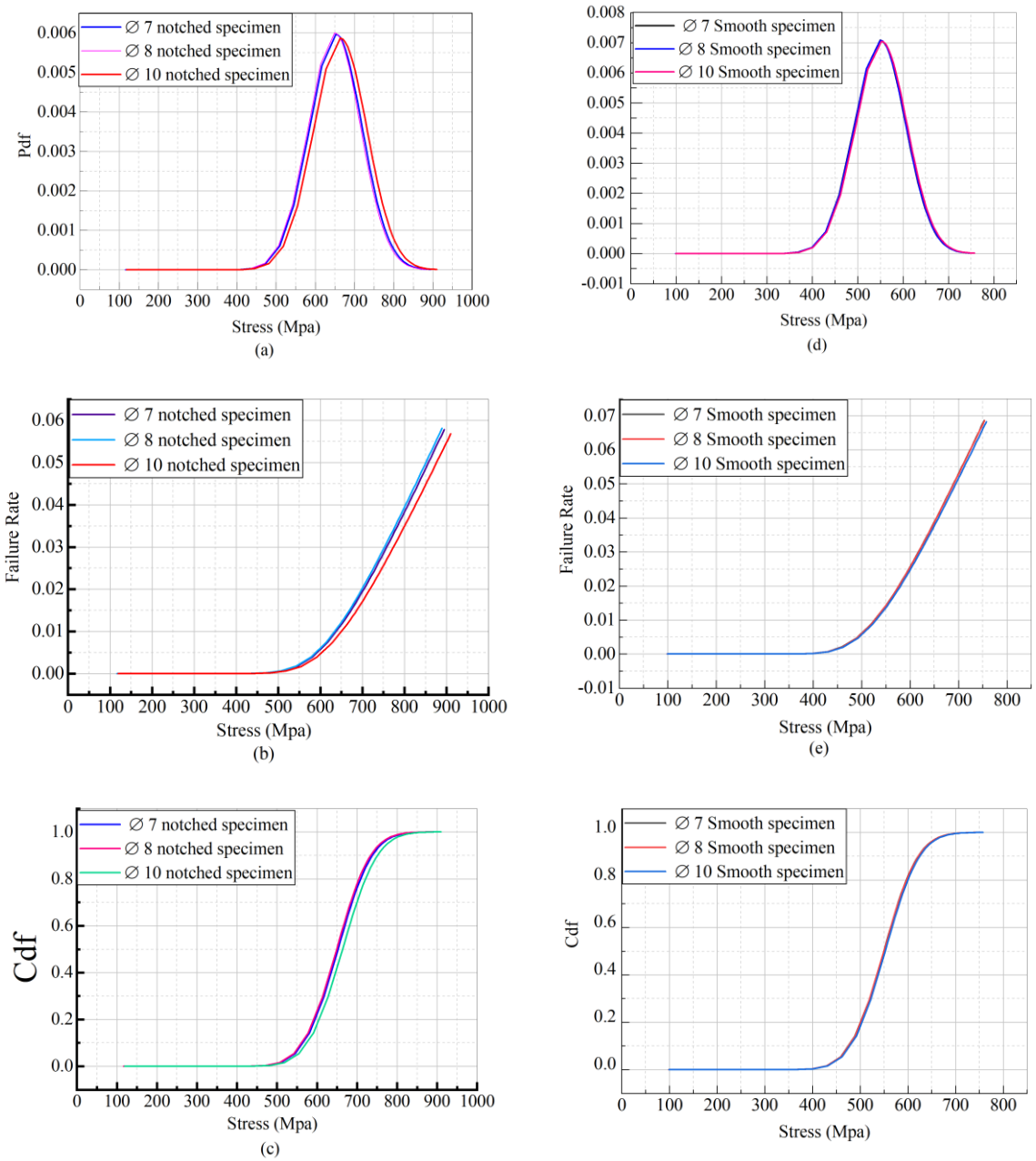

Figure 4.15: Probability density function, failure rate and cumulative density function against stress of a notched and smooth specimen's analysis

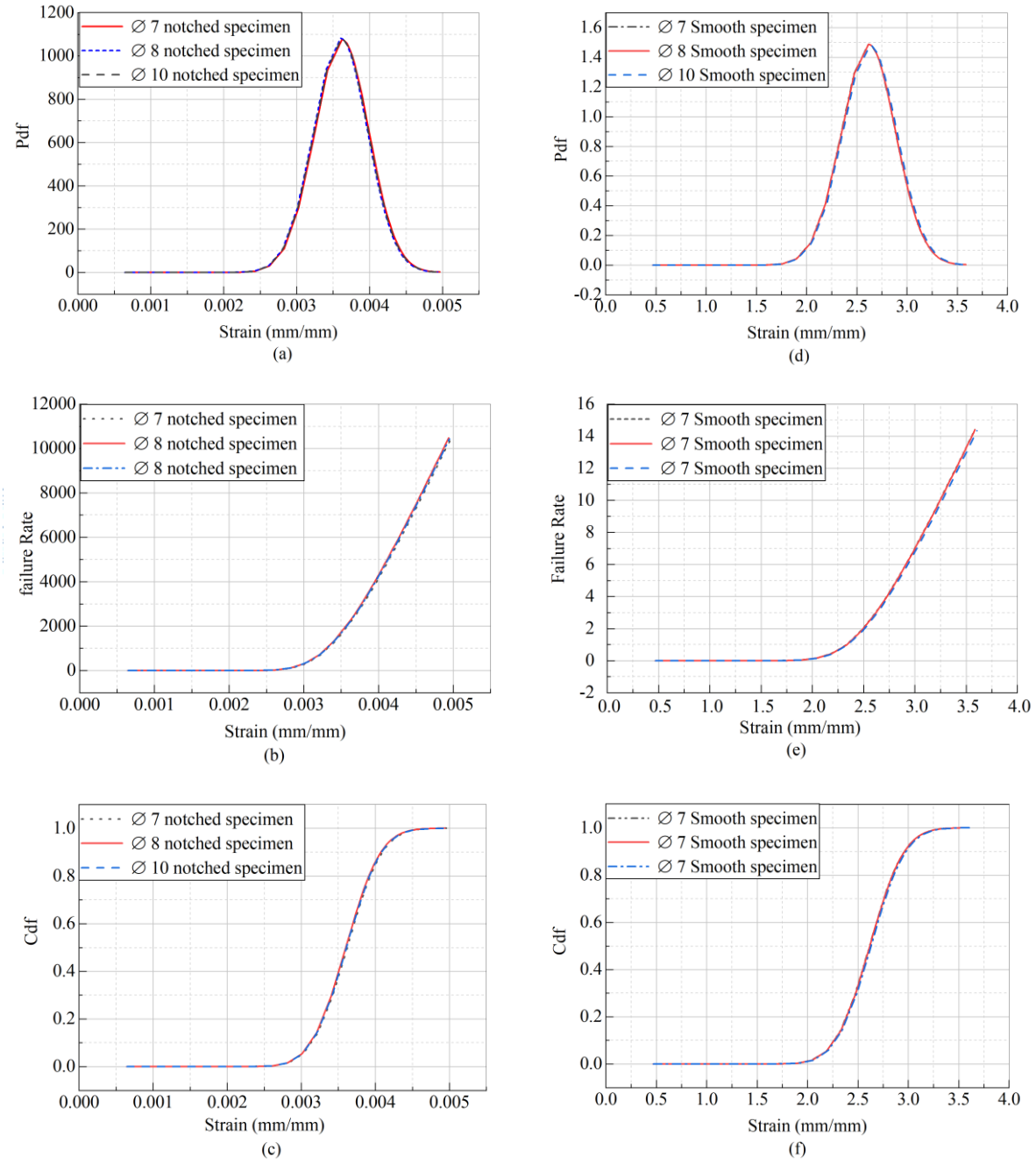

Figure 4.16: Probability density function, failure rate and cumulative density function against strain of a notched and smooth specimen's analysis

For Cdf the horizontal axis is the allowable domain for the given probability function. Since the vertical axis is a probability, it must fall between zero and one. It increases from zero to one as we go from left to right on the horizontal axis. The percent point function (ppf) is the inverse of the cumulative distribution function. For this reason, the percent point function is also commonly referred to as the inverse distribution function. That is, for a distribution function we calculate the probability that the variable is less than or equal to x for a given x as on Figure 4.16.

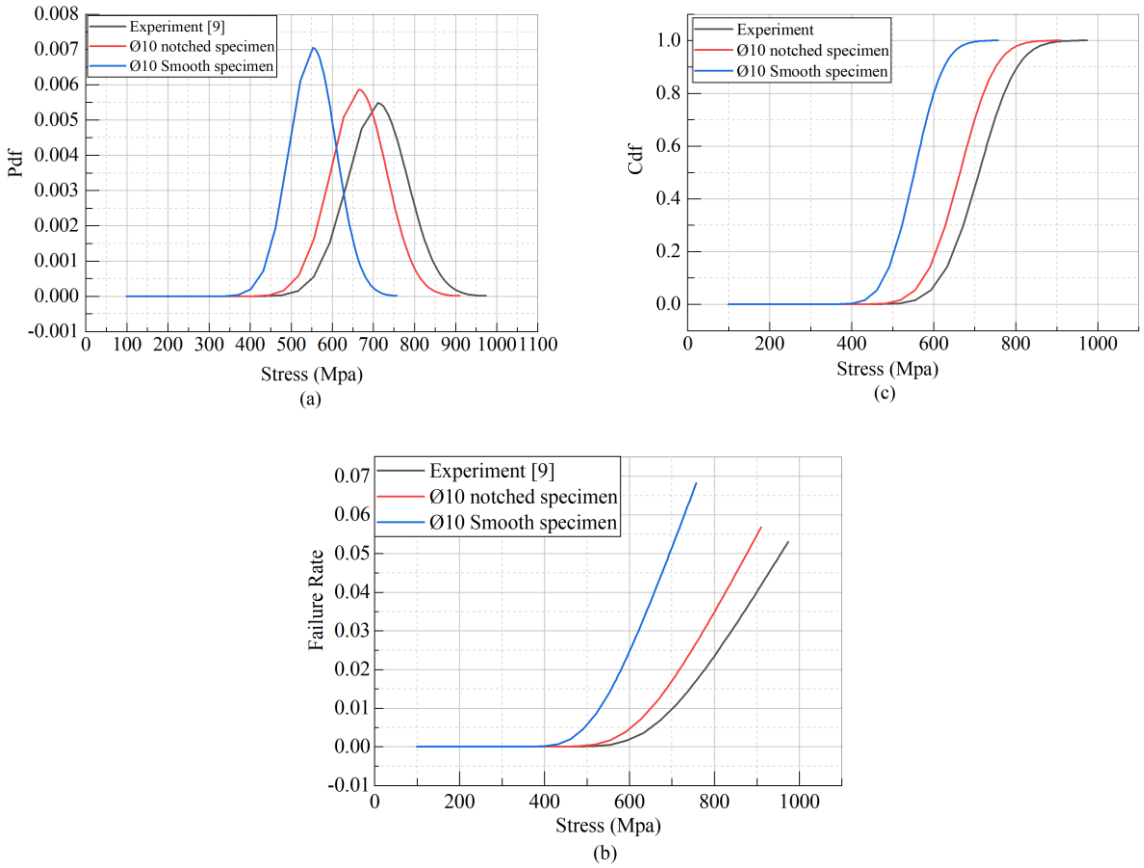

Figure 4.17: Comparing the Probability density function, failure rate and cumulative density function against stress of an experiment specimen and simulation specimen

Figure 4.17 (a), (b) and (c) is a comparison Probability density function, failure rate and cumulative density function against stress of an experiment specimen and simulation specimen. The results indicate that the simulation and experimental results from the literature review have relationship although there are some different variation in terms of the values.

Conclusion and Recommendations

4.6 Conclusion

In this investigation of fatigue failure of a railway axle, it was discovered some of few basic variables that cause fatigue. The following are the three essential variables that induce fatigue and must be considered:

- a sufficiently high maximum tensile stress,
- a sufficiently big variation or fluctuation in the applied stress, and
- a sufficiently many cycles of the applied stress.

There are many types of fluctuating stresses. Among the more common types encountered are displayed in Figure 3.9. A fully reversed stress cycle, where the highest and lowest stress levels are equal, is among the popular commonly used in testing. Another common stress cycle is repeating stress cycle, in which a mean stress ($\mathbf{S_m}$) applied on top of the maximum the same as to minimum stress. Figure 3.10 shows the condition where both stresses (cyclic and applied) are tensile (greater than zero).

Before the materials used for fatigue design, it is important to carryout static analysis. The materials must have high strength to resist static loading because there exists relation between resistance of the materials under static and fatigue. When the given material properties fail due to static loading, obviously not applicable for fatigue design because the life cycle will depend only static application and not the fatigue load. This analysis verified by nCode as shown on Figure 4.8, which indicate failure of materials under static. This ensures that the abilityof axle to withstand fatigue without fail should be designed below the yield point. Above yield point, materials begin to fail due to static loading. In this thesis the finding using FEM indicate that the axle damage occur because of improper design. The improper railway axle design include;

- Improper selection of materials that can resist fatigue load
- Improper fatigue load that the axle can carry it.
- Axle Geometry that cause high stress concentration, especially the radii at the bearing area, wheel seat or gear seat.

However, the axle in fail due to initiation of cracks and cracks growth. These sources of these cracks can be overloading the axle, Scratch and corrosion that can initiate the crack.

4.7 Recommendations

In this analysis using the FEM (ANSYS workbench linked to nCode together), it was found that the materials used to make the railway axle are strong. Analysis was performed for small-scale specimens and full-scale specimen. However, although the materials used to make the railway axles show that they are strong, there are still reports showing the failure of the axles in use. Moreover, the failure of the axle as stated are caused due to present and growth of the cracks. In this case, to prevent failure of the railway axle when in use it is important to conduct more research in the following areas

- Practical investigation of a new materials that are used for railway axle manufacturing
- Investigation of any cracks sources of railway axle when it is in use
- Conducting experimental research on the railway axle after it has been used for a certain interval of time.

References

[1] S. Beretta, M. Carboni, and D. Regazzi, ‘Load interaction effects in propagation lifetime and inspections of railway axles’, *Int. J. Fatigue*, vol. 91, pp. 423–433, 2016, doi: 10.1016/j.ijfatigue.2016.03.009.

[2] S. Executive and R. Court, ‘Railway axle failure investigations and fatigue crack growth monitoring of an axle’, vol. 218, no. March 1996, pp. 283–292, 2004.

[3] P. Hutar and P. Pokorny, ‘Residual fatigue lifetime estimation of railway axles for various loading spectra’, vol. 82, pp. 25–32, 2016, doi: 10.1016/j.tafmec.2015.06.007.

[4] C. Zhu, J. He, J. Peng, Y. Ren, and X. Lin, ‘Failure mechanism analysis on railway wheel shaft of power locomotive’, *Eng. Fail. Anal.*, vol. 104, no. May, pp. 25–38, 2019, doi: 10.1016/j.engfailanal.2019.05.013.

[5] S. Beretta, A. Ghidini, and F. Lombardo, ‘Fracture mechanics and scale effects in the fatigue of railway axles’, *Eng. Fract. Mech.*, vol. 72, no. 2, pp. 195–208, 2005, doi: 10.1016/j.engfracmech.2003.12.011.

[6] M. Novosad, R. Fajkoš, B. Řeha, and R. Řezníček, ‘Fatigue tests of railway axles’, *Procedia Eng.*, vol. 2, no. 1, pp. 2259–2268, 2010, doi: 10.1016/j.proeng.2010.03.242.

[7] Z. Odanovic, M. Ristivojevic, and V. Milosevic-mitic, ‘Investigation into the causes of fracture in railway freight car axle’, *Eng. Fail. Anal.*, vol. 55, pp. 169–181, 2015, doi: 10.1016/j.engfailanal.2015.05.011.

[8] M. Ognjanovic, A. Simonovic, M. Ristivojevic, and T. Lazovic, ‘Research of rail traction shafts and axles fractures towards impact of service conditions and fatigue damage accumulation’, *Eng. Fail. Anal.*, vol. 17, no. 7–8, pp. 1560–1571, 2010, doi: 10.1016/j.engfailanal.2010.06.007.

[9] S. C. Wu, Z. W. Xu, G. Z. Kang, and W. F. He, ‘Probabilistic fatigue assessment for high-speed railway axles due to foreign object damages’, *Int. J. Fatigue*, vol. 117, no. June, pp. 90–100, 2018, doi: 10.1016/j.ijfatigue.2018.08.011.

[10] S. Beretta and D. Regazzi, ‘Probabilistic fatigue assessment for railway axles and derivation of a simple format for damage calculations’, *Int. J. Fatigue*, vol. 86, pp. 13–23, 2016, doi: 10.1016/j.ijfatigue.2015.08.010.

[11] S. Cervello, ‘Fatigue properties of railway axles : New results of full-scale specimens from Euraxles project’, *Int. J. Fatigue*, vol. 86, pp. 2–12, 2016, doi: 10.1016/j.ijfatigue.2015.11.028.

[12] H. Yin, ‘Analysis of transverse cracks forming in a railway axle’, *Mater. Sci. Forum*, vol. 944 MSF, pp. 404–410, 2018, doi: 10.4028/www.scientific.net/MSF.944.404.

[13] P. Jorge, F. Borges, D. Costa, and M. Integrado, ‘Fatigue Reliability Analysis of a Rail Vehicle Axle’, 2020.

[14] V. Grubisic and G. Fischer, ‘Railway axle failures and durability validation’, *Proc. Inst. Mech. Eng. Part F J. Rail Rapid Transit*, vol. 226, no. 5, pp. 518–529, 2012, doi: 10.1177/0954409712442325.

[15] D. Zeng, Y. Zhang, L. Lu, L. Zou, and S. Zhu, ‘Fretting wear and fatigue in press- fi tted railway axle : A simulation study of the in fl uence of stress relief groove’, vol. 118, no. May 2018, pp. 225–236, 2019, doi: 10.1016/j.ijfatigue.2018.09.008.

[16] F. Bayraktar and M. Guclu, ‘Railway Axle Analyses : Fatigue Damage and Life Analysis of Rail Vehicle Axle Railway Axle Analyses : Fatigue Damage and Life Analysis of Rail Vehicle Axle’, no. May, 2020, doi: 10.5545/sv-jme.2011.206.

[17] M. Luke, M. Burdack, S. Moroz, and I. Varfolomeev, ‘Experimental and numerical study on crack initiation under fretting fatigue loading’, *Int. J. Fatigue*, vol. 86, pp. 24–33, 2016, doi: 10.1016/j.ijfatigue.2015.09.022.

[18] M. Filippini *et al.*, ‘ScienceDirect Fatigue strength assessment of railway axles considering small-scale Fatigue railway axles Fatigue strength strength assessment assessment of railway axles considering considering small-scale tests and of damage calculations and calculations’, *Procedia Struct. Integr.*, vol. 4, pp. 11–18, 2017, doi: 10.1016/j.prostr.2017.07.013.

[19] S. Jaap, *Fatigue of structural and materials*, Second Edi. Delft, 2008.

[20] S. Son, H. Jung, T. Kwon, and J. Kim, ‘Fatigue life prediction of a railway hollow axle with a tapered bore surface’, *EFA*, vol. 58, pp. 44–55, 2015, doi: 10.1016/j.engfailanal.2015.08.031.

[21] B. STANDARD, ‘Railway applications — Wheelsets and bogies — Axles — Product requirements-BS EN 13261:2009’, 2010.

[22] ISO, ‘ISO 12107:2012(E) Metallic materials — Fatigue testing — Statistical planning and analysis of data’, *Test*, vol. 2012, no. Reapproved, 2012.

[23] R. et al Li lee, Y;Pa n, J; Hathaway, *Fatigue testing and Analysis*. 2005.

[24] T. Nicholas, *High Cycle Fatigue*. 2006.

[25] F. C. Campbell, ‘Chapter 14: Fatigue’, *Elem. Metall. Eng. Alloy.*, pp. 243–265, 2008.

[26] E. S. N. E. E. NORM, ‘Railway applications - Wheelsets and bogies - Non powered axles - Design method-EN 13103:2009+A2 July’, 2010.

[27] E. S. N. E. E. NORM, ‘Railway applications - Wheelsets and bogies - Powered axles - Design method-EN 13104:2009+A2 October’, 2010.

Appendix

Appendix A: Modelling and assembled parts of wheelset, axle box and track in solid works

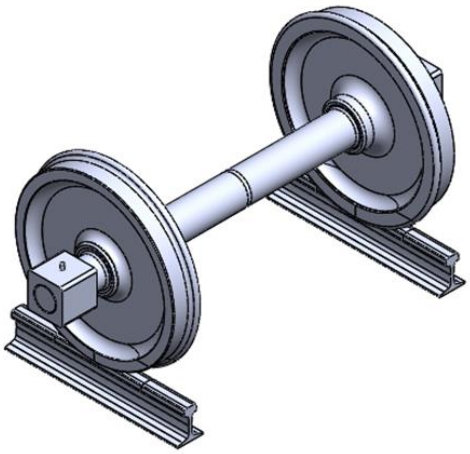

(a) Two side axle box`

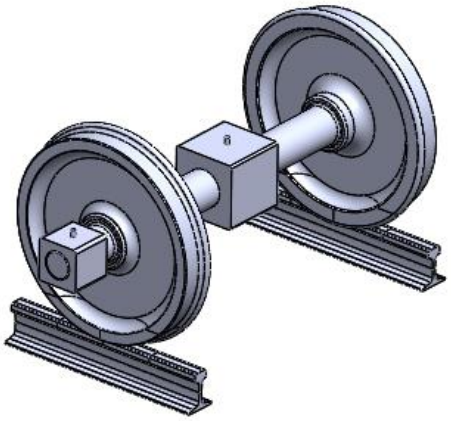

(b) Center axle box

Appendix B: Bodies contact

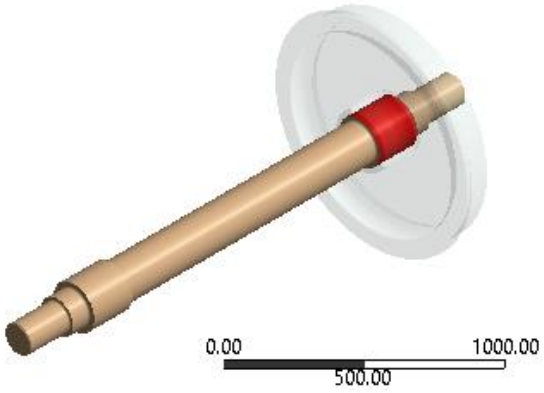

(a) Contact body(bounded)

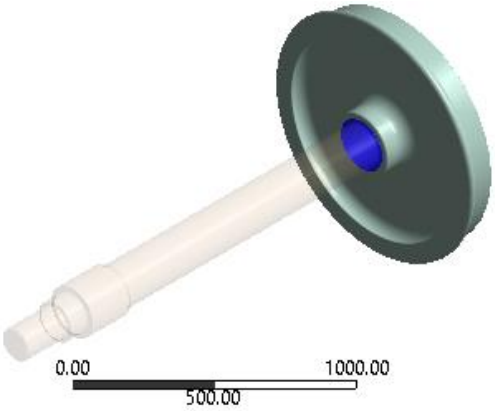

(b) Target body(bounded)

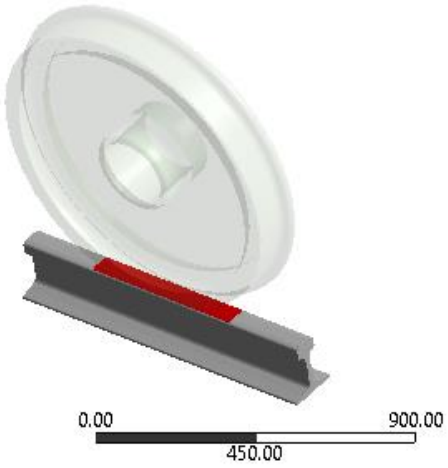

(c) Contact body (Frictional)

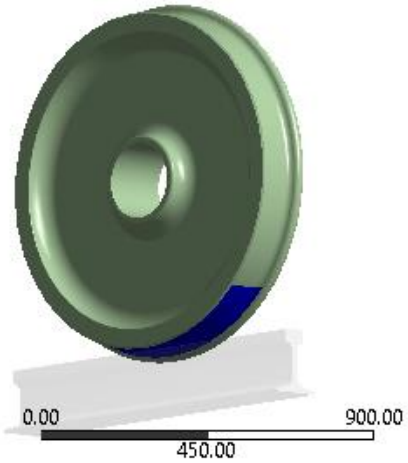

(d) Target body(Frictional)

Appendix C: Static structural analysis showing fixed support, displacement and applied load

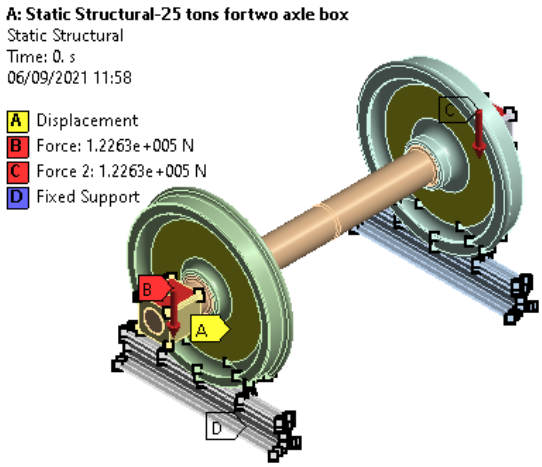

(a)Applied load on two side axle box

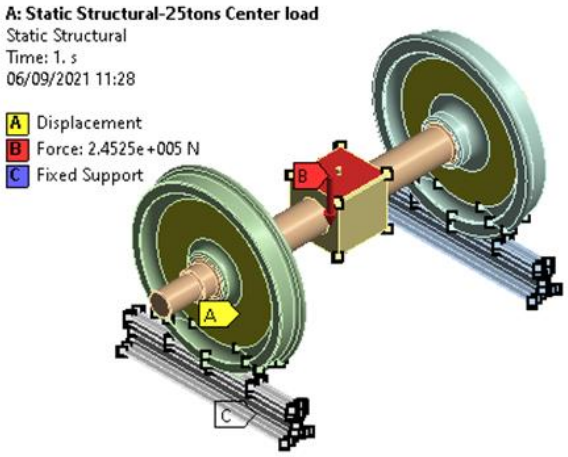

(b) Applied load at the center of axle box

Appendix D: Display of fatigue results using fatigue tool in ANSYS workbench

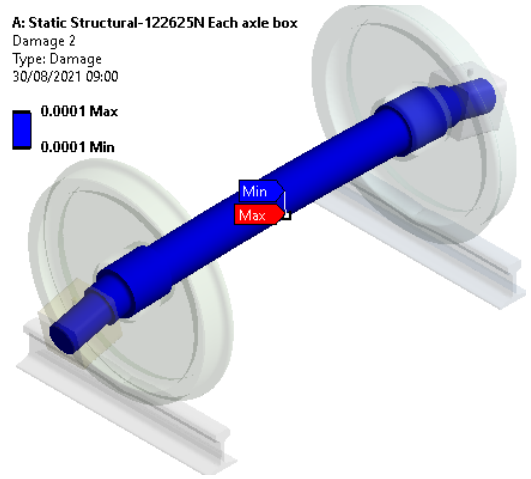

(a) Damage

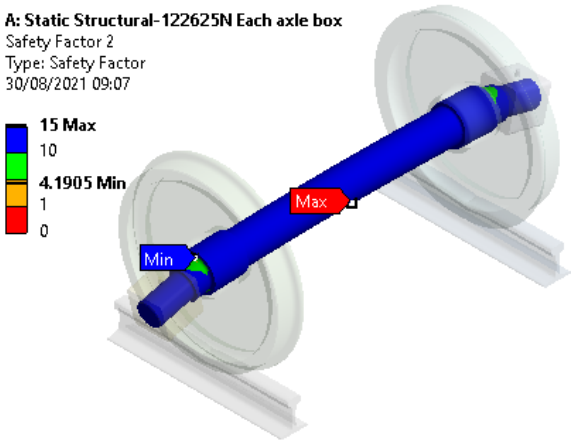

(b) Factor of safety

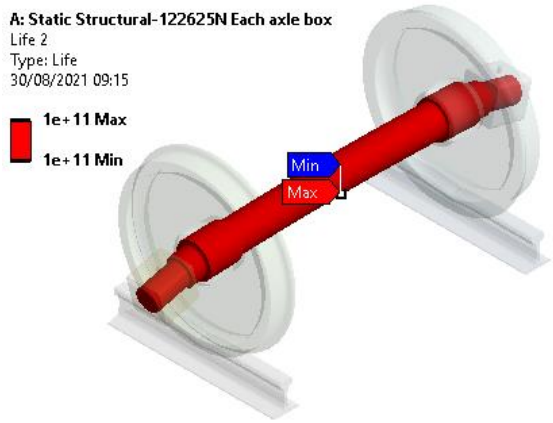

(c) Fatigue life

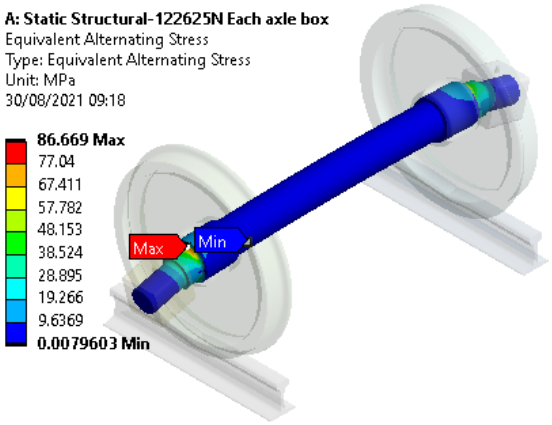

(d) Alternating stress

Appendix E: Static structural results for axle load 30 and 35 tons

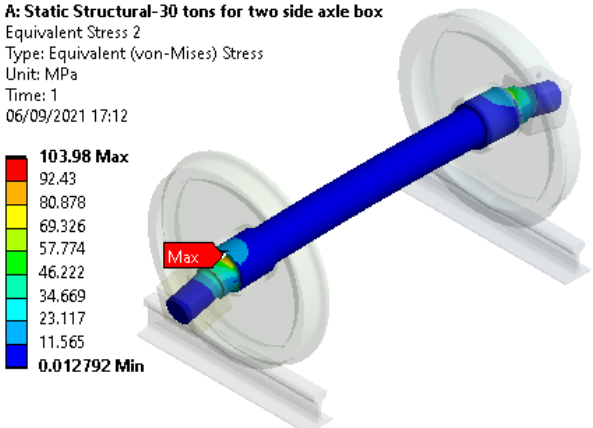

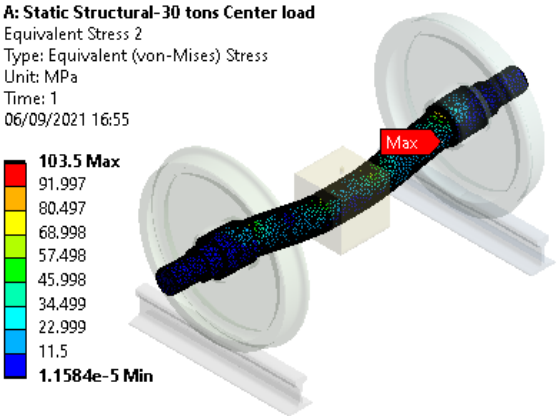

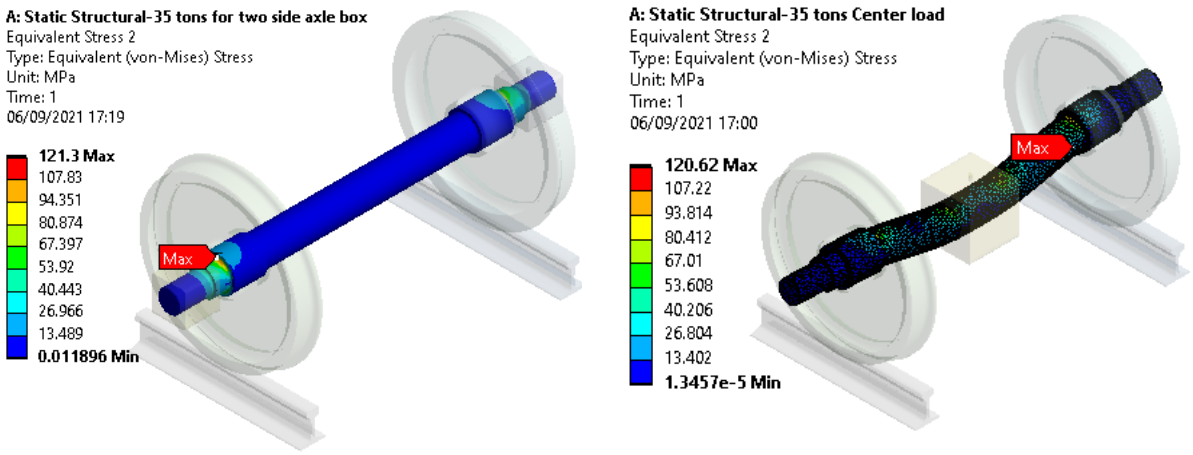

Appendix F: Display results of the of assembly model in nCode fatigue analysis software

DataValuesDisplay1

Export ... Copy

	6	12	13	14	16
Remove Sort	Damage	Max Stress	Min Stress	Part	Life
		MPa	MPa		Repeats
1	6.407e-10	230.5	-230.5	Track left	1.561e+09
2	1.969e-10	207.3	-207.3	Track left	5.078e+09
3	1.543e-10	202.8	-202.8	Track right	6.48e+09
4	9.947e-11	194.9	-194.9	Track left	1.005e+10
5	7.04e-11	189	-189	Track right	1.42e+10
6	6.648e-11	188	-188	Track right	1.504e+10
7	5.905e-11	186	-186	Wheel right	1.693e+10
8	3.877e-11	179.1	-179.1	Wheel left	2.579e+10
9	3.785e-11	178.7	-178.7	Track right	2.642e+10
10	2.253e-11	170.6	-170.6	Axle	4.438e+10
11	2.059e-11	169.2	-169.2	Axle	4.856e+10
12	1.935e-11	168.2	-168.2	Track right	5.168e+10
13	1.778e-11	167	-167	Axle	5.625e+10
14	1.762e-11	166.8	-166.8	Axle	5.674e+10
15	1.744e-11	166.7	-166.7	Axle	5.734e+10
16	1.667e-11	166	-166	Axle	5.998e+10
17	1.65e-11	165.8	-165.8	Axle	6.062e+10
18	1.542e-11	164.8	-164.8	Track left	6.485e+10
19	1.527e-11	164.7	-164.7	Axle	6.549e+10
20	1.524e-11	164.7	-164.7	Axle	6.561e+10
21	1.49e-11	164.3	-164.3	Axle	6.713e+10

TestName: file Channel: 1 Title: Results Table: 1

Appendix G: Fatigue Simulation of imported model from ANSYS workbench in nCode

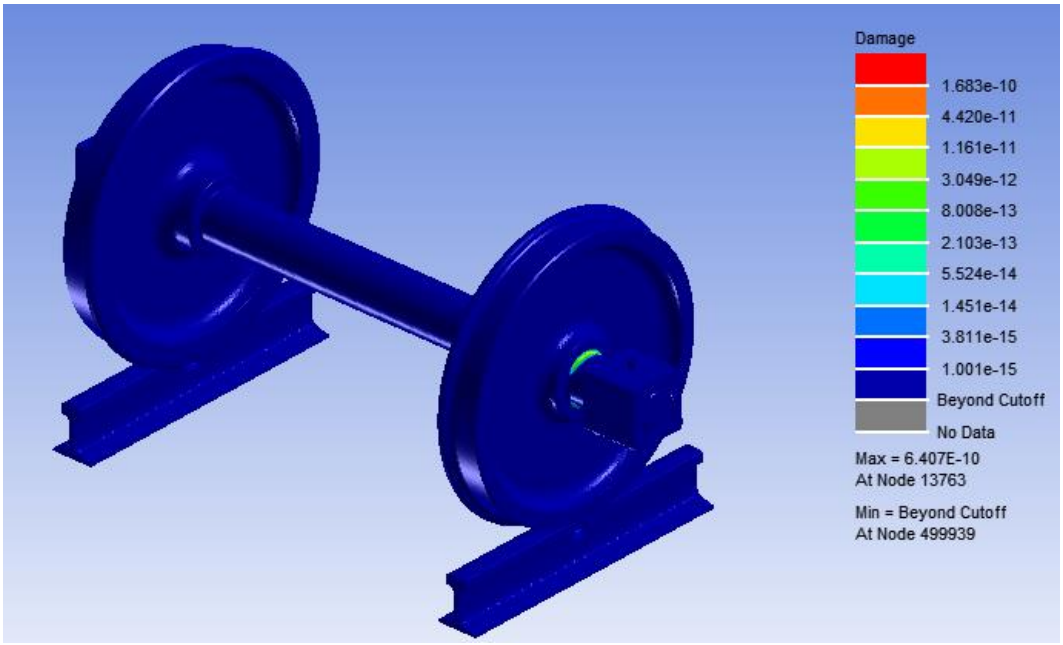

(a) Damage due to fatigue

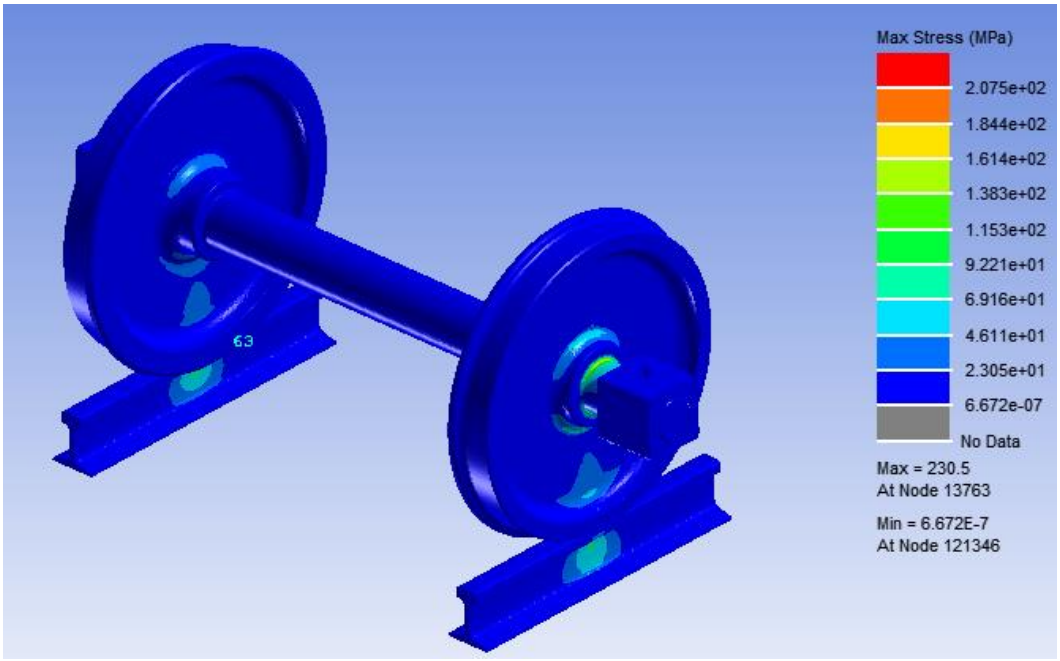

(b) Maximum fatigue stress

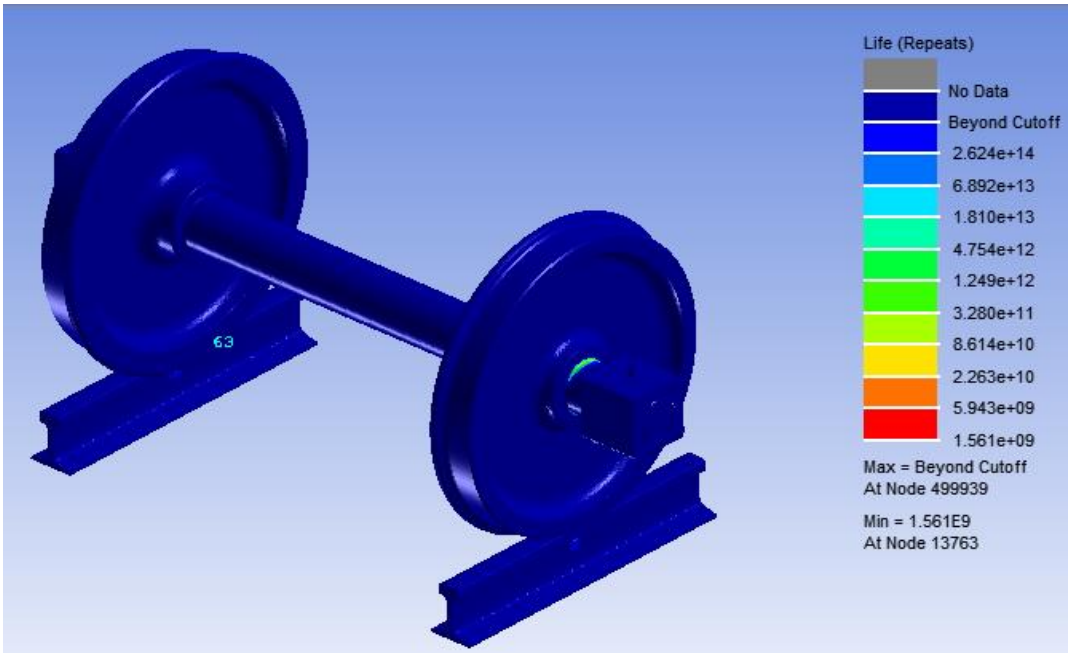

(c) Life cycles

The notched specimen's simulation results is shown from Appendix H to Appendix L.

Appendix H: Stress-strain results of notched specimens of 7mm and 7.5mm diameter

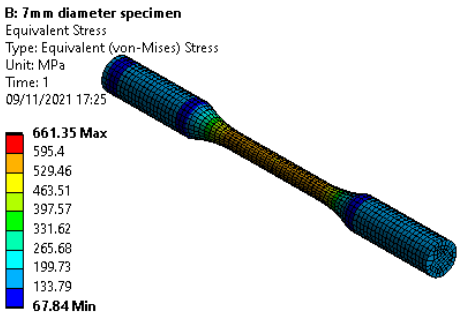

(a) stress result of 7mm diameter of notched specimen

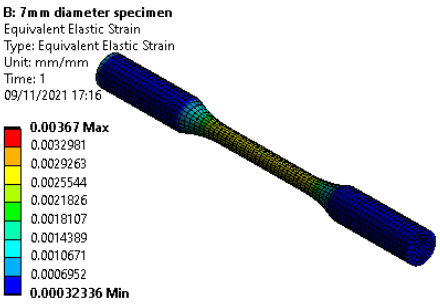

(b) strain result of 7mm diameter of notched specimen

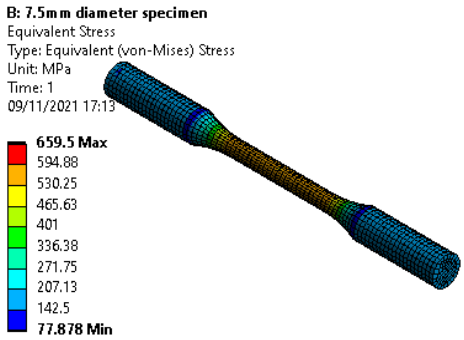

(c) stress result of 7.5mm diameter of notched specimen

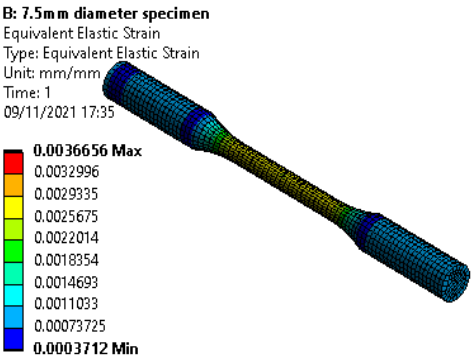

(d) strain result of 7.5mm diameter of notched specimen

Appendix I: Stress-strain results of notched specimens of 8mm and 8.5mm diameter

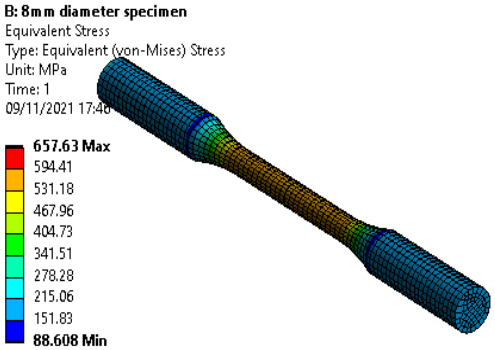

(a) stress result of 8mm diameter of notched specimen

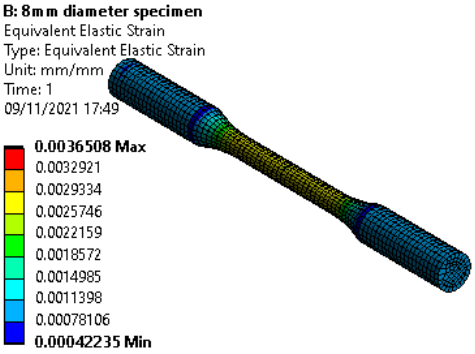

(b) strain result of 8mm diameter of notched specimen

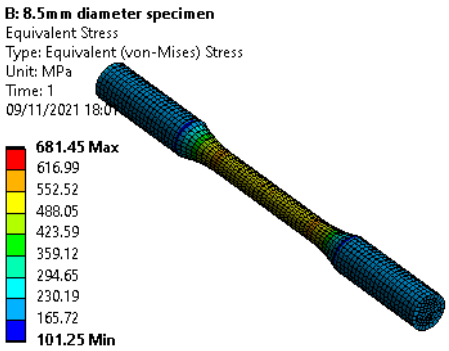

(c) stress result of 8.5mm diameter of notched specimen

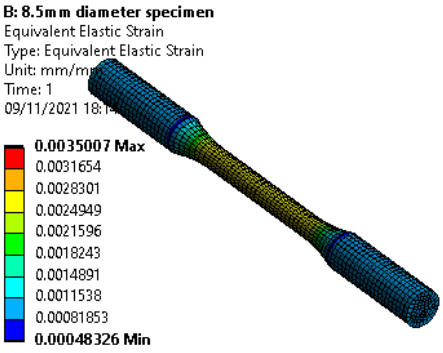

(d) strain result of 8.5mm diameter of notched specimen

Appendix J: Stress-strain results of notched specimens of 9mm and 9.5mm diameter

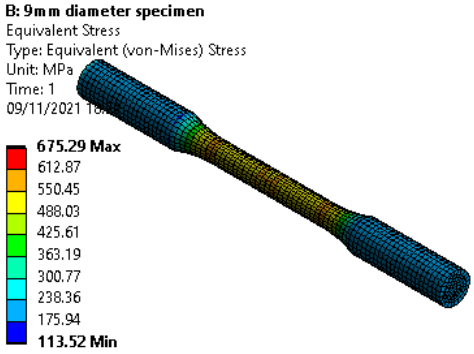

(a) stress result of 9mm diameter of notched specimen

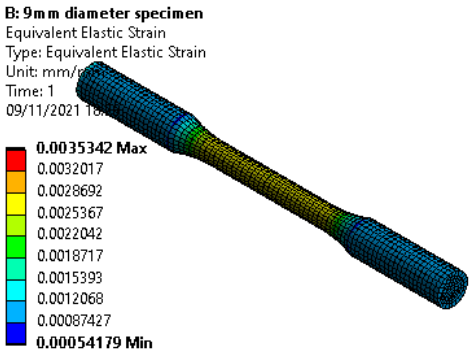

(b) strain result of 9mm diameter of notched specimen

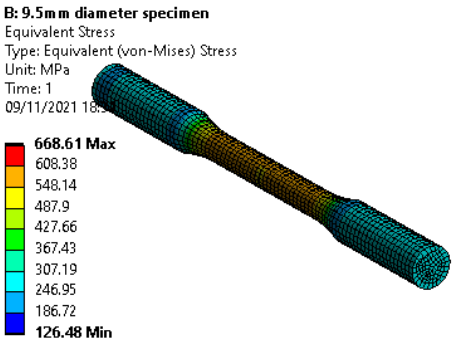

(c) stress result of 9.5mm diameter of notched specimen

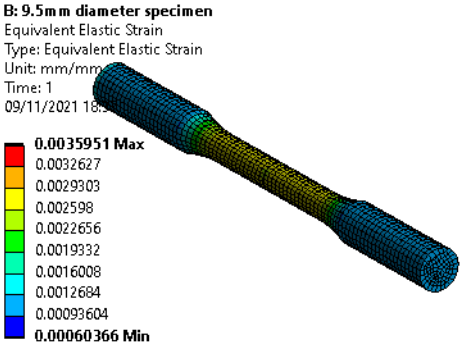

(d) strain result of 9.5mm diameter of notched specimen

Appendix K: Stress-strain results of notched specimens of 10mm and 10.5mm diameter

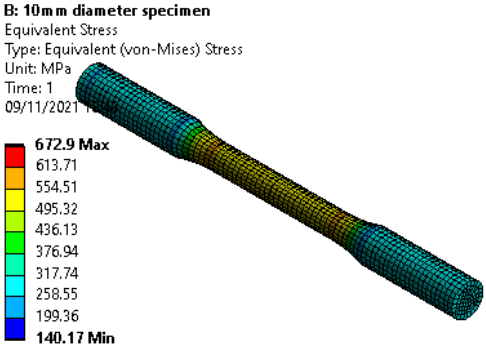

(a) stress result of 10mm diameter of notched specimen

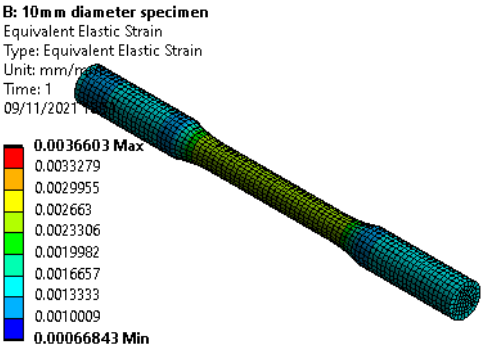

(d) strain result of 10mm diameter of notched specimen

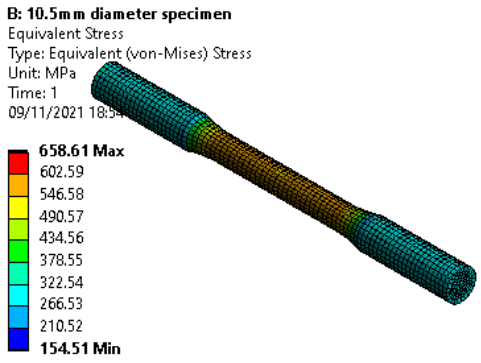

(c) stress result of 10.5mm diameter of notched specimen

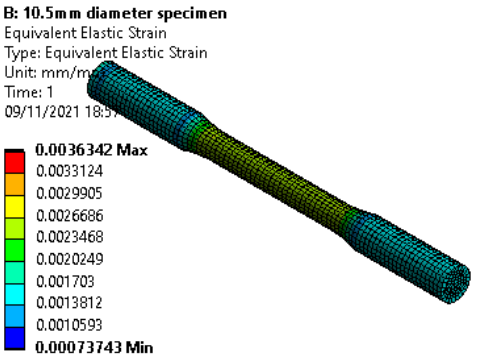

(d) strain result of 10.5mm diameter of notched specimen

Appendix L: Stress-strain results of notched specimens of 11mm and 11.5mm diameter

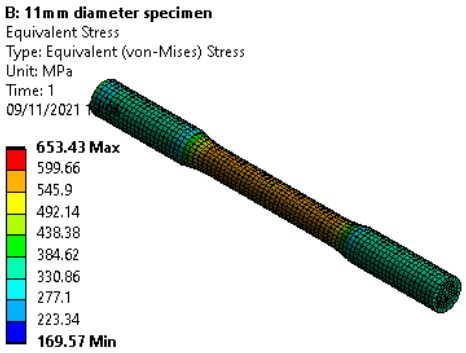

(a) stress result of 11mm diameter of notched specimen

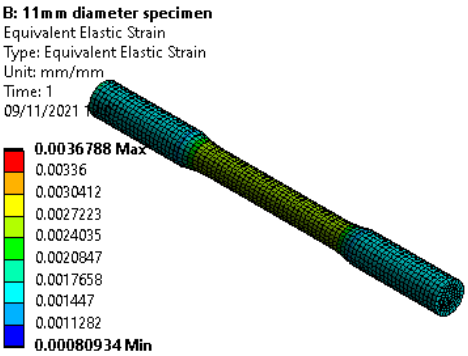

(b) strain result of 11mm diameter of notched specimen

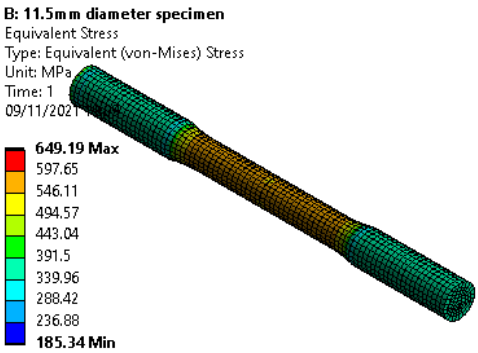

(c) stress result of 11.5mm diameter of notched specimen

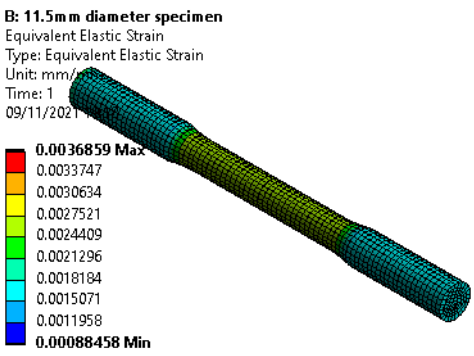

(d) strain result of 11.5mm diameter of notched specimen

The smooth specimen's simulation results is shown from Appendix M to Appendix Q.

Appendix M: Stress-strain results of smooth specimens of 7mm and 7.5mm diameter

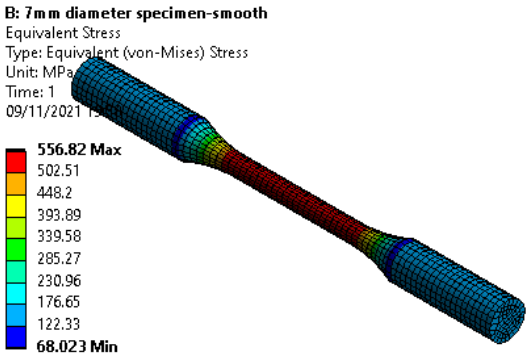

(a) stress result of 7mm diameter of smooth specimen

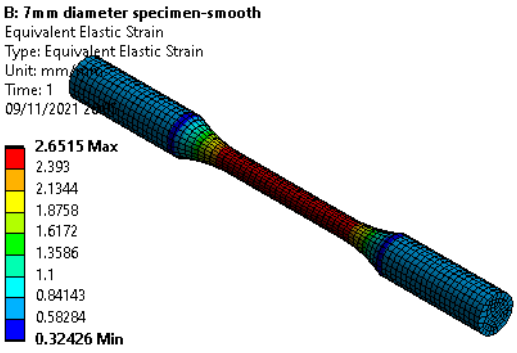

(b) strain result of 7mm diameter of smooth specimen

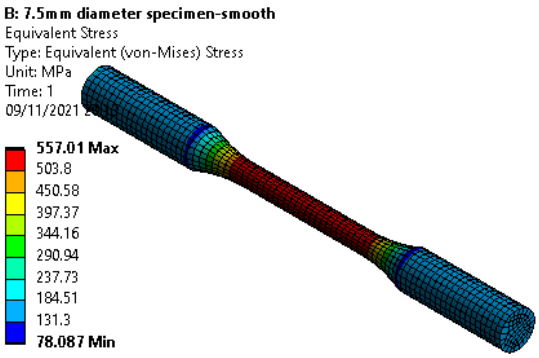

(a) stress result of 7.5mm diameter of smooth specimen

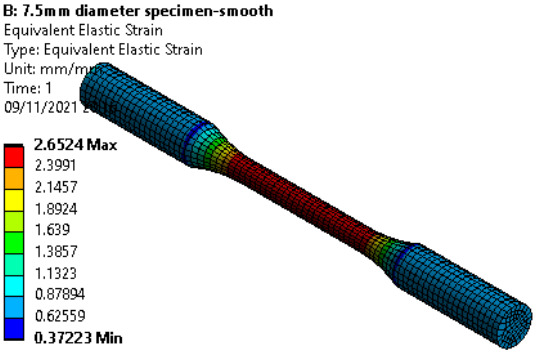

(b) strain result of 7.5mm diameter of smooth specimen

Appendix N: Stress-strain results of smooth specimens of 8mm and 8.5mm diameter

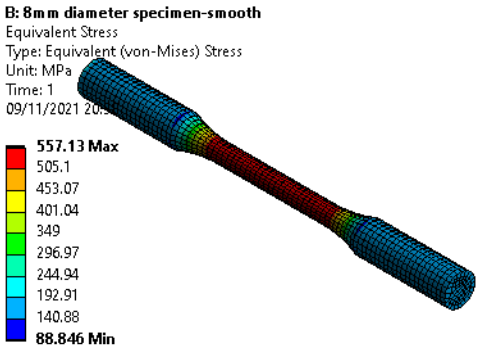

(a) stress result of 8mm diameter of smooth specimen

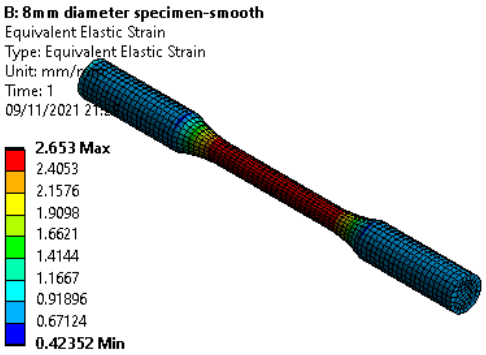

(b) strain result of 8mm diameter of smooth specimen

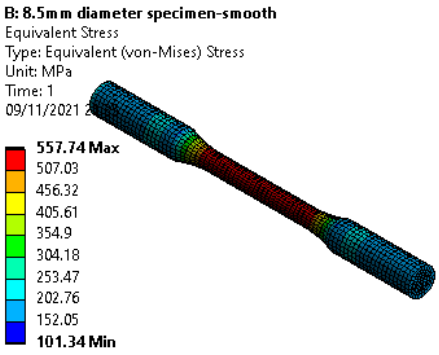

(c) stress result of 8.5mm diameter of smooth specimen

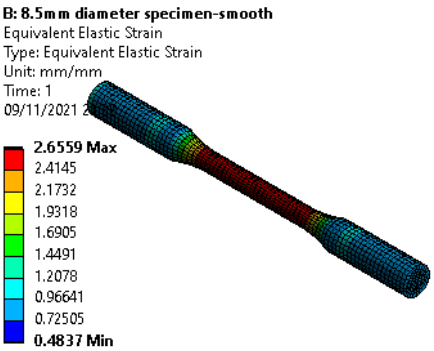

(d) strain result of 8.5mm diameter of smooth specimen

Appendix O: Stress-strain results of smooth specimens of 9mm and 9.5mm diameter

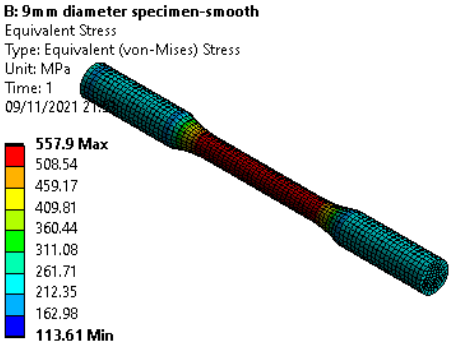

(a) stress result of 9mm diameter of smooth specimen

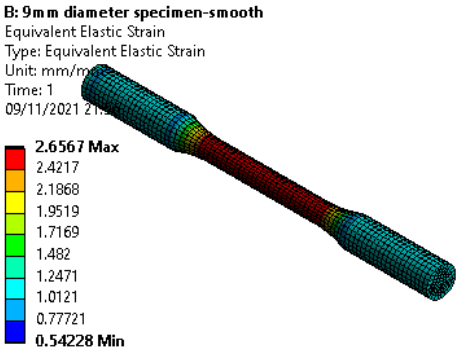

(b) strain result of 9mm diameter of smooth specimen

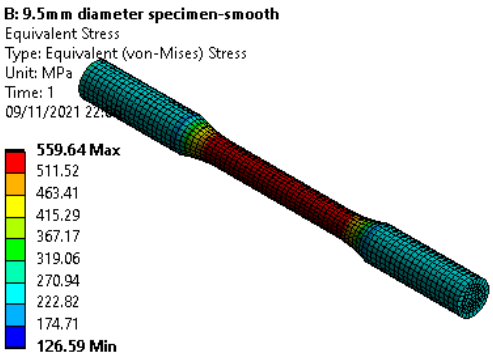

(c) stress result of 9.5mm diameter of smooth specimen

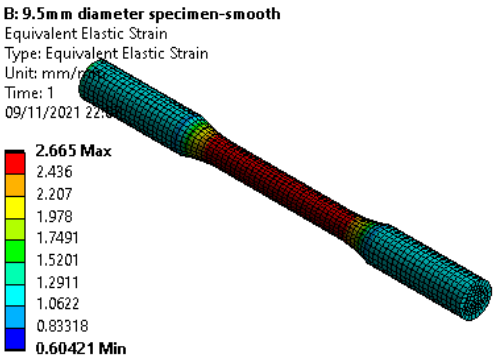

(d) strain result of 9.5mm diameter of smooth specimen

Appendix P: Stress-strain results of smooth specimens of 10mm and 10.5mm diameter

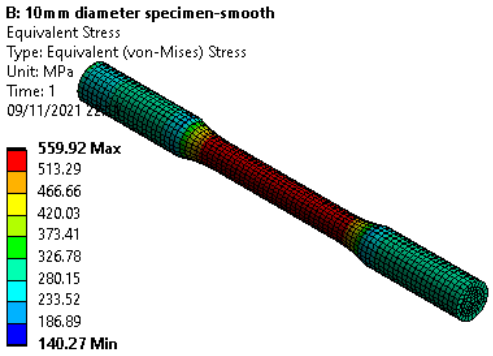

(a) stress result of 10mm diameter of smooth specimen

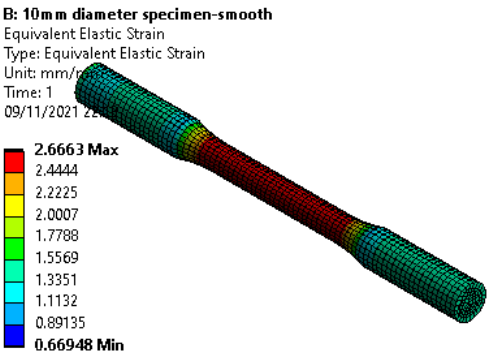

(b) strain result of 10mm diameter of smooth specimen

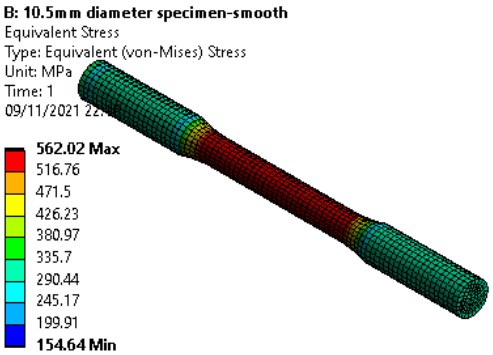

(c) stress result of 10.5mm diameter of smooth specimen

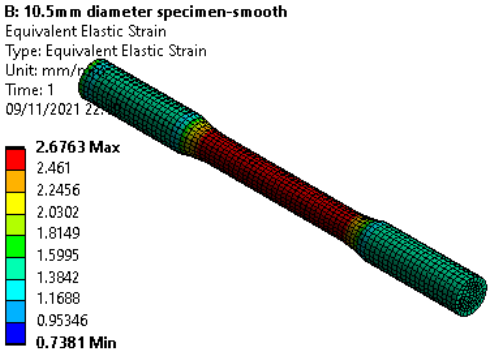

(d) strain result of 10.5mm diameter of smooth specimen

Appendix Q: Stress-strain results of smooth specimens of 11mm and 11.5mm diameter

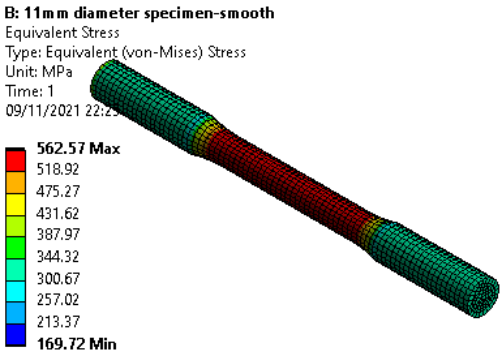

(a) stress result of 11mm diameter of smooth specimen

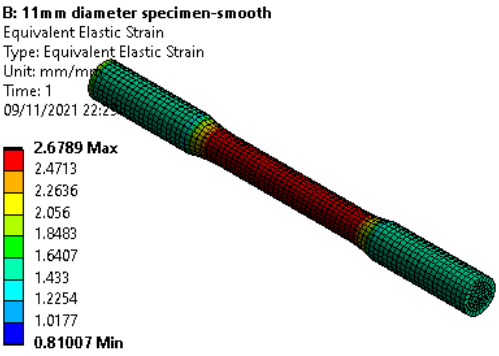

(b) strain result of 11mm diameter of smooth specimen

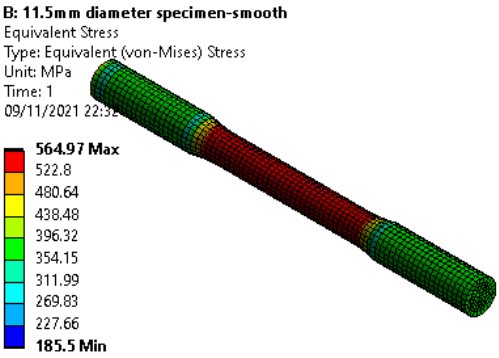

(c) stress result of 11mm diameter of smooth specimen

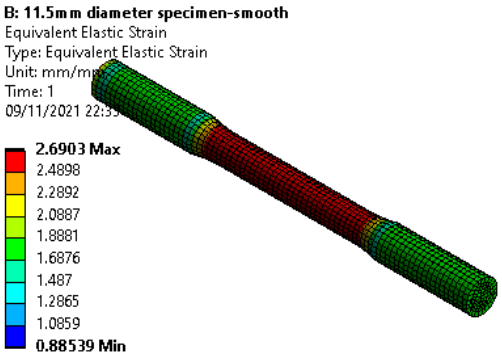

(d) strain result of 11mm diameter of smooth specimen